NTNU
Norwegian University of
Science and Technology

Model-based Detection for Ice on Wind Turbine Blades

Qian Shi

EWEM

TUDelft
Delft University of Technology

NTNU
Norwegian University of
Science and Technology

Model-Based Detection for Ice on

Wind Turbine Blades

Qian Shi

13th July, 2017

Model-Based Detection for Ice on Wind Turbine Blades

Master of Science Thesis

For obtaining the degree of Master of Science in "Technology-Wind Energy" at Norwegian University of Science and Technology, and in "Offshore Engineering and Dredging" at Delft University of Technology.

Qian Shi

NTNU: 471805
TU Delft: 4474945

13th July, 2017

European Wind Energy Master – EWEM

Delft University of Technology
Faculty of Mechanical, Maritime and Materials Engineering
Department of Maritime and Transport Technology
Section of Offshore and Dredging Engineering

Norwegian University of Science and Technology
Faculty of Engineering Science and Technology
Department of Marine Technology

Place: Trondheim   Date: 13th July, 2017   Signature: *Qian Shu*

Acknowledgement

The thesis work is the biggest challenge during my master study. It is also a good practice of the research ability as an engineer. During the thesis work, I had came across with many difficulties and finally made it within very limited time. I am very proud of my thesis work and hope it will be helpful for the future applications.

My thesis work began from February. At that time I did not have a clear mind of what to do, and how to do it. The only thing I am sure is to do fault detection. Then I made much effort to figure out what kind of method is reliable. Then which fault condition can this method are applied. After many attempts, I had made up my mind to do ice on blade detection applying model based detection method. Then I had tried my best to accomplish all the work.

During the time of writing master thesis, Prof. Erin Bachynski gave me a lot of help. We had weekly meeting during the whole thesis work. She had given me a lot of comments on the thesis contents, which were very helpful. She also spent a lot of time and effort to correct my language mistakes. I was inspired by her seriously work manner and tried my best to make the thesis better. I would like to thank Prof. E. Lourens and Prof. Andrei Metrikine of TU Delft. They gave me helpful suggestion and question to make me go further.

I would like to thank my boyfriend Shaojun Ma, a Phd candidate of NTNU. He had given me the strongest support whenever I face with problems. He shows me how to do better and makes me believe in myself. Without him, I will not complete the master study successfully. I would like to thank my friend Jingyi and Rui. They are excellent and I have learned much from them.

Finally, I would like to thank my families and wish they are all happy and healthy.

Trondheim, June 25, 2017

Qian Shi

II

Abstract

Wind power to cold climate sites is attractive because of favorable wind conditions and low population density. However, icing of wind turbine blades remains one of the main challenges for cold climate sites. Ice formation on wind turbine blades causes several problems, such as the loss of power production, unbalanced loads in drive train and ice throw. Most of the existing detection methods need special sensors installed and would be expensive to achieve a satisfied accuracy. In this research, an alternative model-based ice on blade detection method is proposed. There are mainly two advantages of the method. Firstly there are no additional measurements are needed. Secondly the detection method can be implemented for any kind of blade aerodynamic changes, not only ice on blade.

The basis of the mode-based ice-detection method is a reliable linearized wind turbine model. The accuracy of the model is mainly influenced by the number of degrees of freedom (DOFs) and the number of operation points (OP). The most efficient model is the one with less DOFs and OP but without losing much accuracy. The relative importance of DOF and OP is revealed and suggestions are given for an optimum choice of DOF and OP for different quantities. Specifically, for power production properties, increase the number of OP is more efficient. While, for blade and tower related properties, increase the number of DOF is a better choice.

The ice on blade influence of aerodynamic force, power production and structure loads is studied for three ice conditions, which are start ice, light ice and moderate ice. Based on the ice on blade influence and the reliable linearized wind turbine model, the concept of model-based ice-detection is proposed as follows: Firstly ice on blade changes the aerodynamics and the blade mass. Therefore it can be considered as one wind turbine system changed to a different system. That means the outputs of the two systems, with ice and without ice, are different, even the inputs are exactly the same. From the ice-detection point of view, if the difference of outputs between iced system and cleaned one is much larger than modeling error, ice on blade can be detected.

With the proposed model-based detection method, the ice-detection capability of different output quantities is studied. It has been found that the power production related quantities usually have the highest ice-detection capability, while the blade and tower properties have relatively lower capability. In order to verify the ice-detection method for a broad working conditions, implementations are performed for above and below rated wind speed conditions. Successful detections have been achieved for both of them.

For possible measurement errors in reality, they are efficiently considered by introducing uncertainty factors. The ice-detection capabilities with measurement error have been analyzed for three ice conditions and detected based on different quantities. Although a drop in the detection capability has been observed if considering the measurement error, all the quantities still can detect the ice successfully to some degree.

IV

Contents

List of Tables

List of Figures

XVI

Chapter 1 Introduction

1.1 Background and state of art

Wind energy is now established around the world as mainstream sources of energy. It is a clean, renewable energy source and offers many advantages. The 2016 market was more than 54.6 GW, bringing total global installed capacity to nearly 487 GW, led by EU, China, and the US, according to the global wind energy council. Figure 1 display the trend of global wind capacity installation. The market is growing very fast.
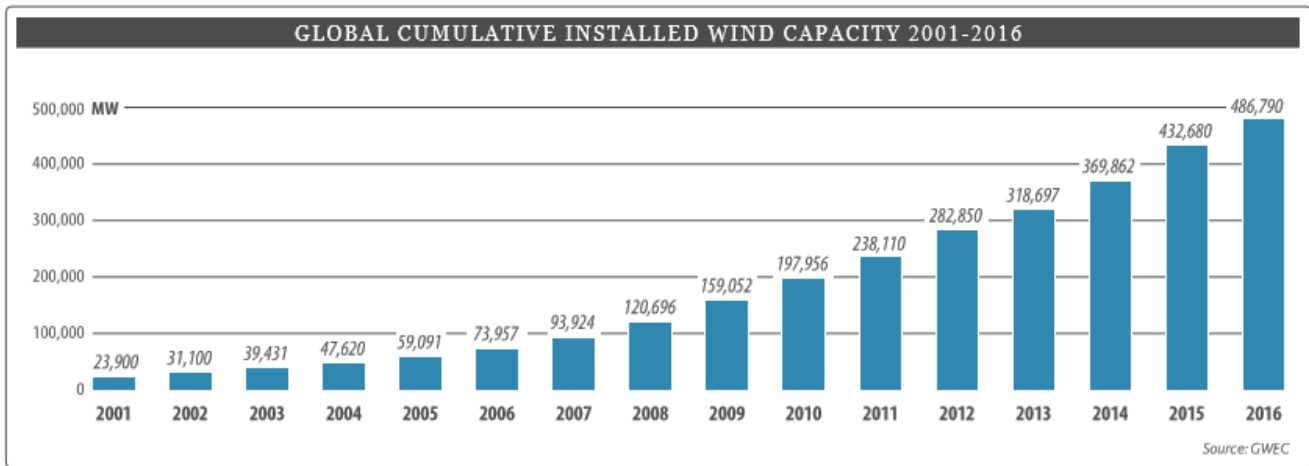
Figure 1 Global cumulative installed wind capacity (Global Wind Report 2016)

Wind power capacity in cold climate is defined as weather conditions of atmospheric icing and low-ambient temperatures which expose wind turbines to conditions outside their normal design limits (IEA Wind Task 19 Group 2011). Building wind power to cold climate sites is attractive because of favorable wind conditions and low population density (Lehtomäki and Wallenius, 2015). Therefore developers and investors are beginning to shift their focus on new sites with attractive wind conditions in areas affected by icing in northern Scandinavia, North America and mountainous regions all over Europe. A marked study by BTM Navigant predicts further strong growth of the cold climate sector in the next years. However, icing of wind turbine blades remains one of the main challenges for cold climate sites. Icing of blades has become more significant while turbine size has increased (Hochart C, 2008).

Ice formation on wind turbine blades causes several problems. Firstly ice on blade changes the airfoil shape of blade, therefore the blades aerodynamic properties changes. This will induce the loss of power production and expected downtime due to icing must be considered in the economic assessment of project. Secondly additional mass on the blade due to icing yields higher inertia forces on the rotor and may change the natural frequencies and loads of the blade. That may decrease the blade life due to fatigue issues. If ice on blade is not symmetric, the asymmetric drive train loading will decrease the life

1

time of drivetrain components. Thirdly possible ice throw from the wind turbines operating under iced condition is an important issue for wind farms near populated areas such as a ski resort or farmlands. (Etemaddar et al.2014).

In this context, an optimized and efficient operation of wind parks under icing conditions has become a very important issue for wind farm operators. On the one hand, it is in the operators' interest to keep the production losses due to icing as low as possible. On the other hand, the safety of passersby and service personnel has to be guaranteed at all times and extreme loads have to be avoided (Cattin, R. 2012).

Icing can be detected either directly or indirectly. The direct methods detect some property change caused by the accretion of ice. These include mass, reflective properties, electrical or thermal conductivity, dielectric coefficient and inductance. The indirect methods are based upon detecting the weather conditions that lead to icing, such as humidity and temperature, or detecting the effects of icing, such as a reduction in power production. They then use a model, either empirical or deterministic, to determine when icing is occurring. There are some commercially available products, which are listed in Table 1 and Table 2 (Cattin, R. et al 2016).

Table 1 Direct ice-detection ptoducts and its principles

Products	Principle	Commercially available
Leine Linde System IPMS	Video livestream	2010
Combitech Ice Monitors	Vertical freely rotating cylinder load cell	2005
Goodrich	Ultrasomic vibrating finger decrease of amplitude during icing	1994
HoloOptics	Reduced infrared reflection when probe covered with ice	2009
Sommer	Change of impedance on surface when probe covered with ice	2016
New Avionics Ice Meister	Change of opacity and index of fraction when probe iced	2014

Table 2 Indirect ice-detection ptoducts and its principles

Products	Principle	Commercially available
Temperature & humidity	Temperature<XX$^\text{o}$C Relative humidity>XX%	Long time
ENERCON Ice-detection System	Actual power output vs. predicted from wind speed	n/a
Heated vs. unheated anemometers	Significant deviation between heated and unheated anemometer	Long time
fos4 Ice-detection	Fiber-optic accelerators change in eigenfrequency when blade is iced	2013
Wolfel SHM Blade	Structural noise sensors(accelerators), detect change of generated noise	2012

The methods using resonant frequency of a probe ice collecting cylinder, change of impedance and two anemometers, as well as the HoloOptics and Sommer sensors all are mounted on the nacelle of the turbine, and have therefore limited applicability for detecting ice on blade. This is due to the rate of ice accretion is directly related to the relative velocity of the super-cooled water droplets, and it is at the blade tip that the highest velocity occurs. What's more the outer ends of the blades sweep a larger volume and collect water or ice from the entire volume.

The method using blade eigenfrequency is widely used with relatively high accuracy. The greatest disadvantage is the difficulty in installing the system in existing blades. This is because the fiber optic cables must be installed during the construction of the blades.

The method using cameras can be useful during testing of various sensors, and to record the conditions at the wind turbine, but have not yet been demonstrated to be suitable for ice-detection. There are two mean reasons. Firstly, in arctic regions there is little light during much of the winter, which requires artificial lighting. The second is the lack of suitable automated image analysis tools, therefore the images should be manual checked. However image analysis is an area in rapid change, which may make this system promising in the near future.

The method applying a change in the frequency of noise will require further investigation to determine how background noise and varying wind speeds affect the data. Actual power output vs. predicted power output is a safety check which should already be implemented and a difference may have other causes than icing of the blades. Moreover it can only be used when wind turbine is operation.

1.2 Scope of the current study

In this research, a model-based detection method for wind turbine ice blade is developed. There are three main advantages of the method. Firstly the model-based ice-detection method is based on the measurements that already exist. By applying the wind turbine model, almost any kind of quantities can be determined including displacements, moments, loads and power production related quantities. Therefore the quantities with measurement value can be selected to detect ice without additional measurements. Secondly the detection method can be implemented for any kind of blade aerodynamic changes, not only ice on blade. Any aerodynamic change will induce the change of output comparing with healthy system, therefore aerodynamic change like blade damage and pitch faults can be detected. Thirdly the linearized healthy wind turbine model can also be applied for design of controllers and states estimators.

There are basically two kinds of models are developed in the thesis. One is nonlinear wind turbine model, and the other is linear wind turbine model. In order to simulate ice on blade in time domain, a nonlinear model of land based NREL 5 MW wind turbine is implemented in FAST. Fast is aero-hydro-servo-elastic system that can conduct the integrated wind turbine system analysis. The aerodynamic part is based on Blade Element Momentum (BEM) theory, and the structural part is based on modal analysis method. The NREL 5MW wind turbine is a pitch regulated wind turbine. Although the nonlinear model is not exactly the same as real wind turbines due to manufacture error as well as the structure change during transport and installation, the model has captured most of the features of wind turbine and is widely used as a benchmark. The nonlinear model is for represent the real operation wind turbine.

However in practice wind turbine model for online detection should be very fast and stable. The nonlinear model is not efficiency enough and consumes much computer time, therefore it is not suitable. A linearized wind turbine model with high efficiency and robust is needed, which captures the most important physical features. Fast is applied for determining the linearized wind turbine model. The accuracy of the linear model is verified in the thesis. Moreover what kind of linearized model is most suitable for ice-detection is also investigated.

The concept of model-based ice-detection is as follows: Firstly ice on blade changes the aerodynamics and the blade mass. Therefore it can be considered as one wind turbine system changed to a different system. That means the outputs of the two systems, with ice and without ice, are different, even the inputs are exactly the same. From the ice-detection point of view, if the difference of outputs between iced system and cleaned one is much larger than modeling error, ice on blade can be detected.

1.3 Structure and innovative of the thesis

 The thesis can be divided into two parts. The first part focuses on modeling the linearized wind turbine system from chapter 2 to 6. The second part focuses on ice on blade detection implementation from chapter 7 to 9. The structure of the thesis is:

In chapter 2, the basic theory of nonlinear wind turbine model in FAST is introduced. After that the theory and steps of linearization method is introduced. Finally the more detailed description of linearization wind turbine components is introduced.

In chapter 3, the definition of NREL 5 MW wind turbine is introduced including the general aerodynamic and structure properties and the detail description of the control system in different regions.

Chapter 4, 5 and 6 is to study the two main modeling parameters, which are the number of degrees of freedom (DOF) and the number of operation points (OP). The aim is to find a suitable DOF and OP for ice-detection. Chapter 4 discusses the influence of number of DOFs for the accuracy of the model. Chapter 5 focuses on the number of OP influence for model accuracy. Chapter 6 studies the total error due to DOF and OP, which is a combination and summary of chapter 4 and 5. In this part all the cases are above wind speed.

Chapter 7 mainly discusses the influence of ice on blade and how to model ice on blade phenomenon. Four ice conditions are considered. And the ice on blade influence on aerodynamic properties and mass are studied as well as other output values of wind turbine. Moreover model-based ice-detection strategies are introduced.

In chapter 8, model-based ice-detection method for above wind speed case is investigated. The ice-detection ability of different quantities, such as power production, blade properties and tower properties, under different DOF, OP and ice categories are studied.

In chapter 9, model-based ice-detection method for below wind speed case is investigated. Firstly the total modeling error is investigated with similar method as chapter 6. Then the ice-detection ability of different quantities, such as power production, blade properties and tower properties, under different DOF, OP and ice categories are studied.

Chapter 10 is a summary of the whole thesis.

The innovative and highlights of the thesis are:

(1) Developed the linearized wind turbine model for ice-detection application. Conducted a systematic analysis on the modeling error. Improved the model in respective of the number of DOFs and OP.

(2) Proposed a detection method for ice on blade based on the previously developed model. Carried out studies to determine the detection capability using different quantities including power production, blade

properties and tower properties. According to my knowledge, there are no studies applying similar methods.

(3) Implemented the model-based ice-detection method for both above rated and below rated wind speed conditions. Suggestions are given for ice-detection under different ice conditions.

Chapter 2 Wind Turbine Modeling Theories

In this chapter, the modeling theories of a wind turbine will be introduced in two steps. Firstly, the nonlinear model will be established with Blade Element Method (BEM) for the aerodynamics and modal method for structure dynamics. Then this nonlinear model will be linearized for convenience in design and simulation. The linearization starts by determining the operation-point (OP) and the nonlinear model will be linearized with respect to this OP. A simple case will also be given to illustrate how the linearization method works.

2.1 Nonlinear wind turbine model

Land based wind turbine is an integrated aero-servo-elastic system with inflow wind, aerodynamics, structure dynamics and control system. In this study, the calculation and analysis are based on the results from FAST, an open source software developed by National Renewable Energy Laboratory (NREL). Therefore, the following theoretical introduction is about the basic theories used in FAST. It should be noted that these theories are general and widely implemented in wind turbine software besides FAST.

All parts in an aero-servo-elastic wind turbine system are shown in Figure 2 . Different parts are related closely and will be introduced one by one here. Aerodynamic module uses inflow wind data and solves for the rotor-wake effects and blade-element aerodynamic loads. The control and electrical system module simulates the controller logic, sensors, and actuators of all control related quantities, such as the blade-pitch, generator-torque, nacelle-yaw, and other control devices. What's more, it can also simulate the generator and power-converter components of the electrical drive. The structural-dynamics module consists of rotor dynamics, drivetrain dynamics, power generation, nacelle dynamics and tower dynamics. Within this module, the elasticity of the rotor, drivetrain, and support structure are simulated according to the control and electrical system reactions as well as the aerodynamic and gravitational loads. The modular interface and coupler enables interactions between all modules.
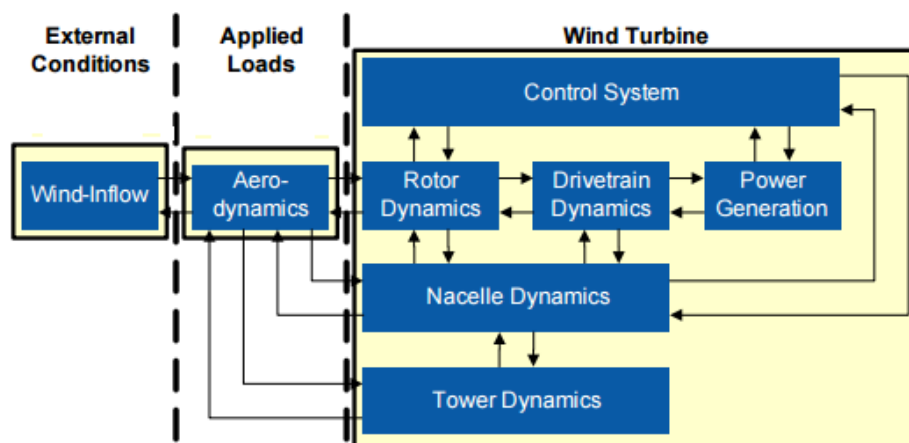
Figure 2 Coupled aero- servo-elastic interaction (Jonkman J M, 2013)

The aerodynamics module, structure dynamics module and control system are three key parts of the wind turbine modeling, and thus they will be thoroughly introduced in the following sections. For the aerodynamics module, the Blade Element Momentum (BEM) theory is implemented with some corrections in the coefficients. For the structure dynamics module, the blades, drivetrain and tower are considered as flexible structures and simulated by modal analysis method. As for the other parts, such as nacelle, rotor and generator, are considered as rigid body. Some structure parts are modeled in the earth fixed coordinate system, while others have their own local coordinate system. The multi-body dynamics theory is applied to assemble all the structure motions in earth fixed coordinate. Finally, the Newton Second Law is applied to analysis dynamic response of structures. A three-blade land based wind turbine will be taken as an example. Its definition of Degrees of Freedom (DOFs) and coordinate systems will be introduced first, and then the focus will be put on the theories of aerodynamics and structure dynamics implemented in FAST. As the control strategies are quite different from one turbine to another, I will introduce the control system in Chapter 3 for a NREL 5MW wind turbine, which will be used as the object for all the later simulations.

2.1.1 Degrees of freedom and coordinates

The FAST code can model a three-bladed land based Horizontal Axial Wind Turbine (HAWT) consisting of nine rigid and five flexible bodies through 18 DOFs. The rigid bodies include the earth, base plate, nacelle, armature, gears, hub, tail, and structure furling with the rotor. The flexible bodies include the tower, three blades, and drive shaft. Detailed information for these 18 DOFs are given in Table 3.

Table 3 Definition of DOF

Body	No. of DOF	Detail Description
3 Blades	9	1st and 2nd flap-wise modes 1st edge-wise mode
	1	blade pitch
Tower	4	1st and 2nd Bending mode in longitudinal and transverse direction
Nacelle	2	Yaw and tilt
Generator	1	Variable speed
Drivetrain	1	Torsion motion
Rotor	1	Tilt

Figure 3 shows the definitions of different DOFs. The first nine DOFs are the blade first and second flapwise mode and blade first edgewise mode. As shown in Figure 3, bending can occur both in the rotor plane and out of the rotor plane. Besides, the blades also have aerodynamic pitch though bearings at the

8

root of blades, which can be considered as another DOF of blades since all three blades pitch simultaneously. The next four DOFs account for tower motion: two of them are the first and second longitudinal modes and the other two are the first and second lateral modes. The tower is assumed cantilevered to the earth and can bend in two directions, producing the fore-aft and side-side motions. These bending flexibilities are modeled by two modes in each direction. Yawing motion of the nacelle provides another DOF. The yaw bearing allows everything above the tower to rotate as the wind direction changes. Moreover, nacelle can be allowed to tilt as well. The next DOF is for the generator azimuth angle, which means the generator rotation speed can be controlled. Another DOF is the compliance in the drivetrain between the generator and hub/rotor. These DOFs account for variable rotor speed and drive-shaft flexibility. The rotor consists of a hub, and rotor blades. A teeter hinge connects between the rotor and the low-speed shaft, which allows the rotor to tilt. For floating wind turbines there are another six DOFs corresponding to the platform translational and rotational motions. For land based wind turbine these DOFs will be omitted.
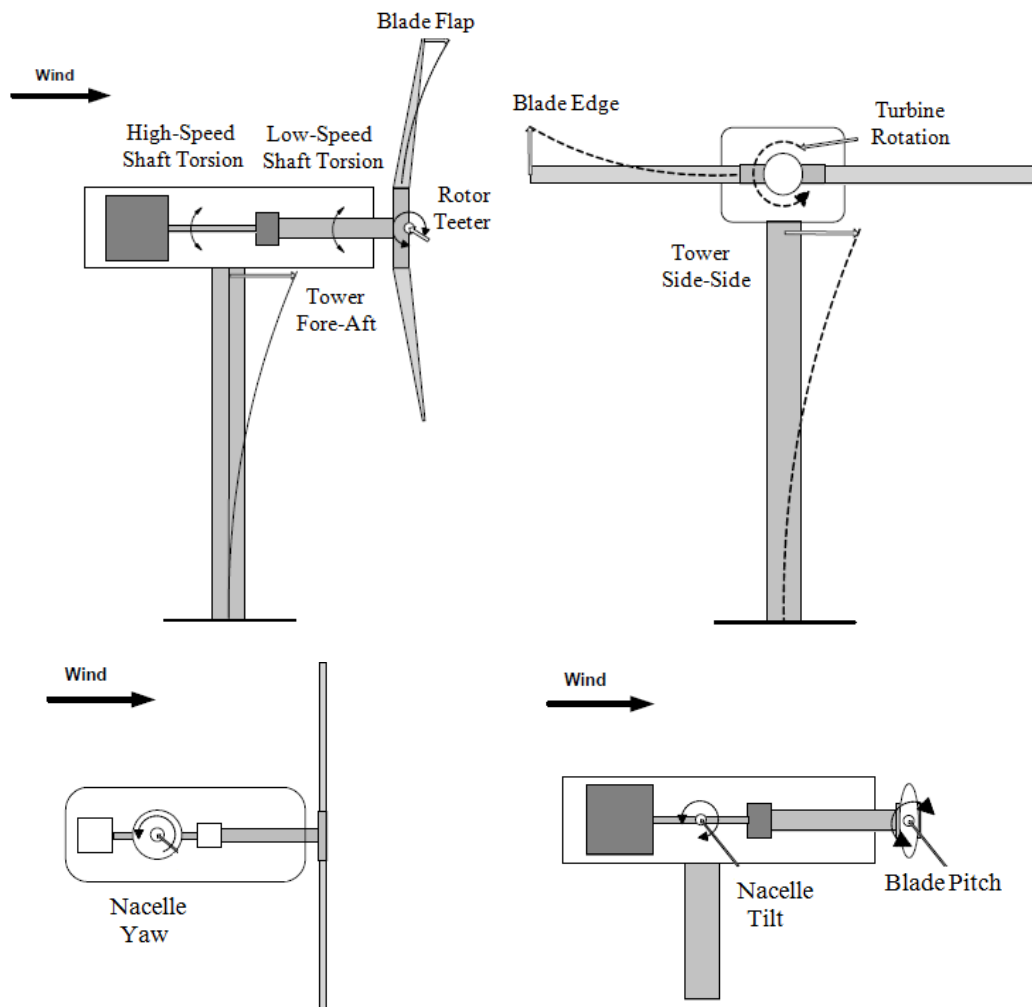
Figure 3 Typical turbine degrees of freedom and motions (Alan D. Wright 2004)

9

The tower related coordinate systems are shown in Figure 4. The Tower-Base Coordinate System coordinate system is fixed in the support tower. So that it translates and rotates together with the platform for floating wind turbine and it is the same as earth fixed coordinate for land based wind turbine. The Tower-Top coordinate system is fixed to the top of the tower. For land based wind turbine it translates and rotates as the tower bends, but it does not yaw with the nacelle. The Nacelle/Yaw coordinate system translates and rotates with the top of the tower, and it has the yaw motion with the nacelle.

Moreover, there are also local coordinate systems defined for the shaft, hub and every blade as shown in Figure 5. The shaft coordinate system does not rotate with the rotor, but it translates and rotates with the tower and it yaws with the nacelle and furls with the rotor. The hub coordinate system rotates with the rotor and the axis orientation does not include a cone angle. The coned coordinate system for each blade rotates with the rotor and includes the cone angle. The coordinate system does not pitch with the blades. The blade coordinate systems are the same as the coned coordinate systems, except that they pitch with the blades and their origins are at the blade root.
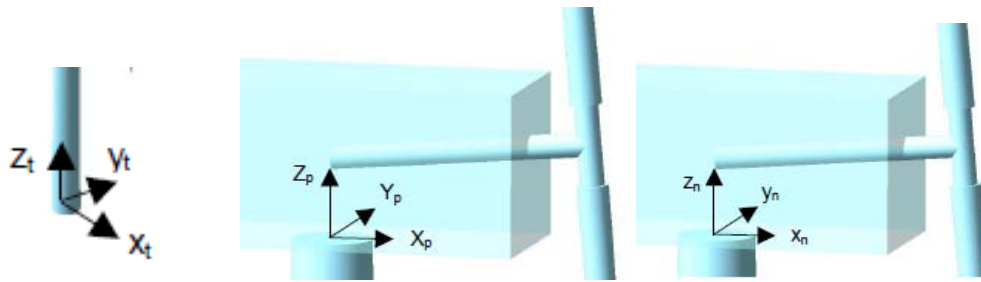
Figure 4 Tower-Base Coordinate System (left) Tower-Top/Base-Plate Coordinate System (middle) Nacelle/Yaw Coordinate System (right) (Jonkman, J. M 2005)
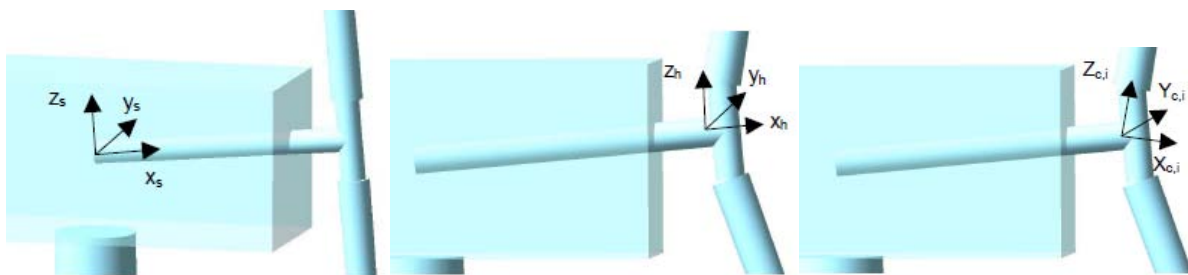
Figure 5 Shaft Coordinate System (left) Hub Coordinate System (middle) Coned Coordinate Systems (right) (Jonkman, J. M 2005)

2.1.2 Aerodynamics—BEM

The BEM method implemented in the current study is a combination of blade element method and momentum method. The assumptions of one-dimensional momentum theory include homogeneous, incompressible and steady-state flow, no friction drag, no flow through stream tube boundary, infinite blades, uniform thrust over disk, non-rotating wake and pressure equal to ambient pressure far from disk.
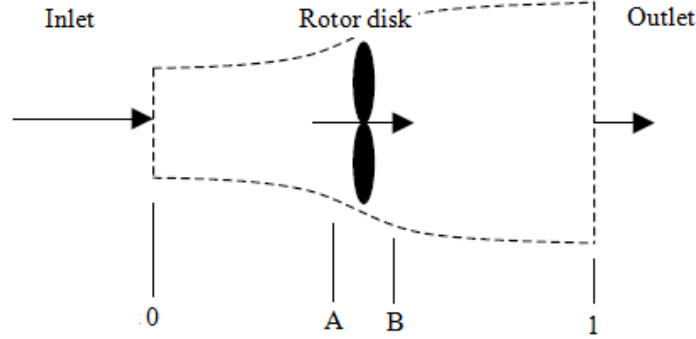
Figure 6 Control volume for actuator disc model (J.M. Jonkman 2003)

Figure 6 shows the one-dimensional actuator disk model. Here we define v_0 as the velocity at inlet of control volume, and v_1 as the velocity at outlet of control volume. At position just before and after the rotor plane, the velocities are defined as v_A and v_B respectively. For convenience in the later expression, we further defined two non-dimensional factors, axial induction factor a and angular induction factor a'.

$$a = \frac{v_0 - v_A}{v_0}, \quad a' = \frac{\omega}{2\Omega} \tag{1}$$

According to the momentum method, the thrust force T can be expressed as

$$T = \frac{1}{2}\rho A(v_0^2 - v_1^2) \tag{2}$$

where ρ is the air density and A the area of rotor plane.

The power P is equal to the change of kinetic energy, which can be calculated as

$$P = \frac{1}{2}\dot{m}(v_0^2 - v_1^2) = \frac{1}{2}\rho A v_0^3 4a(1-a)^2 \tag{3}$$

where $\dot{m}$ donates the air flux through the rotor plane.

From the above formulations, it can be seen that the factors a and a' are the key to determine thrust load and power. They can be determined as follows. We can write the thrust dT and torque dQ acting on an annular ring based on momentum theory

11

$$dT = 4a(1-a)\frac{1}{2}\rho v_0^2 2\pi r dr \qquad (4)$$

$$dQ = 4a'(1-a)\frac{1}{2}\rho v_0 \Omega r^2 2\pi r dr \qquad (5)$$

where r and dr is the radius and thickness of the annular ring.

If the blade element theory is applied, a force normal to the rotor plane p_N and a force tangential to the rotor plane p_T can be determined as shown in Figure 7.
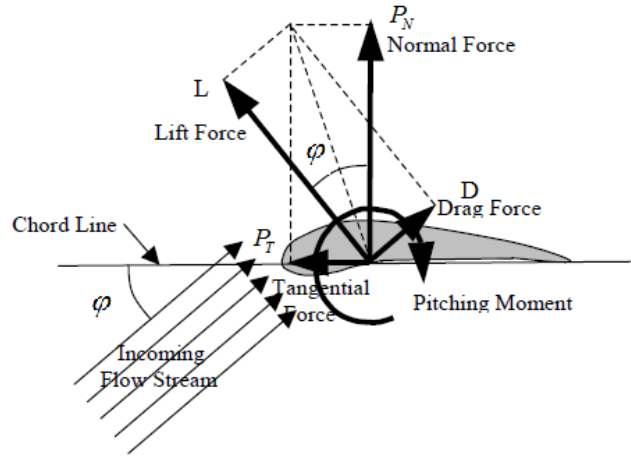
Figure 7 Airfoil section in the rotor plane (J.M. Jonkman 2003)

The thrust and torque can be calculated as

$$dT = BP_N dr = B(L\cos\varphi + D\sin\varphi)dr \qquad (6)$$

$$dQ = BP_T dr = Br(L\sin\varphi - D\cos\varphi)dr \qquad (7)$$

Where B is the number of blades, dr is the length of a strip along the blade.

Combining equation(6) and (4) we can get

$$a = \frac{1}{\dfrac{4\sin^2\varphi}{\sigma C_n}+1} \qquad (8)$$

Combining equation(7) and (5) we can get

$$a' = \frac{1}{\dfrac{4\sin\varphi\cos\varphi}{\sigma C_t}+1} \qquad (9)$$

12

A typical solution procedure is: (1) Guess starting values for a and a'; (2) Calculated φ and the corresponding α, C_l and C_d; (3) Update a and a'; (4) Check for convergence with a given tolerance, and if not, repeat the procedures.

Additionally, there are two corrections applied, which are the Prandtl correction and Glauert correction. The air tends to flow around the tip of the blade from the lower to upper side of the lifting surface. Therefore, the tip of the blade produces less aerodynamic force. This reduction of forces due to finite blade length is accounted by multiplying the Prandtl correction factor F

$$F = \frac{2}{\pi}\cos^{-1}\left[\exp\left(-\frac{B(1-r/R)}{2r\sin\varphi/R}\right)\right] \tag{10}$$

The wind velocity in the far field wake would be negative, and because of this effect, BEM theory is not valid for induction factors greater a than 0.5. The Glauert correction is used for the cases with large induction factors. For $a>0.4$, the empirical thrust curve recommended by Burton et al [10] can be written as

$$a = \frac{(C_T/F - C_{T1})}{C_{T2} - C_{T1}}(a_2 - a_1) + a_1 \tag{11}$$

where $a_2 = 1.0$, $C_{T2} = 1.82$, $a_1 = 1.0 - 0.5\sqrt{C_{T2}}$, $C_{T1} = 4a_1(1-a_1)$, and F is the Prandtl factor.

2.1.3 Structure dynamics

In the structural model, the blades and tower is considered to be flexible cantilevered beams, which are fixed at one end and free at the other end. They both have point masses attached at the free end, which are the nacelle for tower and the tip brakes for blade. In theory, such continues bodies possess an infinite number of DOFs. However, in practice, such bodies are modeled as a linear sum of known shapes of the dominant normal vibration modes. The deflection of a cantilever beam can be represented as a linear combination of the known shapes of the first several normal vibration modes. This technique reduces the number of DOFs from infinity to a finite number N and is known as the normal mode summation method. This method is used to represent the beam bending in two different directions. In order to give greater accuracy, more than one mode can be used. Specifically, the tower in two directions and blade deflection in flapwise direction is modeled by two modes. The in-plane deflection of the blade is modeled with only one mode since the flexibility in this direction is much lower.

The blades are treated as flexible beams fixed at the hub and free at the tip. Since the blade have structural pre-twist, the definition of the deflections in two directions will change along the twisted beam, which brings some complex. A method to make it easier is to define the total blade curvature as the combination of curvature in each direction, oriented by the structural pre-twist. This curvature is resolved into two directions, which are in-plane and out-of-plane. The two components are then

13

integrated twice to get the deflection shape. The local curvature in the flapwise direction and edgewise direction can be expressed as

$$\tilde{u}''(z,t) = q_1(t)f_1''(z) + q_2(t)f_2''(z) \tag{12}$$

$$\tilde{v}''(z,t) = q_3(t)g''(z) \tag{13}$$

where z is the coordinate along the blade, f_1 and f_2 are the first and second flapwise mode shapes for the non-pre-twisted blade, g is the edgewise mode shape for the non pre-twisted blade, q_1, q_2 and q_3 are the their associated generalized coordinates.

If the local pre-twist angle is $\theta_0(z)$ in element local coordinate, then the local coordinate system can be transformed back to the system fixed at the blade root. The out-of-plane curvature can be written as

$$u''(z,t) = \cos\theta_0 \left\{ q_1(t)f_1''(z) + q_2(t)f_2''(z) \right\} - \sin\theta_0 \left\{ q_3(t)g''(z) \right\} \tag{14}$$

And the in-plane curvature can be expressed as

$$v''(z,t) = \sin\theta_0 \left\{ q_1(t)f_1''(z) + q_2(t)f_2''(z) \right\} + \cos\theta_0 \left\{ q_3(t)g''(z) \right\} \tag{15}$$

These two curvatures can also be represented by twisted shape functions as follows:

$$u'' = q_1\phi_1'' + q_2\phi_2'' + q_3\phi_3''$$
$$v'' = q_1\psi_1'' + q_2\psi_2'' + q_3\psi_3'' \tag{16}$$

where $\phi_1'' = \cos\theta_0 f_1''(z)$, $\phi_2'' = \cos\theta_0 f_2''(z)$, $\phi_3'' = -\sin\theta_0 g''(z)$, $\psi_1'' = \sin\theta_0 f_1''(z)$, $\psi_2'' = \sin\theta_0 f_2''(z)$ and $\psi_3'' = \cos\theta_0 g''(z)$. These functions can be integrated twice with respect to z, to get the overall mode shapes with twist for in-plane and out-of-plane bending. The deflection of the blade in two directions can then be expressed as equation(17). It should be noted that since the local blade segment is vibrating, its position is expressed in the root-fixed coordinates

$$u(z,t) = \sum_{i=1}^{3} q_i(t)\phi_i(z)$$
$$v(z,t) = \sum_{i=1}^{3} q_i(t)\psi_i(z), \quad i = 1,2,3 \tag{17}$$

The generalized mass and stiffness m_{ij} and k_{ij} are defined in terms of the kinetic energy T, and potential energy V, as expressed in equation(18) and(19). The energies T and V can also be expressed by

14

integrated formula containing $u(z,t)$ and $v(z,t)$. By relating (17), (18) and (19), m_{ij} and k_{ij} can be easily determined from $\phi_i(z)$ and $\psi_i(z)$.

$$T = \frac{1}{2}\sum_{i=1}^{N}\sum_{j=1}^{N}m_{ij}\dot{q}_i(t)\dot{q}_j(t) \tag{18}$$

$$V = \frac{1}{2}\sum_{i=1}^{N}\sum_{j=1}^{N}k_{ij}q_i(t)q_j(t) \tag{19}$$

Similar modal analysis method is applied for tower. It is easier due to symmetric vibration in two directions and without structure twist. Therefore it will not be explained in detail here.

There are several coordinate systems for different flexible and rigid bodies. Once the motions are defined in their local reference frames, the kinematics of the system can be expressed. Vectors from any of the above coordinate systems can be used, since they are easily transformed to a common coordinate system. The accelerations of points in the system can be expressed using velocities and angular velocities. Velocities and angular velocities can be determined according to the relationship of different reference frames.

The equations of motion according to Newton's Second Law can be assembled with expressions for the accelerations and external forces determined.

$$F_r + F_r^* = 0, \quad F_r = \sum_i F_i, \quad F_r^* = \sum_i (-m_i a_i) \tag{20}$$

Where F_r are generalized active forces and F_r^* are generalized inertia forces, respectively. The generalized active forces include all external forces acting on the body

$$F_r\big|_{Total} = F_r\big|_{Aero} + F_r\big|_{Gravity} + F_r\big|_{Drive} + F_r\big|_{Elastic} \tag{21}$$

These generalized active forces are aerodynamic forces, gravity, drive train forces, and elastic restoring forces of the flexible bodies. The aerodynamic forces have been introduced in section 2.2.1. During start-up and stopping operations, significant drive train loads can occur. During start-up, the rotor starts as a result of the generator acting as a motor. At that time the drive shaft acts as a torsional spring and may cause large torsional oscillations. The elastic restoring forces of the flexible bodies are induced by the bending of elastic bodies, which produces forces that restore the bodies to their non-deflected position. The generalized active forces based on these restoring forces can be computed from the potential energy V of a bent beam.

The generalized inertia forces can be written as

$$F_r^*\big|_{Total} = F_r^*\big|_{Tower} + F_r^*\big|_{Nacelle} + F_r^*\big|_{Hub} + F_r^*\big|_{Blades} \tag{22}$$

The generalized inertia forces consist of all effects of linearly and angularly accelerating mass. All bodies that have mass, including the tower, nacelle, hub, and blades makes a contribution to the generalized inertia forces.

2.2 Linearization theory

The model linearization process in FAST consists of two steps. The first step is to compute a periodic steady state operating point condition. The second step is to linearize the FAST model about this steady state operating point to form state matrices. It should be noted that the state matrices are related to rotor azimuth angle, which means there are state matrices at each azimuth angle. Therefore the state matrices can be azimuth-averaged for non periodic development. During the second step, the control system, which includes pitch controller and variable generator speed controller, is neglected.

2.2.1 Periodic Operating-Point (OP) determination

Operation point (or fixed-point) determination is the first step in the linearization process. An operating point is a set of values of the system that characterize a steady condition of the wind turbine, such as DOF displacements, velocities, accelerations, wind inputs, and control inputs. For a wind turbine operating in steady winds, this operating point is periodic which means the OP. values depend on the rotor azimuth orientation. This periodicity is induced by aerodynamic loads, which depend on the rotor azimuth position in the presence of prescribed shaft tilt, tower shadow, or wind shear. Furthermore, gravitational loads also drive the periodic behavior. For a nonlinear system, a linear representation is only valid for small perturbations from an OP. This means the linearized model is only accurate for the inputs and DOFs values that are close to the operating point values. Therefore, it is important to determine an accurate operating point. The procedure to determine periodic steady state computation is shown in Figure 8.
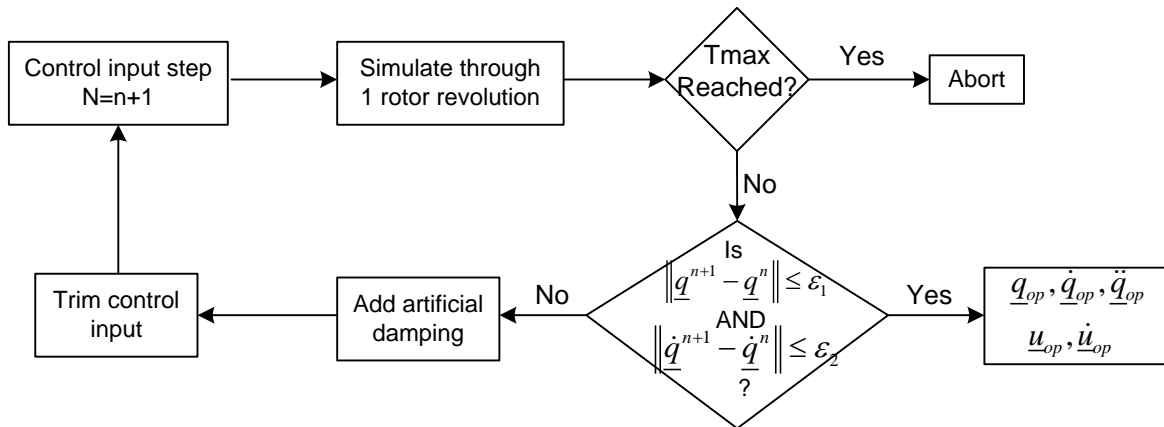
Figure 8 Periodic Steady State Computation (Jonkman, J. M, et al. 2005)

16

During the process of finding a steady state solution, FAST integrates the nonlinear equations of motion in time until the solution converges. At the first time step the control input is the initial value set by the users. Then nonlinear simulation though one iteration, or one period of the rotor revolution, is conducted. The convergence is checked unless the maximum time is reached. Convergence is defined as a L2-norm of the differences between the states computed at the beginning and at the end of the iteration. The preset convergence tolerances ε_1 and ε_2 are chosen to be very small. A L2-norm is computed for the angular displacement vector $\underline{q}$ and angular velocity vector $\underline{\dot{q}}$. If the computed L2-norm is larger than the convergence tolerance, an artificial damping will be added and the control inputs, such as blade pitch or generator torque, are also changed. The simulation continues until the solution is considered to have converged. Otherwise, the iteration stops if the solution has not converged by the time Tmax is reached. One thing should be noted is that the control input to be trimmed depends on the operation region of wind turbine. Generator torque will be trim in region 2, while blade pitch will be trimmed in region 3. Once the OP is determined the model linearization will be conducted.

2.2.2 Model linearization

In the model linearization step, FAST numerically linearizes the nonlinear aero-elastic model at the operating point. Since the OP of each azimuth angle is different, the OP is a function of rotor azimuth angle. Therefore at each azimuth angle there is a set of state matrix.

The fully nonlinear aeroelastic equations of motion can be expressed as:

$$M\left(\underline{q},\underline{u},t\right)+f\left(\underline{q},\underline{\dot{q}},\underline{u},\underline{u}_d,t\right)=\underline{0} \tag{23}$$

where M is the mass matrix, f is the force function vector, $\underline{q}$ is the vector of displacements (periodic), $\underline{\dot{q}}$ and $\underline{\ddot{q}}$ are velocities and accelerations respectively (periodic), $\underline{u}$ is the control inputs vector, $\underline{u}_d$ is the wind input perturbing vector, and t is the time.

Then this nonlinear aeroelastic model will be numerically linearized at the O.P. The motions and inputs and be expressed as the summation of O.P. value and the disturbance values expressed as:

$$\begin{aligned}
\underline{q}=\underline{q}_{op}+\Delta q, \quad \underline{\dot{q}}=\underline{\dot{q}}_{op}+\Delta\dot{q}, \quad \underline{\ddot{q}}=\underline{\ddot{q}}_{op}+\Delta\ddot{q}, \\
\underline{u}=\underline{u}_{op}+\Delta u, \quad \underline{u}_d=\underline{u}_{dop}+\Delta u_d
\end{aligned} \tag{24}$$

The second-order linearized system can be obtained by substituting equation(24) into the equations of motion expressed in(23), and expanding as a Taylor series approximation.

$$M\Delta\underline{\ddot{q}}+C\Delta\underline{\dot{q}}+K\Delta\underline{q}=F\Delta\underline{u}+F_d\Delta\underline{u}_d \tag{25}$$

where M is the mass matrix, C is the damping matrix, K is the stiffness matrix, F is the control input matrix and F_d is the wind input disturbance matrix. The matrixes are determined be first Taylor expansion at the operation point

$$M = M\big|_{op}, \quad C = \frac{\partial f}{\partial \underline{\dot{q}}}\bigg|_{op}, \quad K = \left[\frac{\partial M}{\partial \underline{q}}\underline{\ddot{q}} + \frac{\partial f}{\partial \underline{q}}\right]\bigg|_{op}$$

$$F = -\left[\frac{\partial M}{\partial \underline{u}}\underline{\ddot{q}} + \frac{\partial f}{\partial \underline{u}}\right]\bigg|_{op}, \quad F = -\frac{\partial f}{\partial \underline{u}_d}\bigg|_{op}$$

(26)

The partial derivatives in equation(26) are computed using the central difference perturbation numerical technique within FAST. For example the partial derivatives of mass matrix to control input can be expressed as

$$\frac{\partial M}{\partial \underline{u}}\bigg|_{op} = \frac{M\left(\underline{u}\big|_{op} + \Delta\underline{u}, \ \underline{q}\big|_{op}, \ t\big|_{op}\right) - M\left(\underline{u}\big|_{op} - \Delta\underline{u}, \ \underline{q}\big|_{op}, \ t\big|_{op}\right)}{2\Delta\underline{u}}$$

(27)

Besides the linearized equations of motion, a linearized system associated with output measurements y can be developed. The measurement can be quantities related to generator and rotor, blade pitch angle, structure motion and moment, etc. The second order linearized representation of the output system can be expressed as:

$$\underline{y} = VelC \cdot \Delta\underline{\dot{q}} + Dsp \quad C\Delta\underline{q} + D \cdot \Delta\underline{u} + D_d \cdot \Delta\underline{u}_d$$

(28)

where $VelC$ is the velocity output matrix, $DspC$ is the displacement output matrix, D is the control input transmission matrix, and D_d is the wind input disturbance transmission matrix.

The second order motion and measurement representations can be rewrite for a first order equation with the DOF displacement, velocity and acceleration disturbing vectors replaced by the first-order state vector $\underline{x}$ and the state derivative vector $\underline{\dot{x}}$.

$$\underline{x} = \begin{bmatrix} \Delta\underline{q} \\ \Delta\underline{\dot{q}} \end{bmatrix}, \quad \underline{\dot{x}} = \begin{bmatrix} \Delta\underline{\dot{q}} \\ \Delta\underline{\ddot{q}} \end{bmatrix}$$

(29)

Therefore the first order expression of the system is

$$\underline{\dot{x}} = A\underline{x} + B\Delta\underline{u} + B_d\Delta\underline{u}_d$$
$$\underline{y} = C\underline{x} + D\Delta\underline{u} + D_d\Delta\underline{u}_d$$

(30)

18

where A is the state matrix, B is the control input matrix, B_d is the wind input disturbance matrix, and C is the output state matrix. All matrixes can be derived from their second-order counterparts as follows:

$$A = \begin{bmatrix} 0 & I \\ -M^{-1}K & -M^{-1}C \end{bmatrix}, \quad B = \begin{bmatrix} 0 \\ M^{-1}F \end{bmatrix}$$

$$B_d = \begin{bmatrix} 0 \\ M^{-1}F_d \end{bmatrix}, \quad C = \begin{bmatrix} DspC & VelC \end{bmatrix} \tag{31}$$

The control input transmission matrix D and wind input disturbance matrix D_d of first order representations are identical with second-order representations of the linearized system.

The wind turbine system is an aeroelastic system with several modules which are summarized in Table 4. The relationship of the inputs and outputs of these modules is illustrated in Figure 9. In the following, the modules, states, inputs, and outputs will be introduced one by one. There are three modules taking parts in the linearization, which are Inflow Wind (IfW), Aerodynamics (AD) and Structure Dynamics (ED). The purpose of IfW is to generate wind field according to the input disturbance wind speed, power-law shear exponent and wind direction. There are no DOFs included in this module, therefore also no states included. The next module is AD, which is applied to determine the aerodynamic force. Wind velocity, which is the output of IfW, is one of the inputs of AD. Blade pitch is another input, which can be used to calculate the angle of attack to get lift and drag coefficient. It should be noted that in the integrated nonlinear model, blade pitch is determined by the wind turbine control system. However in linear model, the blade pitch comes from the measured inputs. Due to the coupling between aerodynamic and structure dynamic, the calculation of aerodynamic force should consider the motions of structures. Therefore, the displacements and velocities of blades and tower, which are outputs of ED, are inputs for AD. There are no DOFs included in this AD module, therefore no states as well. The next module is ED with the purpose of determining the structure motions and generator speed. Besides the aerodynamic force from AD, the inputs of ED should include generator torque as an external force. With all the forces and structure properties, the flexible and rigid body motions can be determined as outputs.

Overall, if we make the IfW, AD and ED modules as an integral closed system, the inputs are wind field properties, blade pitch angle and generator torque, and the outputs are wind velocity, aerodynamic forces and flexible and rigid body motions. The states only come from ED, which are the modal displacements and modal velocities for flexible body and rigid body displacements and velocities.
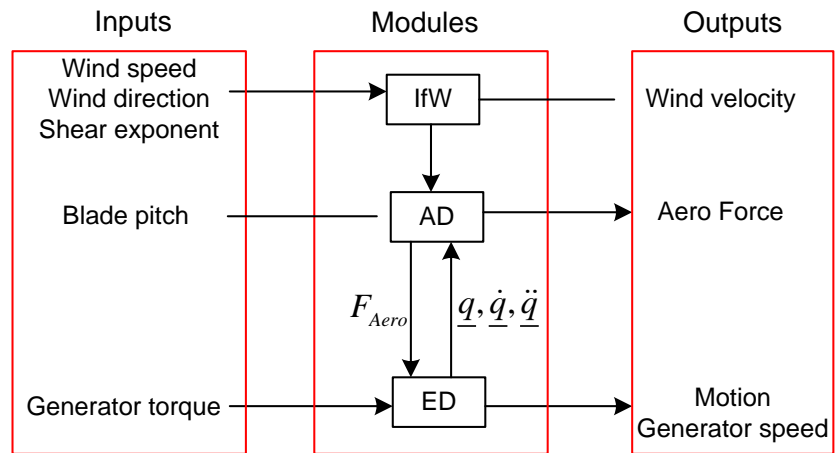
Figure 9 Relationship of modules and the inputs and outputs

Table 4 Module states, inputs, and outputs in the linearization process

Module	States	Inputs	Outputs
Inflow Wind (IfW)	None	• Disturbance of wind speed, power-law shear exponent, and wind direction	• Undisturbed wind velocity
Aerodynamics (AD)	None	• Displacements • Velocities • Blade pitch angle	• Aerodynamic loads
Structure dynamics (ED)	• Displacements • Velocities	• Aerodynamic loads • Generator torque	• Displacements • Velocities • Accelerations • Reaction loads • Generator speed

20

2.3 Linearization of wind turbine model

Although FAST can output the state space matrix conveniently, it is very helpful to introduce the detailed linearization theories for aerodynamics and structure dynamics, in order to have a better understanding of the physics.

2.3.1 Aerodynamics linearization

Wind turbine extract kinetic energy of wind to make the rotor rotate. The available power of the wind is determined by the circular cross section, which has the same area as the rotor disc. The power coefficient C_p should be considered, since only a part of the available power P_w can be converted to rotor power P_r, which has nonlinear expression as

$$P_r = P_w C_p = \frac{1}{2} \dot{m} v^2 C_p = \frac{1}{2} \rho \pi R^2 v^3 C_p \tag{32}$$

where $\dot{m}$ is the mass flow of the wind, v is the wind speed, R is the radius of the rotor disc and ρ is the air density.

The aerodynamic forces acting on the rotor consists of two parts: torque and thrust. The nonlinear aerodynamic torque and thrust can be expressed as

$$T_{tq} = \frac{P_r}{\Omega_r} = \frac{\frac{1}{2} \rho \pi R^2 v^3 C_p \left(\frac{v}{\Omega_r R}, \beta \right)}{\Omega_r} \tag{33}$$

$$T_{thr} = \frac{1}{2} \rho \pi R^2 v^2 C_T \left(\frac{v}{\Omega_r R}, \beta \right) \tag{34}$$

The power coefficient C_p and thrust coefficient C_T are functions of blade pitch angle β, the rotor rotational speed Ω_r and the wind speed v. The power and thrust coefficient and be calculated by BEM theory as shown in section 2.1.2. In the following, we will conduct the linearization of torque, thrust and power.

For the aerodynamic torque force T_{tq} it is a continuous function of wind speed v, rotor-speed Ω_r, and pitch angle β. It can be expanded as a Taylor series in terms of v, Ω_r and β:

$$T_{tq} = T_{tq}\left(v_0, \Omega_{r0}, \beta_0\right) + \left.\frac{\partial T_{tq}}{\partial v}\right|_{v_0} \delta v + \left.\frac{\partial T_{tq}}{\partial \Omega_r}\right|_{\Omega_{r0}} \delta\Omega_r + \left.\frac{\partial T_{tq}}{\partial \beta}\right|_{\beta_0} \delta\beta + O^2\left(v, \Omega_r, \beta\right) + \dots \tag{35}$$

where $v_0, \Omega_{r0}, \beta_0$ are the nominal wind speed, rotor speed and blade pitch angle at the operation point. δv, $\delta\Omega_r$ and $\delta\beta$ are perturbations (e.g. $\delta\Omega_r = \Omega_r - \Omega_{r0}$). The left terms in the equation stands for the second and higher order terms, which will be neglected in the linearization. The only control input to this model will be rotor collective pitch β, which means that the pitch angle of each blade is identical.

The perturbation of aerodynamic force can be expressed as

$$\delta T_{tq} = T_{tq}\left(v,\Omega_r,\beta\right) - T_{tq}\left(v_0,\Omega_{r0},\beta_0\right)$$
$$= \left.\frac{\partial T_{tq}}{\partial v}\right|_{v_0} \delta v + \left.\frac{\partial T_{tq}}{\partial \Omega_r}\right|_{\Omega_{r0}} \delta\Omega_r + \left.\frac{\partial T_{tq}}{\partial \beta}\right|_{\beta_0} \delta\beta = \alpha\delta v + \gamma\delta\Omega_r + \zeta\delta\beta \tag{36}$$

The individual partial derivatives of equation(36) can be derived as

$$\left.\frac{\partial T_{tq}}{\partial v}\right|_{v_0} = \frac{1}{\Omega_{r0}}\left.\frac{\partial P_r}{\partial v}\right|_{v_0}$$

$$\left.\frac{\partial T_{tq}}{\partial \Omega_r}\right|_{\Omega_{r0}} = \frac{1}{\Omega_{r0}}\left.\frac{\partial P_r}{\partial \Omega_r}\right|_{\Omega_{r0}} - \frac{P_{r0}}{\Omega_{r0}^2} \tag{37}$$

$$\left.\frac{\partial T_{tq}}{\partial \beta}\right|_{\beta_0} = \frac{1}{\Omega_{r0}}\left.\frac{\partial P_r}{\partial \beta}\right|_{\beta_0}$$

Similarly, the partial derivatives of P_r in equation(37) can be expressed as

$$\left.\frac{\partial P_r}{\partial v}\right|_{v_0} = \frac{1}{2}\rho\pi R^2 3v_0^2 C_{P0} + v_0^3 \left.\frac{\partial C_P}{\partial \lambda}\right|_{\lambda_0}$$

$$\left.\frac{\partial P_r}{\partial \Omega_r}\right|_{\Omega_{r0}} = \frac{1}{2}\rho\pi R^2 v_0^3 \left.\frac{\partial C_P}{\partial \lambda}\right|_{\lambda_0} \cdot \left.\frac{\partial \lambda}{\partial \Omega_r}\right|_{\Omega_{r0}} \tag{38}$$

$$\left.\frac{\partial P_r}{\partial \beta}\right|_{\beta_0} = \frac{1}{2}\rho\pi R^2 v_0^3 \left.\frac{\partial C_P}{\partial \beta}\right|_{\beta_0}$$

where λ is the tip speed ratio, which can be expressed as $\lambda = \dfrac{v}{\Omega_r R}$.

For the aerodynamic thrust, it can be linearized with similar methods as torque.

$$\delta T_{thr} = T_{thr}\left(v,\Omega_r,\beta\right) - T_{thr}\left(v_0,\Omega_{r0},\beta_0\right) = \left.\frac{\partial T_{thr}}{\partial v}\right|_{v_0}\delta v + \left.\frac{\partial T_{thr}}{\partial \Omega_r}\right|_{\Omega_{r0}}\delta\Omega_r + \left.\frac{\partial T_{thr}}{\partial \beta}\right|_{\beta_0}\delta\beta \tag{39}$$

During the above linearization process, there are aerodynamic phenomena omitted. As mentioned earlier, the aerodynamic coefficients are only valid under the assumption of a steady-state mass flow of the air.

In reality the mass flow does not settle to a new equilibrium infinitely fast during a transition, and thus contributions from the dynamics of the fluid (air) should be added to the coefficients. These contributions are significant and can lead to an aerodynamic damping of the interaction between the wind and the rotor. If the blades are pitching fast or even oscillating, the actual coefficients might differ significantly from the quasi-stationary coefficients. Hence, care should be taken not to induce such a situation during control of the wind turbine.

Moreover, the rotor blades are bended backwards in steady state operation. This means the blades are not rotational symmetric with regards to their masses and when pitched this gives rise to oscillations in both blades and tower. This oscillating behavior also disrupts the quasi-stationary assumptions of the power and thrust coefficients.

And finally as mentioned the wind section, the wind shear is also omitted from the model2.4.2 Structural Dynamics Linearization

2.3.2 Structural dynamics linearization

2.3.2.1 Electrical generator linearization

The mechanical power of the rotor side will be transferred to electrical generator via the drive train shaft. The generator imposes an electrical counter torque on the drive shaft and thereby extracts electrical power. However, due to less than perfect efficiency, such as losses in drivetrain bearings, gearbox etc, the generator is not able to convert all of the mechanical power to electrical power. The electrical power can be expressed as

$$P_e = \eta P_m = \eta \Omega_g Q_g \tag{40}$$

For a linear generator, it can be linearized as

$$P_e \cong P_{e0} + \frac{\partial P_e}{\partial \Omega_g}\bigg|_{\Omega_{g0}} \delta\Omega_g + \frac{\partial P_e}{\partial Q_g}\bigg|_{Q_{g0}} \delta Q_g \tag{41}$$

2.3.2.2 Flexible drivetrain shaft linearization

If the generator and rotor speed states and drive-train torsion state are considered, we have a model with three states, which are rotor speed Ω_r, generator Ω_g and the azimuth angle difference between rotor and generator $\phi\Delta$. In this case the rotor, generator, drivetrain system can be modeled as a 2-mass, 1-spring, and 1-damper system. Rotor and generator can be modeled as two mass. However the drivetrain will be modeled as a spring and damper.

$$\dot{\phi}_r = \Omega_r, \quad \dot{\phi}_g = \Omega_g, \quad \phi\Delta = \phi_r - \frac{\phi_g}{N_g} \tag{42}$$

The equation for rotor and generator can be expressed as equation (43)

$$I_{rot}\ddot{\phi}_r = T_{tq} - T_{shaft}$$
$$I_{gen}\delta\ddot{\phi}_g = T_{shaft} - T_{gen} \tag{43}$$

Here, T_{tq} is the rotor aerodynamic torque, and T_{shaft} is the reaction torque from the shaft. I_{rot} and I_{gen} are the rotor and generator rotational inertia respectively. The shaft force can be expressed as a combination of stiffness and damping term.

$$T_{shaft} = K_d\phi\Delta + C_d\left(\Omega_r - \frac{\Omega_g}{N_g}\right) \tag{44}$$

Let's assume that we have constant generator torque in region 3, which means that

$$\delta T_{gen} = 0 \tag{45}$$

Substitute (44) into (43), it can be derived as

$$I_{rot}\ddot{\phi}_r = T_{tq} - T_{shaft} = T_{tq}\left(v_0, \Omega_{r0}, \beta_0\right) + \delta T_{tq} - T_{shaft_0} - \delta T_{shaft} \tag{46}$$

Where T_{shaft_0} is the shaft torque at equilibrium. Since at equilibrium, rotor acceleration is zero, and perturbations in aerodynamic torque and shaft torque are zero. Thus

$$I_{rot}\delta\ddot{\phi}_r = \delta T_{tq} - \delta T_{shaft} \tag{47}$$

Substituting the expression of disturbance torque and shaft force, we can derive

$$I_{rot}\delta\ddot{\phi}_r = \alpha\delta v + \gamma\delta\Omega_r + \zeta\delta\beta - K_d\delta\phi\Delta - C_d\left(\delta\Omega_r - \frac{\delta\Omega_g}{N_g}\right) \tag{48}$$

Again, at equilibrium, the generator acceleration is zero. We can use a similar argument as before to show that at equilibrium, the shaft torque and generator torque are equal. Thus

$$I_{gen}\delta\ddot{\phi}_g = \delta T_{shaft} - \delta T_{gen} = K_d\delta\phi\Delta - C_d\left(\delta\Omega_r - \frac{\delta\Omega_g}{N_g}\right) \tag{49}$$

There are two inputs for the system, disturbing wind speed δv and disturbing blade pitch angle $\delta\beta$. There are three states in the system. The state space model can be written as

$$
\begin{bmatrix} \delta\dot{\Omega}_r \\ \delta\dot{\Omega}_g \\ \delta\dot{\phi}\Delta \end{bmatrix} = \begin{bmatrix} \dfrac{\gamma - C_d}{I_{rot}} & \dfrac{C_d}{I_{rot}N_g} & -\dfrac{K_d}{I_{rot}} \\[3mm] \dfrac{C_d}{I_{gen}N_g} & \dfrac{-C_d}{I_{gen}N_g^2} & \dfrac{K_d}{I_{gen}N_g} \\[3mm] 1 & -\dfrac{1}{N_g} & 0 \end{bmatrix} \begin{bmatrix} \delta\Omega_r \\ \delta\Omega_g \\ \delta\phi\Delta \end{bmatrix} + \begin{bmatrix} \dfrac{\zeta}{I_{rot}} \\[2mm] 0 \\ 0 \end{bmatrix} \delta\beta + \begin{bmatrix} \dfrac{\alpha}{I_{rot}} \\[2mm] 0 \\ 0 \end{bmatrix} \delta v \tag{50}
$$

2.3.2.3 Flexible tower linearization

The thrust exerted by the wind on wind turbine makes the flexible tower to bend fore-aft and side-side. In this example only the back and forth motion of the nacelle is modeled in simplification. The displacement of the nacelle from its original position is denoted as q_t, where the displacement of the nacelle in steady state is

$$
q_{t0} = F_{thr} / K_t \tag{51}
$$

The equation for the tower first fore-aft mode motion can be written:

$$
M_t \delta\ddot{q}_t + C_t \delta\dot{q}_t a + K_t \delta q_t = \delta F_{th} \tag{52}
$$

Since we did not include the blade displacement modes, there is no coupling items equation (52). If the blade motion is considered there is coupling at mass term, damping term and stiffness term. The state space model can be written as:

$$
\begin{bmatrix} \delta\dot{q}_t \\ \delta\ddot{q}_t \end{bmatrix} = \begin{bmatrix} 0 & 1 \\[2mm] -\dfrac{K_t}{M_t} & -\dfrac{D_t}{M_t} \end{bmatrix} \begin{bmatrix} \delta q_t \\ \delta\dot{q}_t \end{bmatrix} + \begin{bmatrix} 0 \\[2mm] \dfrac{1}{M_t} \end{bmatrix} \delta F_{thr} \tag{53}
$$

For the disturbance of thrust we can substitute the linearization expression equation(39) to get the state space model.

Chapter 3 Definition of 5 MW Wind Turbine

In the thesis the NREL 5 MW wind turbine is studied. It is a baseline wind turbine developed by the National Renewable Energy Laboratory (NREL). It is widely used for control system design and support structure design. What's more it is validated by many researchers applying different wind turbine analysis codes and softwares.

3.1 General aerodynamic and structure properties

The general aerodynamic and structure properties are listed in Table 5. The 3 blade upwind wind turbine is pitch regulated with rated wind speed 11.4 m/s. The rated power is 5 MW.

Table 5 General Properties of the NREL 5-MW Baseline Wind Turbine

Rating	5 MW
Rotor Orientation, Configuration	Upwind, 3 Blades
Control	Variable Speed, Collective Pitch
Drivetrain	High Speed, Multiple-Stage Gearbox
Rotor Diameter	126 m
Hub Height	90 m
Cut-In, Rated, Cut-Out Wind Speed	3 m/s, 11.4 m/s, 25 m/s
Cut-In, Rated Rotor Speed	6.9 rpm, 12.1 rpm
Rotor Mass	110,000 kg
Nacelle Mass	240,000 kg
Hub Mass	56,780 kg
Blade Mass	17613kg

3.2 Control system

For the NREL 5-MW wind turbine, a conventional variable-speed, variable blade pitch to feather configuration is chosen. In such wind turbines, the conventional approach for controlling power-production operation relies on the design of two basic control systems: a generator torque controller and a full span rotor collective blade pitch controller. These two control systems are designed to work independently, for the most part. At the below-rated wind speed range the generator torque controller works. At the above-rated wind-speed range, the blade pitch controller works. The goal of the generator torque controller is to maximize power production below the rated operation point. The goal of the blade

pitch controller is to regulate generator speed above the rated operation point, since there are limitations for generator speed due to noisy.
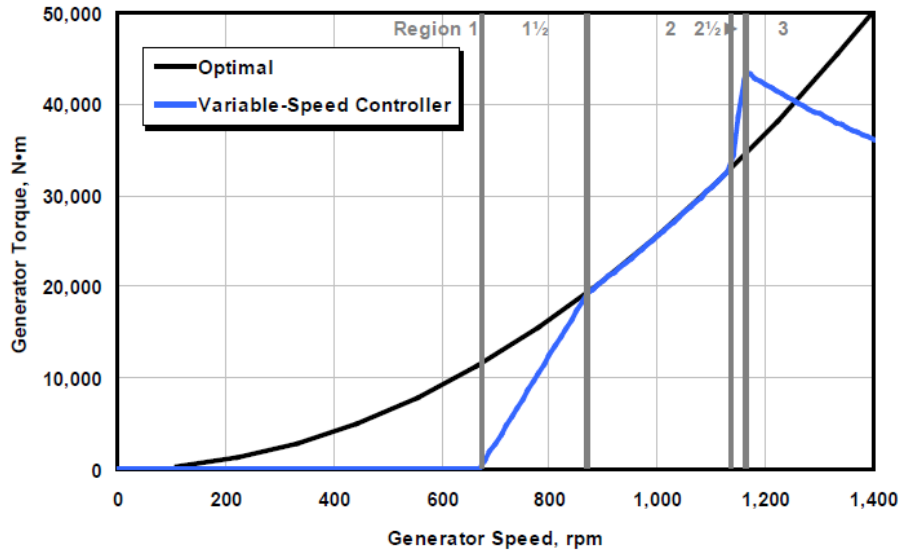
Figure 10 Torque versus speed response of the variable speed controller (J. Jonkman 2009)

Baseline Generator-Torque Controller

The generator torque is computed as a tabulated function of the filtered generator speed, incorporating five control regions: 1, 1½, 2, 2½, and 3. Region 1 is a control region before cut-in wind speed, where the generator torque is zero and no power is extracted from the wind; instead, the wind is used to accelerate the rotor for start-up. Region 2 is a control region for optimizing power capture. Here, the generator torque is proportional to the square of the filtered generator speed to maintain a constant (optimal) tip-speed ratio. In Region 3, the generator power is held constant so that the generator torque is inversely proportional to the filtered generator speed. Region 1½, a start-up region, is a linear transition between Regions 1 and 2. This region is used to place a lower limit on the generator speed to limit the wind turbine's operational speed range. Region 2½ is a linear transition between Regions 2 and 3 with a torque slope corresponding to the slope of an induction machine. Region 2½ is typically needed (as is the case for my 5-MW turbine) to limit tip speed (and hence noise emissions) at rated power.

Baseline Blade Pitch Controller

The baseline blade pitch controller works in Region 3, which is computed using gain-scheduled proportional-integral (PI) control. The proportional coefficient is proportional to the speed error between the filtered generator speed and the rated generator speed. The integral coefficient is proportional to the integral of speed error between the filtered generator speed and the rate generator speed. We designed the blade-pitch control system using a 1 DOF model of the wind turbine. This DOF is the angular rotation of the shaft.

28

3.3 Definition of modeling errors

The linearization model is an approximate of nonlinear model. There can be many simplifications. There are two main simplifications. One is that linear model only includes partly DOFs. The other is linearization at one operation point. That means the total error includes both error due to not enough DOF and error due to linearization. Therefore it is valuable to investigate their influence to the modeling error.

Figure 11 illustrates the definition and relationship of different kind of errors. The total modeling error is the difference between nonlinear full DOF model and linear part DOF model. In order to investigate the two parts of error separately, the nonlinear model with part DOF is introduced. The error between nonlinear full DOF model and nonlinear part DOF model is the error due to lack of DOFs. While the error between linear part DOF model and nonlinear part DOF model is the error due to linearization process.
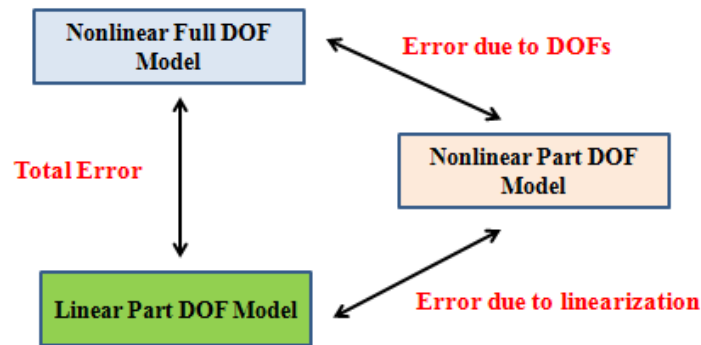
Figure 11 Definition and Relationship of Errors

The meaning of investigate errors are: The objective of an optimal system is to provide control capability with a minimum number of required measurements.

Chapter 4 Modeling Error Due to limited number of DOFs

In this chapter, the influence of DOFs will be analyzed with focus put on which DOFs are more important. Therefore, we can model the linear state space model with the most important DOFs involved and without losing much accuracy. The importance of a DOF depends on which variable we care most. For example, if we would like to study the blade properties, the DOFs related to blade modes would be important. While if we focus on the tower response, the importance of tower bending modes will increase. In addition, it may not be possible to obtain all the measurements due to the limitation of time and money. For example, the measurements of blade deflections can be obtained in some wind turbines, while for other wind turbines tower top bending moment can be acquired. In order to make the investigation to be widely applicable, different properties of wind turbine are studied. The variables are grouped into three categories. The first group includes properties related to wind turbine power production. The second group is related to blade properties, such as blade tip deflection and root bending moment. The third group is tower top bending moments. The detailed description is shown in Table 6. All the following study will analyze quantities listed below.

Table 6 Quantities related to ice-detection

		Unit	
Power production	Gen Power	kW	Generator power
	Gen Torque	kN	Generator torque
	Blade Pitch	deg	Blade collective pitch angle
	Rotor Speed	rpm	Rotor speed
Blade	OoPDefl1	m	Blade 1 tip out-of-plane deflection
	IpDefl1	m	Blade 1 tip in-plane deflection
	RootMxc1	kNm	Blade 1 root in-plane bending moment
	RootMyc1	kNm	Blade 1 root out-of-plane bending moment
	RootMzc1	kNm	Blade 1 root torsion moment
Tower	RotThrust	kN	Rotor thrust
	YawBrMxp	kNm	Tower top side-side bending moment
	YawBrMyp	kNm	Tower top fore-aft bending moment
	YawBrMzp	kNm	Tower top torsional moment

Six cases which include different DOFs are investigated and the results are compared with full DOFs nonlinear model. Table 7 lists the cases as well as the corresponding DOFs. For power production, the generator DOF is the most important, therefore it is included in all the cases. Case number 2 aims to investigate the influence of flexibility in the drivetrain on the wind turbine power production. The drivetrain DOF accounts for drivetrain flexibility associated with torsional motion between the generator and the hub/rotor. Cases 3 and 4 are designed to study the blade 1st flap wise and edge wise influence on power production and blade properties. Similarly, the aim of cases 5 and 6 is to have a better understanding of the influence of tower 1st fore-aft and side-side mode on power production and bending moment. Finally, the case where all 18 DOFs are active is a reference. This means it includes all the 2nd modes.

Table 7 Definition of Cases with different DOFs

Case	DOF_1	DOF_2	DOF_3	DOF_4	DOF_5	DOF_6	DOF_all
DOF	Variable generator speed	DOF_1+ Drivetrain rotation	DOF_2+ 1st Blade flap	DOF_3+ 1st Blade edge	DOF_4+ 1st Tower Fore-aft	DOF_5+ 1st Tower side-side	DOF_6+ Second order

In order to have a detail study about the influence of different DOFs, an above rated wind speed case is analyzed. Figure 12 displays the time series and spectrum of wind speed. The 10 minutes average wind speed is 18 m/s. The wind speed ranges from 14 m/s to 22 m/s, which are all above rated wind speed. For below-rated wind speed cases, they will be individually analyzed in Chapter 9.
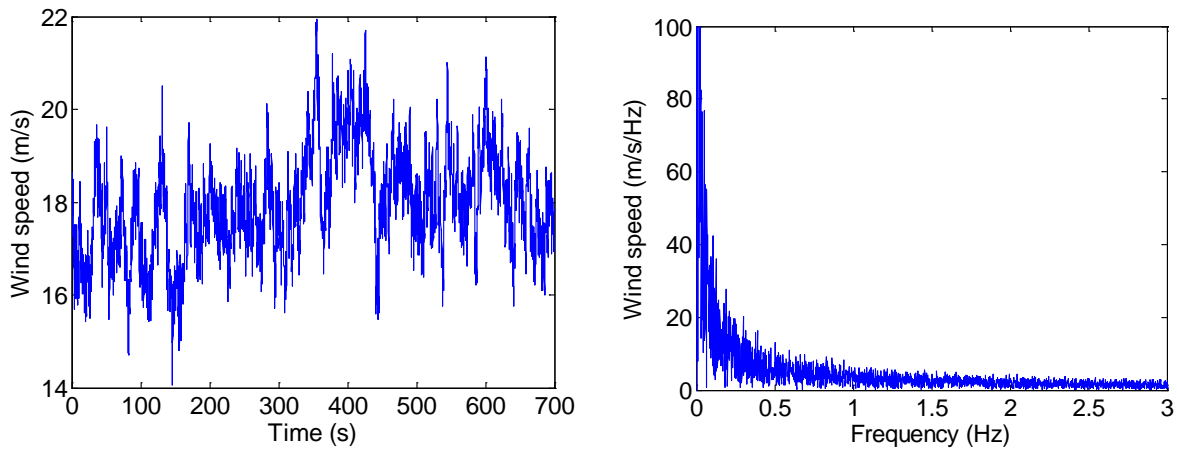
Figure 12 Wind speed time series (left) wind speed spectrum (right)

The following part of this section will analyze the L_2 error of varies quantities between nonlinear model with part DOFs and nonlinear model with full DOFs.

4.1 Natural frequency analysis

For the wind turbine dynamic system, natural frequency analysis is helpful to have a better understanding of the system and will be referred to in the later analysis of this Chapter. The natural frequencies and eigenmodes are determined under free vibration condition. For the undamped system the governing equation can be written as

$$M \Delta \ddot{\underline{q}} + K \Delta \underline{q} = 0 \qquad (54)$$

To find the natural frequencies of the system, the following determinant should be set to zero:

$$\det\left[-\omega^2 M + K \right] = 0 \qquad (55)$$

Undamped natural frequencies can be found by finding the eigenvalues of the matrix KM^{-1}. The normal modes of the free vibrations can be found by searching for the eigenvectors of the matrix KM^{-1}. For the wind turbine system in this study, the damping has little influence and can be neglected.

In order to carry out quantitative analysis, it is necessary to non-dimensionalize the mode shape magnitude of each DOF in order to ensure that the magnitude of the entire mode shape has the same units (here they are all in unit of radians). All rotational DOFs already have the units of radians, but the tower deflection, and blade deflection DOFs have the units of meters. They are rescaled with respect to individual characteristic length.

The calculated natural frequencies and corresponding non-dimensional mode shapes are shown in Table 8 and Table 9. The first column in the tables is the state quantities included, and the second column gives the scaling parameter for non-dimensionalization. The rest 16 columns in the tables are the natural frequency and modes. Since the different quantities in a mode are already non-dimensionalized, they can be directly compared. Roughly speaking, a larger non-dimensional magnitude of a state quantity in a certain mode may indicate that this degree of freedom is the main cause of that natural mode. These information can be significant helpful to analysis the behavior of a wind turbine model. For each natural mode in the tables, the state quantity with the largest non-dimensional magnitude is found and marked red.

Table 8 Natural frequency and mode shape magnitude

Mode No.		1	2	3	4	5	6	7	8
Natural Freq (Hz)		0.00061	0.32105	0.32447	0.66148	0.67045	0.69131	1.07760	1.09292
States	Scaling	Mag (rad)	Mag (rad)	Mag (rad)	Mag (rad)	Mag (rad)	Mag (rad)	Mag (rad)	Mag (rad)
1st tower F-A	0.0114	1.86E-08	1.13E-04	3.63E-03	5.55E-06	1.37E-05	5.35E-05	4.43E-06	1.90E-06
1st tower S-S	0.0114	7.09E-08	4.90E-03	9.20E-05	3.67E-06	3.56E-06	1.30E-06	3.89E-06	2.00E-05

2st tower F-A	0.0114	2.41E-11	1.81E-08	4.24E-08	1.92E-07	5.62E-07	2.17E-07	2.43E-07	1.68E-07
2st tower S-S	0.0114	2.54E-10	1.62E-06	3.35E-08	4.87E-08	1.67E-08	1.36E-08	2.54E-08	1.08E-07
Nacelle Yaw	1.0000	1.30E-07	4.06E-05	1.60E-06	6.31E-05	2.09E-05	1.62E-06	1.69E-05	2.24E-05
Gen DOF	1.0000	**8.96E-01**	**8.02E-03**	1.63E-05	8.92E-06	2.27E-05	1.43E-04	6.18E-06	3.24E-05
Drivetrain	1.0000	2.84E-07	1.87E-04	3.76E-07	8.85E-07	2.32E-06	1.56E-05	1.62E-06	8.77E-06
1st flap B1	0.0163	7.38E-07	1.90E-04	**3.87E-03**	1.13E-04	4.55E-04	**3.53E-03**	2.09E-05	6.34E-06
1st flap B2	0.0163	3.04E-03	9.08E-04	3.04E-03	1.21E-03	**3.53E-03**	9.00E-04	4.64E-05	1.97E-04
1st flap B3	0.0163	7.57E-04	5.94E-04	1.54E-04	**3.60E-03**	1.19E-03	9.23E-05	2.03E-04	5.92E-05
1st edge B1	0.0163	1.47E-07	1.21E-04	2.56E-04	6.10E-06	2.33E-05	1.67E-04	7.36E-07	4.02E-06
1st edge B2	0.0163	6.47E-03	1.49E-03	1.97E-04	2.22E-05	6.52E-05	1.08E-05	4.40E-04	**2.28E-03**
1st edge B3	0.0163	5.39E-05	4.19E-05	2.35E-04	6.48E-05	2.14E-05	2.25E-05	**2.31E-03**	4.30E-04
2st flap B1	0.0163	4.00E-08	2.04E-05	2.65E-04	6.27E-07	5.13E-06	1.34E-04	6.40E-06	2.58E-06
2st flap B2	0.0163	7.38E-04	1.69E-04	7.53E-05	3.14E-05	9.13E-05	4.02E-05	4.60E-05	2.34E-04
2st flap B3	0.0163	7.78E-05	2.59E-05	2.62E-05	8.81E-05	2.91E-05	4.16E-06	2.35E-04	4.55E-05

Table 9 Natural frequency and mode shape magnitude (continued)

Mode No.		9	10	11	12	13	14	15	16
Natural Freq (Hz)		1.69573	1.91310	1.92058	2.00750	2.91633	2.95361	3.92761	6.14209
States	Scaling	Mag (rad)	Mag (rad)	Mag (rad)	Mag (rad)	Mag (rad)	Mag (rad)	Mag (rad)	Mag (rad)
1st tower F-A	0.0114	8.65E-07	3.01E-06	1.24E-06	9.33E-06	2.16E-08	7.23E-08	7.54E-08	3.10E-09
1st tower S-S	0.0114	6.30E-06	3.60E-07	5.12E-07	3.98E-08	8.03E-08	1.86E-08	5.14E-07	3.48E-07
2st tower F-A	0.0114	1.25E-08	1.12E-06	4.60E-07	1.39E-07	4.33E-06	2.41E-07	4.39E-09	2.65E-10
2st tower S-S	0.0114	1.65E-06	4.08E-08	9.32E-08	3.17E-08	1.35E-07	6.08E-06	6.42E-07	5.09E-08
Nacelle Yaw	1.0000	1.27E-05	3.21E-05	7.52E-05	4.95E-07	1.41E-07	6.06E-06	1.11E-05	2.04E-04
Gen DOF	1.0000	**2.22E-03**	1.49E-06	1.84E-06	2.53E-05	4.68E-07	1.18E-05	1.90E-04	3.43E-06
Drivetrain	1.0000	1.46E-03	1.24E-06	1.55E-06	2.32E-05	6.70E-07	3.39E-05	**6.67E-04**	3.07E-05
1st flap B1	0.0163	2.65E-04	3.85E-06	1.60E-06	8.28E-05	3.70E-05	1.82E-04	1.41E-04	1.42E-06
1st flap B2	0.0163	3.35E-07	1.02E-04	4.24E-05	3.54E-06	5.94E-04	4.97E-05	1.86E-06	1.05E-05
1st flap B3	0.0163	2.36E-06	3.88E-05	9.17E-05	7.87E-07	2.17E-05	9.64E-05	2.83E-05	**3.45E-04**
1st edge B1	0.0163	1.49E-03	9.03E-06	5.28E-06	1.78E-04	3.41E-05	**8.31E-04**	6.37E-04	6.50E-06
1st edge B2	0.0163	4.92E-06	1.45E-04	6.53E-05	1.86E-05	1.60E-04	6.69E-05	1.21E-05	4.66E-05
1st edge B3	0.0163	1.12E-06	6.70E-05	1.47E-04	4.67E-06	9.08E-05	3.11E-05	6.30E-06	7.14E-05
2st flap B1	0.0163	1.29E-04	6.49E-05	2.93E-05	**1.26E-03**	7.18E-05	1.07E-04	7.58E-05	7.37E-07
2st flap B2	0.0163	1.22E-06	**1.22E-03**	4.97E-04	1.48E-04	**6.24E-04**	4.91E-05	1.51E-06	7.24E-06
2st flap B3	0.0163	4.35E-06	5.26E-04	**1.23E-03**	5.09E-06	1.90E-05	1.02E-04	2.21E-05	2.26E-04

4.2 Power production properties

Figure13 shows the time series and spectrum of power. It can be seen that the power is around 5000 kW, and there is no significant difference between the cases in both time series and spectrum. From the spectrum it can be seen that most of the responses are focused at wind frequency. The spectrum at low frequency is consistent with wind spectrum. That indicates the wind speed is the dominant factor for power production properties. For different case there is no difference on peak frequencies, however with difference on peak amplitude. The main difference lays in peak value at around 1.7 Hz. From modal analysis in Table 8 and Table 9, it can be seen that 1.7 Hz frequency is much influenced by generator DOF. With more DOFs included, such as blade and tower mode, the generator DOF response can be estimated more accurately. For other quantities related to power production, such as generator torque blade pitch and rotor speed, the trend of time series and spectrum is similar to that of generator power, Therefore, they are not be analysis in detail and the figures of time series and spectrum are in the appendix A1.
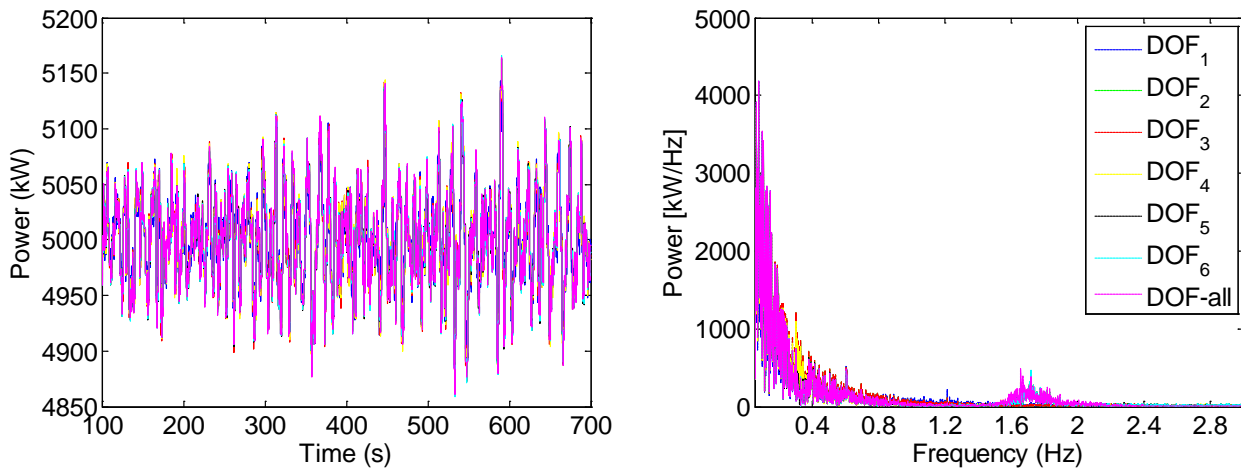
Figure13 Time series of power (left) Spectrum of power (right)

Table 10 displays the error of mean value for power. It should be noted that the error of mean value at different DOFs are all positive, which means cases with less DOFs have larger power production. That may due to no flexible structures influence the wind energy.

Table 10 Mean value error at different DOFs of power

	DOF_1	DOF_2	DOF_3	DOF_4	DOF_5	DOF_6
Error	0.0271	0.0286	0.0013	0.0030	0.0027	0.0011

In order to show the accuracy of models with different DOFs more clearly, we hereby calculate the L2 error for different DOF cases. Figure 14 displays the L_2 error of power, torque, pitch and rotor speed at different DOFs. The changing trend of these plots is similar, i.e. the errors decrease monotonously with

the increase of DOFs. It should be noted that the L_2 error is already smaller (smaller than 1%) even if only 1 DOF used. This means the oscillations of the blades and tower will not have much impact on the power production. However, for the purpose of ice-detection at the start stage, the model with only 1 DOF may be not accurate enough. Therefore, the following analysis will be focused on how the rest DOFs influence the results.

The L_2 error does not change from DOF 1 to DOF 2, which means the drivetrain flexible DOF does not influence the results, which can be neglected. If the blade 1st flapwise mode is opened from DOF 2 to DOF 3, the L_2 error will drop dramatically to half of the value. The reason may be that the flapwise tip motion range of blades is relatively large (about 3 meters). The large deflection changes the relative wind speed and converts the wind kinetic energy to structure elastic potential energy. As a result it is important to include blade flapwise motion to achieve more accurate power production property. The next case DOF 4 include blade edgewise motion, where the L_2 error decreases a little. That indicates blade edgewise DOF is less important than flapwise motion. One possible reason is that the stiffness of blade at edgewise direction is much larger than flapwise. Therefore, the motion range of edgewise is much smaller (about 1 meter). The influence of power production is also small. Another error drop occurs when tower fore-aft motion is include in DOF 5. That means tower fore-aft mode has much influence on the power production properties. The reason is similar to that of blade flapwise mode. Although the stiffness of the tower at all directions is the same, the motion face wind direction is larger due to the thrust in wind direction. It can be conclude that the tower fore-aft mode is the second most important DOF to be included to get accurate power production properties. At last the errors of DOF 6 are at a very small level, no more than 0.1%, which means second order modes almost have nothing to do with power production properties. That would be proper to neglect the second order mode DOFs.
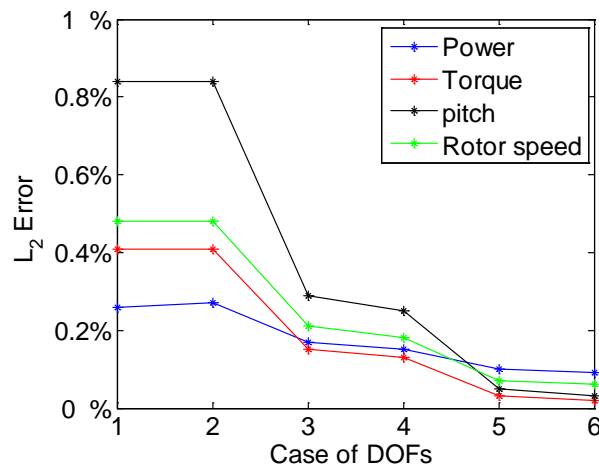
Figure 14 L_2 error of power production properties under different DOFs

4.3 Blade properties

Blade properties include blade deflection and bending moment. Firstly the blade out-of-plane deflection and the corresponding bending moment are analyzed. Table 11 shows the L_2 error of blade out-of-plane deflection and bending moment under different DOFs. The blade is considered as a rigid body for DOF 1 and DOF 2, so there is no deflection at all. As a result the L_2 error is 100%. For DOF 3 blade out-of-plane deflection is included. The error drops dramatically from 100% to about 10%. As more DOFs are included, the error doesn't drop much. In case DOF 6, with all the first order DOFs included and second order DOFs neglected, the error is still relatively large at about 8%. That means the flapwise deflection is influenced by second order mode of blade and tower. The blade root bending moment at y direction is induced by forces aligned with the blade flapwise and tower fore-aft motions. Therefore, it is influenced by blade out of plane deflection most, since there is large drop of errors from DOF 2 to DOF 3. Moreover, the tower fore-aft DOF also plays an important role, since there is large drop of errors from DOF 4 to DOF 5.

Table 11 L_2 error of blade out-of-plane deflection and bending moment under different DOFs

Error[%]	DOF_1	DOF_2	DOF_3	DOF_4	DOF_5	DOF_6
OoPDefl1	100.00	100.00	10.56	8.47	7.67	7.67
RootMyc1	10.24	10.27	3.62	3.31	1.13	1.12

The time history and spectrum of out of plane deflection and bending moments are shown in Figure 15 and Figure 16. From the time series it can be seen that the oscillation trends of different cases are similar. There is positive offset of both deflection and moment. From the spectrum it can be seen that case DOF 3 has much higher peak at 0.2 Hz than others, which means the first-order flapwise deflection and bending moment are greatly influenced by gravity. However gravity should have the most influence on edgewise deflection and moment theoretically. The reason might be that the gravity influence to edge wise will transfer to flapwise, since the blade flapwise and edgewise deflection are coupled by twist. That means that the edge wise deflection should be included as well to get a relatively accurate flapwise deflection and moment. Besides the rotational frequency 0.2 Hz, another dominant frequency is the wind frequency (low frequency). For the bending moment, there are also peaks at frequencies of 0.4 Hz, 0.6 Hz, 0.8 Hz, 1.0 Hz and 1.2 Hz induced by tower shadow effects. Each time the blades pass by the tower, there will be a change of motion and moment due to the change of wind field around the tower. It should be noted that bending moment of DOF 1 (blue line) has high response at higher frequencies, since there is no deflection in blade flapwise DOF, forces acting on rigid body are larger than that of flexible one. There are peaks induced by tower shadow for out of plane deflection as well, however it is not such significant.
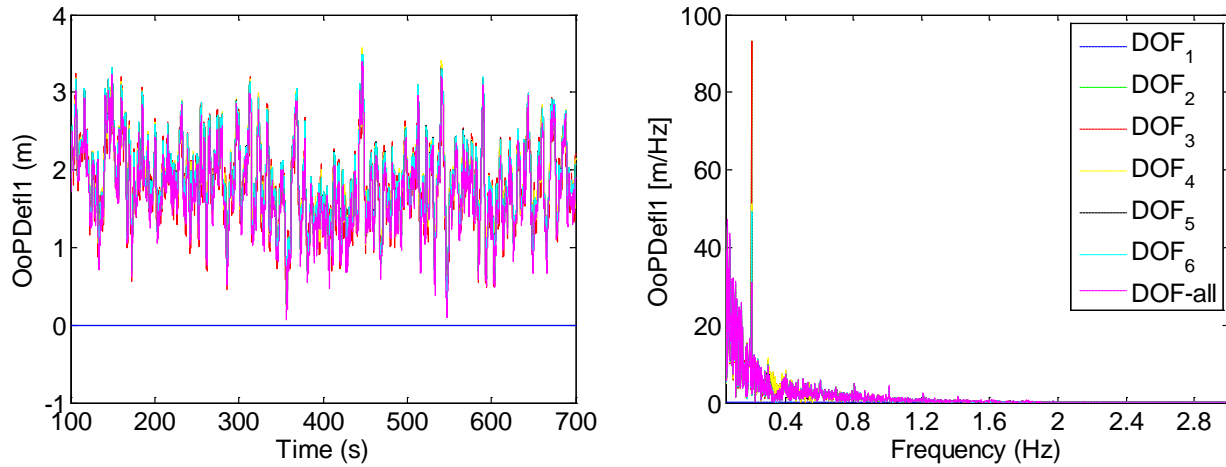
Figure 15 Time series (left) and spectrum (right) of blade 1 out-of -plane deflection

Figure 16 Time series (left) and spectrum (right) of blade 1 root out-of -plane bending moment

Table 12 shows the L_2 error of blade in-plane deflection and bending moment under different DOFs. Again, since the blade is considered as a rigid body in DOF 1 and DOF 2, there is no deflection at all. As a result the L_2 error is 100%. For the next case the blade out-of-plane deflection is included. The error drops dramatically from 100% to about 50%. Moreover the in-plane deflection DOF is another critical reason in decreasing errors from about 50% to about 5%. The blade root bending moment at x direction is induced by forces aligned with blade in-plane deflection DOF. Therefore it is influenced by blade in-plane deflection most.

Table 12 L_2 error of blade in- plane deflection and bending moment under different DOFs

Error[%]	DOF_1	DOF_2	DOF_3	DOF_4	DOF_5	DOF_6
IpDefl1	100.00	100.00	46.32	5.82	4.95	4.95
RootMxc1	3.27	3.45	2.70	1.50	1.11	1.09

The time history and spectrum of in-plane deflection and bending moments are shown in Figure 17 and Figure 18. From the time series it can be seen that there is a negative offset in deflection and positive offset in bending moment mainly induced by the lift force acting on the blade. The oscillation is mainly due to the gravity effect which can be verified in the spectrum with high peak in 0.2 Hz. The time series of different cases in bending moment match well in the rotational frequency of 0.2 Hz. For the two spectrums, there is a peak in the response at 0.2 Hz, which means the gravity has the most influence on the in-plane deflection. This influence is much larger than wind frequency. All the cases with different DOFs can capture the rotational frequency 0.2 Hz correctly. The main difference of different cases is the peak value. The more DOFs are considered, the more accurate of the result becomes.
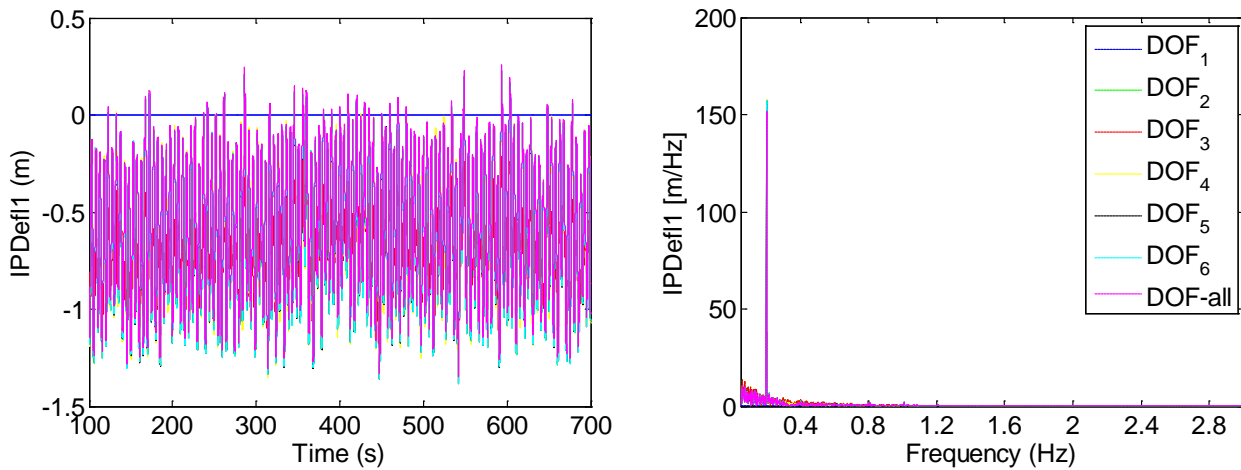
Figure 17 Time series (left) and spectrum (right) of blade 1 in-plane deflection
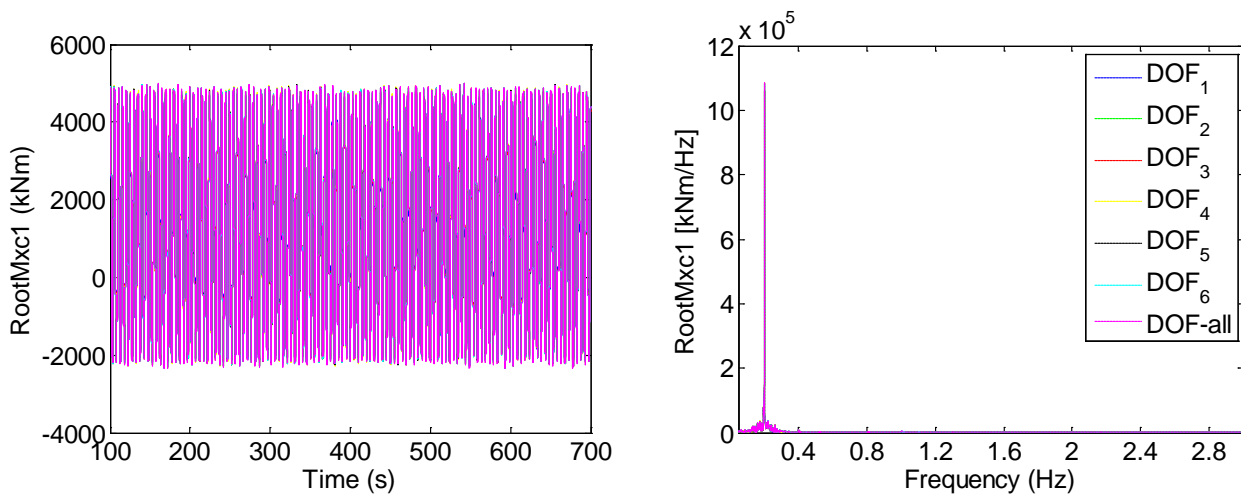
Figure 18 Time series (left) and spectrum (right) of blade 1 root in-plane bending moment

Table 13 shows the L_2 error of blade torsional moment under different DOFs. It can be seen that the blade torsional moment is influenced by the blade in-plane DOF most (from DOF 3 to DOF 4). Flexible tower has a little influence (from DOF 4 to DOF 6). Figure 19 shows the time series and spectrum of

39

blade root torsional moment. The blade torsional moment is induced by both aerodynamic force and gravity. The aerodynamic lift and drag forces contribute to the mean value of torsional moment, which can be seen in the time series there is a negative offset. The aerodynamic force frequency is consistent with wind frequency, and cases with different DOFs match well at wind frequency. However for gravity induced torsional moment, large error occurs when blade is considered rigid. Therefore the blade 1st order DOFs must be included to achieve a relatively accurate result.

Table 13 L_2 error of blade torsional moment under different DOFs

Error[%]	DOF_1	DOF_2	DOF_3	DOF_4	DOF_5	DOF_6
RootMzc1	44.89	44.87	35.97	5.45	2.33	2.34

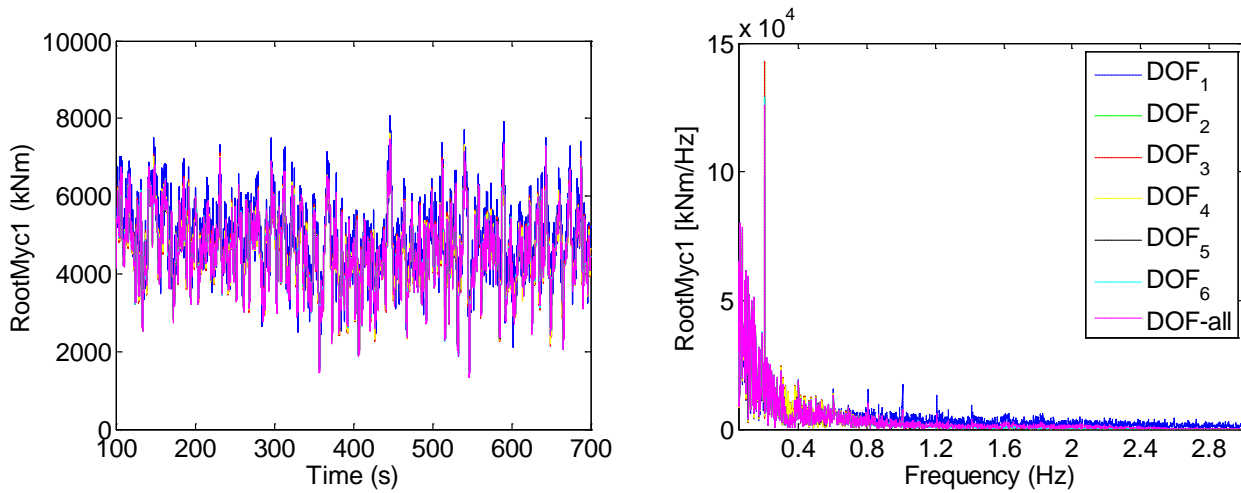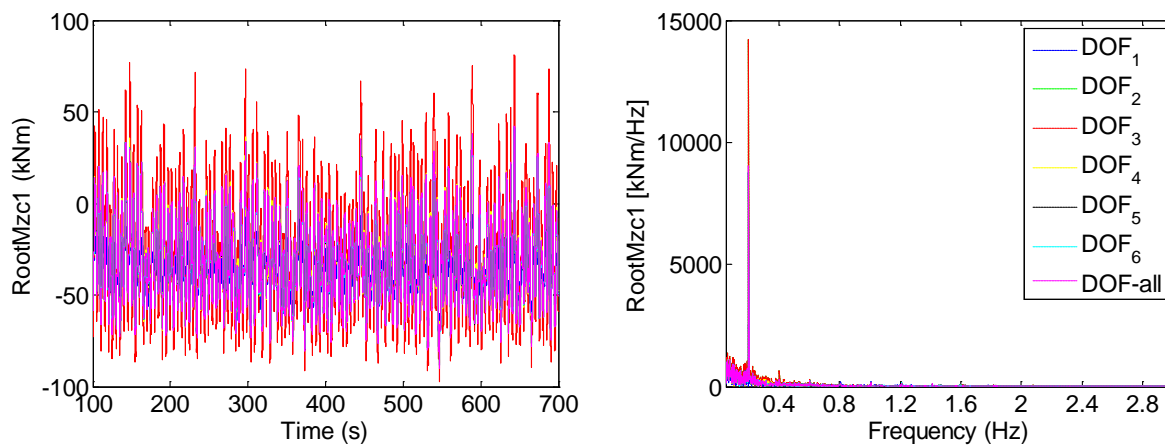
Figure 19 Time series (left) and spectrum (right) of blade 1 root torsional moment

Figure 20 shows the L_2 error of blade properties under different DOFs as a summary, the overall trend of quantities is similar. At the first four DOFs, the L_2 error decreases significantly. And as more DOFs are included, the L_2 errors become stable at a relatively low level. However for each quantity, the decrease range of L_2 error is quite different.
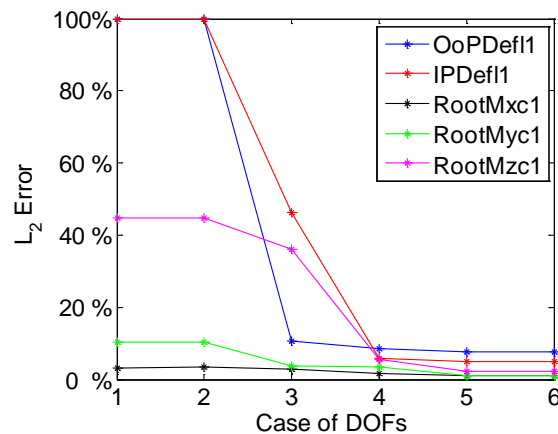
Figure 20 L_2 error of blade properties under different DOFs

4.4 Tower properties

Tower properties include rotor thrust and tower top bending moment. Firstly the thrust is analyzed. Table 14 shows the L_2 error of rotor thrust under different DOFs. The error drops dramatically from DOF 4 to DOF 5, which indicates that the tower fore-aft DOF has the largest effect. Another drop of L_2 error occurs from DOF 2 to DOF 3, which means the blade out-of-plane DOF has the second largest effect. That is reasonable since a flexible tower and blade will change the relative wind velocity, then changing the aerodynamic force. The error can be less than 1% at DOF 6, so 2nd order DOFs do not have much influence. Figure 21 displays the time series and spectrum of rotor thrust. From time series in Figure 21, it can be seen that the low frequency of different cases match well, while difference occurs in high frequency. Look into spectrum, wind frequency is dominant. There is a significant peak at about 0.3Hz, corresponding to the 1st tower bending mode. For case DOF 1 (blue line), the peaks of high frequency are larger than others. That means the differences between rigid and flexible blade and tower focus on high frequency part. For a more accurate rotor thrust response in high frequency, the blade and tower DOF can be included.

Table 14 L_2 error of rotor thrust under different DOFs

Error[%]	DOF_1	DOF_2	DOF_3	DOF_4	DOF_5	DOF_6
RotThrust	8.14	8.17	5.40	5.27	0.96	0.95
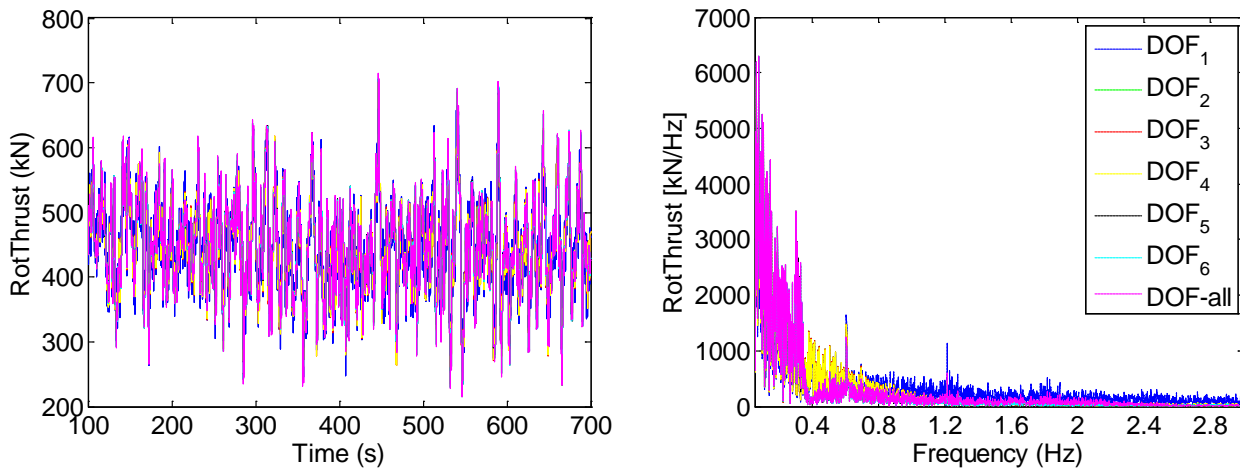
Figure 21 Time series (Left) and spectrum (Right) of rotor thrust

The L_2 errors of tower top side-side bending moment under different DOFs are all very small, as shown in Table 15. Figure 22 shows the time series and spectrum of tower top side-side bending moment. Even with only 1 DOF included, the model is very accurate. One possible reason is that tower top side-side bending moment is mainly induced by torque, which is little influenced by the flexibility of blades and tower. Therefore the dominant frequency is wind frequency, as shown in the spectrum in Figure 22. At low frequencies, the time series as well as spectrum of different cases match well. Similar to power

production property, the peaks of different cases at frequency around 1.7 Hz are different. The reason is also similar to that of power production, as previously explained.

Table 15 L_2 error of tower top side-side bending moment under different DOFs

Error[%]	DOF_1	DOF_2	DOF_3	DOF_4	DOF_5	DOF_6
YawBrMxp	2.19	2.65	2.03	1.96	1.94	1.70

Figure 22 Time series (Left) and spectrum (Right) of tower top side-side bending moment

Table 16 shows the L_2 error of tower top fore-aft bending moment under different DOFs. The tower top fore-aft bending moment is mainly induced by thrust force, which influenced by tower fore-aft and blade out-of-plane DOFs most. In case DOF 6, the error is about 8%, which means 2nd order DOFs have significant influence. From the time series and spectrum in Figure 23, it can be seen that the cases with different DOFs don't match well with each other in high frequencies. Wind frequency has some influence. However the dominant frequencies are 0.3Hz, 0.6Hz, 1.2Hz, 1.8Hz and 2.4Hz. From the natural frequency analysis in section 4.1, it can be seen that 1st tower fore-aft and blade flapwise DOFs have most influence around 0.3 Hz. If blade and tower is considered flexible the response at about 0.3 Hz can be captured. Therefore error decreases significantly. Obviously blade rotational and tower shadow effect is significant, since the peak at 0.6Hz is the largest. The reason can be explained as follows. The rotational frequency is 0.2Hz. For a 3 blade wind turbine, each time one blade pass by the tower, the aerodynamic force will change. Therefore the total thrust force will has a frequency at 0.6Hz and the thrust induced tower bending moment has a change of 0.6Hz as well. Moreover tower top fore-aft bending moment is influenced by not only thrust force but also the arm of force. The imbalanced force acting on blade will cause a 0.6Hz change in the thrust force arm and that is exactly in phase with the thrust force. As a result the integrated influence is at 0.6 Hz.

Table 16 L_2 error of tower top fore-aft bending moment under different DOFs

Error[%]	DOF_1	DOF_2	DOF_3	DOF_4	DOF_5	DOF_6
YawBrMyp	49.04	49.46	34.14	31.57	8.39	8.06
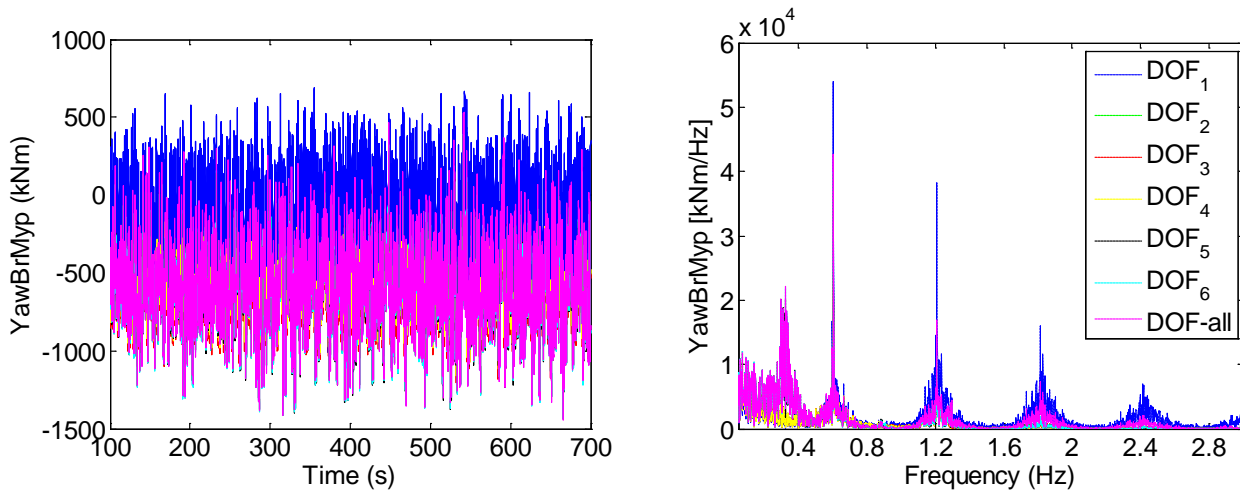
Figure 23 Time series (Left) and spectrum (Right) of tower top fore-aft bending moment
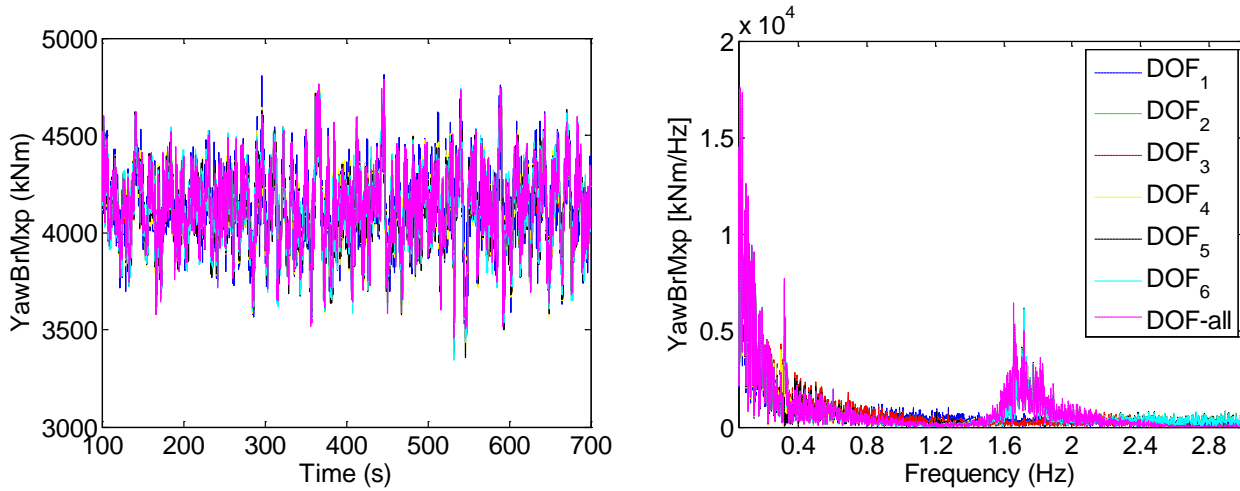
Table 17 shows the L_2 error of tower top torsional moment under different DOFs. It can be seen that the L_2 error of tower top torsional moment is greatly influenced by blades and tower flexibility much, since there are relatively large drops of errors from DOF 2 to DOF 3 and from DOF 4 to DOF 5. The torsional moment is induced by the unbalanced aerodynamic force in out-of-plane direction. Therefore any factor that influences aerodynamic force has an influence on torsional moment. Figure 24 displays time series and spectrum of tower top torsional moment. From the time series it can be seen that cases of different DOFs match well at low frequency and the difference occur at high frequencies. From the spectrum it can be seen that the frequencies where peaks occurs are similar with that of tower top fore-aft bending moment. For the torsional moment, 0.6Hz is definitely the most significant frequency for 3 blades turbine rotating at 0.2 Hz since the torsional moment is closely related with the position of blades. Other frequencies that are multiples of 0.6Hz are induced by the combination of rotor rotation and the tower shadow effect. However these peaks are not that large.

Table 17 L_2 error of tower top torsional moment under different DOFs

Error[%]	DOF_1	DOF_2	DOF_3	DOF_4	DOF_5	DOF_6
YawBrMzp	11.85	11.94	7.69	5.88	4.27	4.13
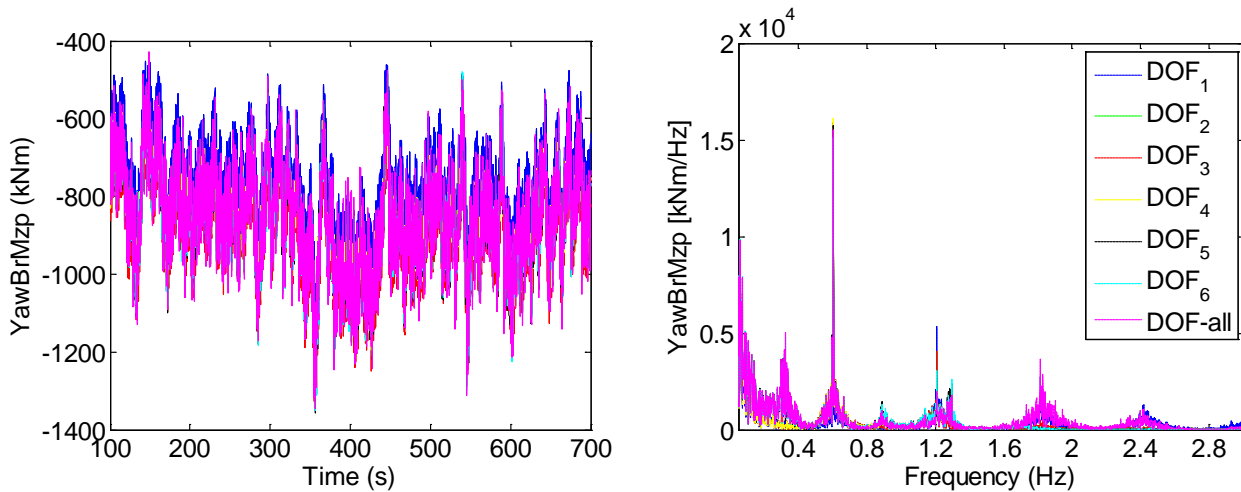
Figure 24 Time series (Left) and spectrum (Right) of tower top torsional moment

Figure 25 shows the L_2 error of tower properties under different DOFs as a summary, the overall trend of quantities is similar. At the first four DOFs, the L_2 error decreases significantly. While as more DOFs included, the L_2 errors become stable at a relatively low level. However the error levels are quite different. Specifically, tower top fore-aft bending moment has the largest error, which means it is sensitive to DOFs. It is influenced much by not only 1st order modes but also 2nd order modes. The L_2 error of the tower top torsional moment has the second largest value, stable at about 4%. The L_2 error of rotor thrust and tower top fore-aft bending moment is quite small at case 6, around 1%.
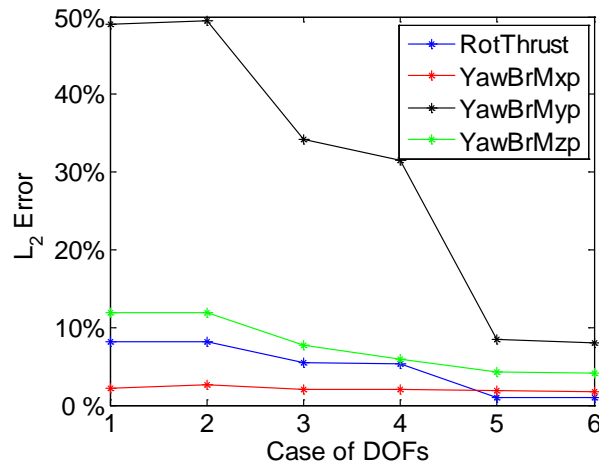
Figure 25 L_2 error of tower properties under different DOFs

4.5 Summary

Although all the DOFs have some influence on the modeling accuracy, their importance can be different for a certain quantity. Table 18 lists the most and second most important DOF for different quantities. In order to achieve a better modeling accuracy, the DOFs listed in the table are strongly suggested to be included.

Table 18 The most and second most important DOF for different quantities

	Most Important DOF	2nd Most Important DOF
Gen Power	Blade Flap	Tower Fore-aft
Gen Torque	Blade Flap	Tower Fore-aft
Blade Pitch	Blade Flap	Tower Fore-aft
Rotor Speed	Blade Flap	Tower Fore-aft
OoPDefl1	Blade Flap	Blade Edge
IpDefl1	Blade Flap	Blade Edge
RootMxc1	Blade Edge	Blade Edge
RootMyc1	Blade Flap	Tower Fore-aft
RootMzc1	Blade Edge	Blade Flap
RotThrust	Tower Fore-aft	Blade Flap
YawBrMxp	Blade Flap	Tower Side-side
YawBrMyp	Blade Edge	Blade Flap
YawBrMzp	Blade Flap	Blade Edge

Chapter 5 Modeling Error Due to Linearization

Error due to linearization is an important part of the total modeling error. As introduced in section 3.3, the error between linear model with part DOF and nonlinear model with the same DOFs is the error due to linearization process. In this chapter we aim to find the most efficient way to minimize error due to linearization. The linearization error is influenced by both number of operation points and interpolation method.

In this chapter, the same wind case as Chapter 4 is studied as shown in Figure 26. The range of wind speed is from 14m/s to 22m/s, and the 10 minutes mean wind speed is 18m/s. Noted that all the cases in this chapter have the same number of DOFs: DOF 6.
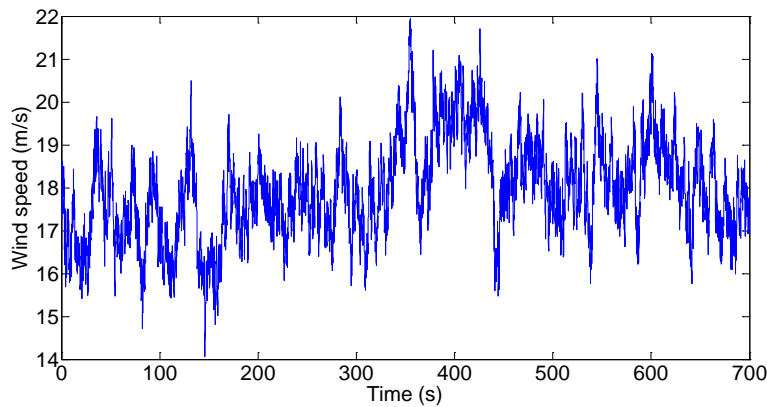
Figure 26 Time series of wind speed

5.1 Number of operation points

Each linearization is about one operation point as introduced in chapter 2. If the wind speed is far from the operation point, the estimation will be inaccurate. It is important to investigate within what range an operation point works well. In this study, 5 cases are investigated, where the number of operation points is 1, 2, 3, 5 and 9. The corresponding wind speeds are listed in Table 19.

Table 19 Details of operation points

No. of OP.	1	2	3	5	9
OP.[m/s]	18	17, 19	16, 18, 20	14, 16, 18, 20, 22	14, 15, 16, 17, 18, 19, 20, 21, 22

If more than one operation point is chosen, the weight, also known as interpolation method, should be determined as well. In this study the linear interpolation method is applied first. The following figures display the choice of operational points and the weight function shape.

47

Case 1: 1 operation point 18m/s
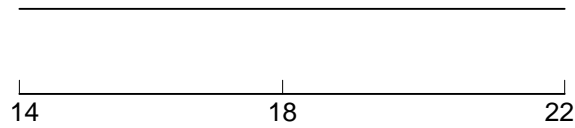
Case 2: 2 operation point 17m/s and 19m/s
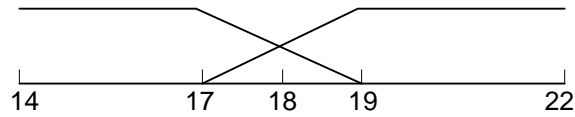
Case 3: 3 operation point 16m/s, 18m/s and 20m/s
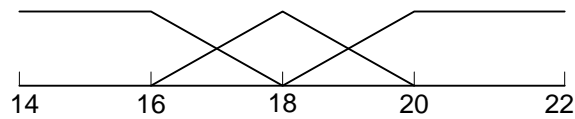
Case 4: 5 operation point 14m/s, 16m/s, 18m/s, 20m/s and 22m/s
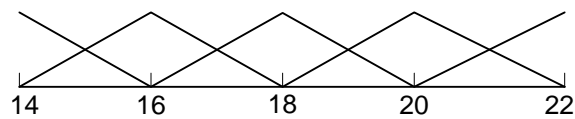
Case 5: 9 operation point 14m/s, 15m/s, 16m/s, 17m/s, 18m/s, 19m/s, 20m/s, 21m/s and 22m/s
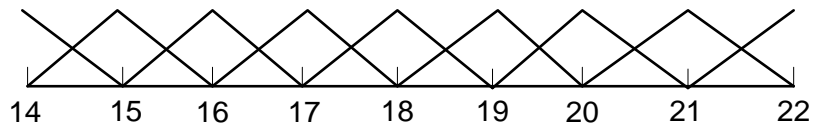
Figure 27 shows the flow chart of the calculation steps of applying two operation points as an example.

Step 1: At time step n, the input to the state space model is the perturbing wind speed generator torque and blade pitch with respect to different operation points.

Step 2: Substitute inputs into the discrete state space equation $\Delta x_{n+1} = A\Delta x_n + B\Delta u_n$. The perturbing states of next time step Δx_{n+1} can be determined.

Step 3: This step is aim to do the weight average of the state at two OP, where the weights corresponding to the linear interpolation function. It should be noted that the states obtained from state space equation are the fluctuating from operation points. Therefore the true states can be determined by sum up the states operation point and the state fluctuating.

Step 4: With the perturbing input of time n+1 and states of time n+1, the calculation of next time step can be obtained. It should be noted that the states perturbing of each system for next time step are the true states deduct the corresponding operation points of states.
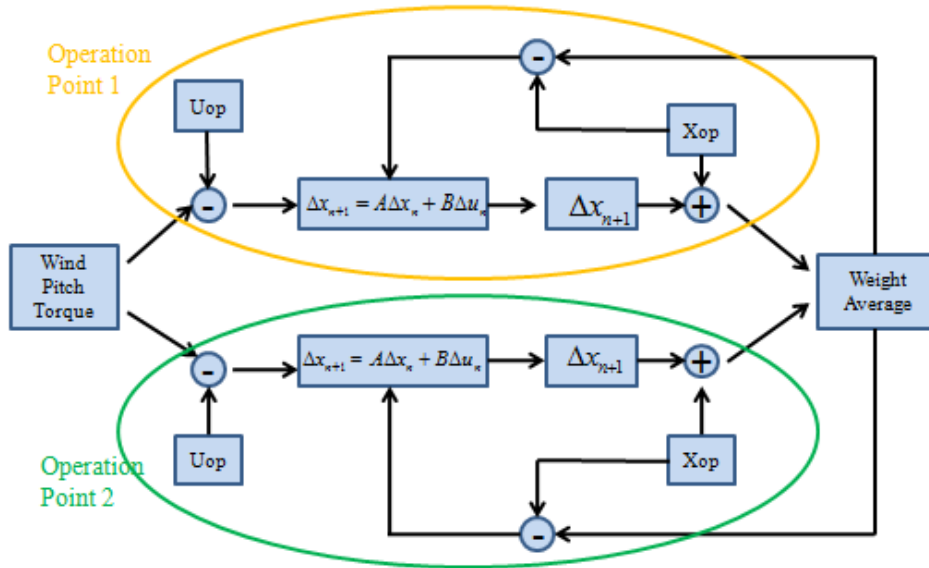
Figure 27 Linearization step of two operation points

With all the inputs and weight averaged states, the output disturbance, such as power production, blade and tower properties can be determined using $\Delta y_{n+1} = C\Delta x_n + D\Delta u_n$. The final outputs are summation of disturbances and operation point values $y_{n+1} = y_{op} + \Delta y_{n+1}$. It should be noted that the operation point may change with the azimuth angle. For power and rotor speed the operation point does not change with azimuth angle, they are constant as 5MW and 12.1 rpm respectively under wind speed 18 m/s. However for quantities, such as in-plane deflection, blade and tower bending moment, the operation points change with azimuth angle. Figure 28 shows the OP of blade in-plane deflation and tower fore-aft bending moment as an example. The OP of other quantities is shown in the appendix A2. For the in-plane deflection, the offset is due to aerodynamic force and the sine shape variation is induced by gravity. For the tower fore-aft bending moment, there are three significant peaks due to 3 blades. The OP under different wind speed is quite different, while they have similar trend.
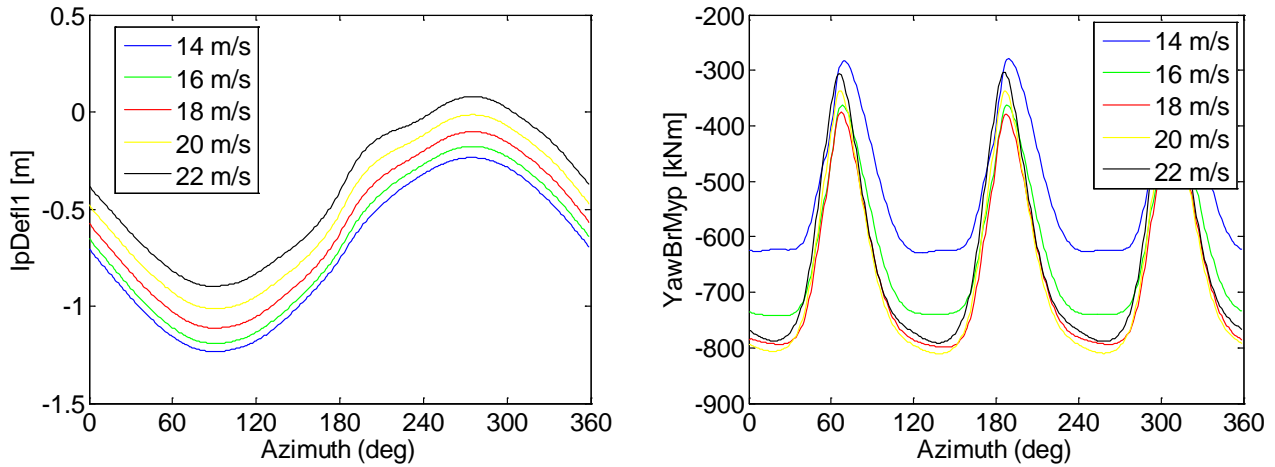
Figure 28 Blade in-plane deflation and tower fore-aft bending moment OP at different azimuth

5.1.1 Power production properties

Figure 29 displays the trend of L_2 error for different numbers of OPs. Overall the error of power is larger than that of rotor speed at all cases. It can be concluded that for power and rotor speed, the L2 error decreases as the No. of OP increases. Theoretically if there is infinite number of operation points, the linearization error will be zero. The two dashed lines represent the error due to DOFs (6 DOFs), blue dashed line for power and red dashed line for rotor speed. It is clear that the error due to DOFs is much smaller compared to the linearization error. Therefore the dominant error is linearization error, and the most efficient method to decrease error is to use more operation points.
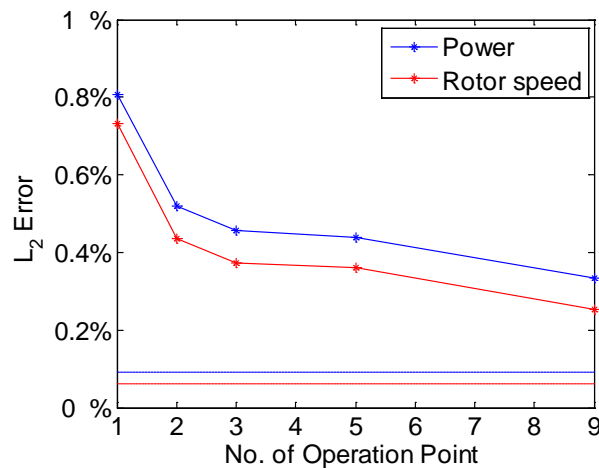
Figure 29 L_2 error of power and rotor speed under different No. of OP.

Figure 30 displays the time series of power and error under different No. of OP, it can be seen that for most time all of the cases match well. However there is large deviation at some time segments. The time series of error show that large error will not occur at cases with more OP, which means increasing the

50

No. of OP is efficient for reducing errors. This phenomenon demonstrates that the error due to linearization will decrease if the disturbance is small. Applying more operation points can make quantities not far away from the operation points. In terms of rotor speed, time series of error distribution are similar.
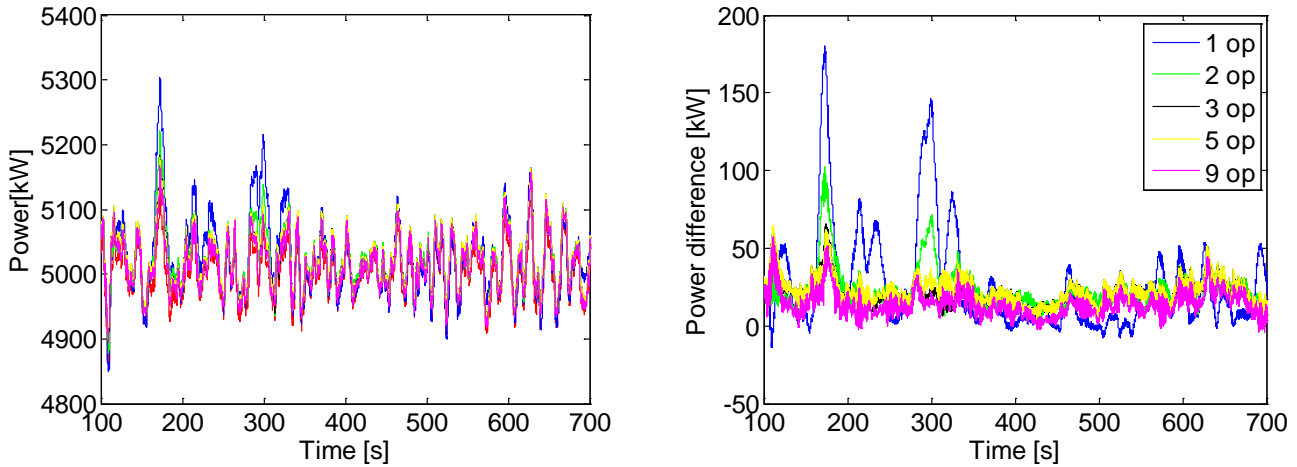
Figure 30 Time series of power (left) and error (right) under different No. of OP

5.1.2 Blade properties

Figure 31 displays L_2 error of blade properties under different No. of OP. Overall blade in-plane deflection has the largest linearization error, while blade out-of-plane bending moment has the smallest error level. The errors of more than one OP are all no more than 3%, which means the error due to linearization is not large. This can be seen in Figure 31. We take blade out-of-plane deflection as an example. Figure 32 shows the time series and spectrum of blade out-of-plane deflection at different No. of OP. All cases with different No. of OP match well in both time series and spectrum. The time series and spectrum of other blade quantities are similar, which are displayed in the appendix A3. It seems that increasing No. of OP does not make much difference. That indicates the dominant factor that induces linearization error is not the number of operation points. Simplification of physical phenomenon induces the error.

The separated dashed lines in Figure 31 display the corresponding error due to DOFs. It is clear that the error due to DOFs is much larger than linearization error for blade out-of-plane deflection (blue dash line) and in-plane deflection (red dashed line). That means some important phenomenon are neglected due to not enough DOFs, and the most efficient way to decrease error is to include more DOFs. In contrary, the errors due to DOFs of blade root bending moment are quite small, around 1%. Therefore for these two quantities the dominant error is linearization error, and the most efficient method to decrease error is to use more operation points.

51
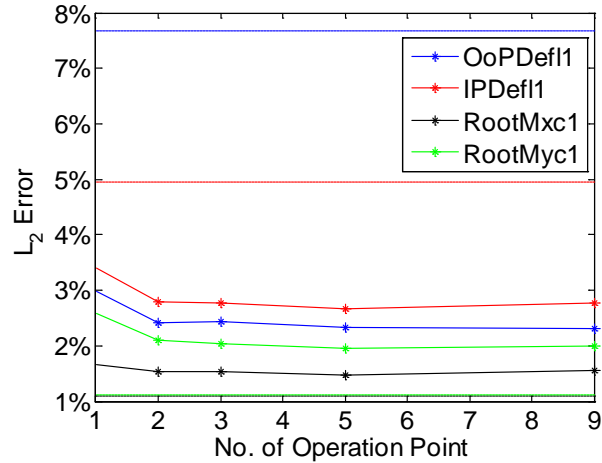
Figure 31 L_2 error of blade properties under different No. of OP.
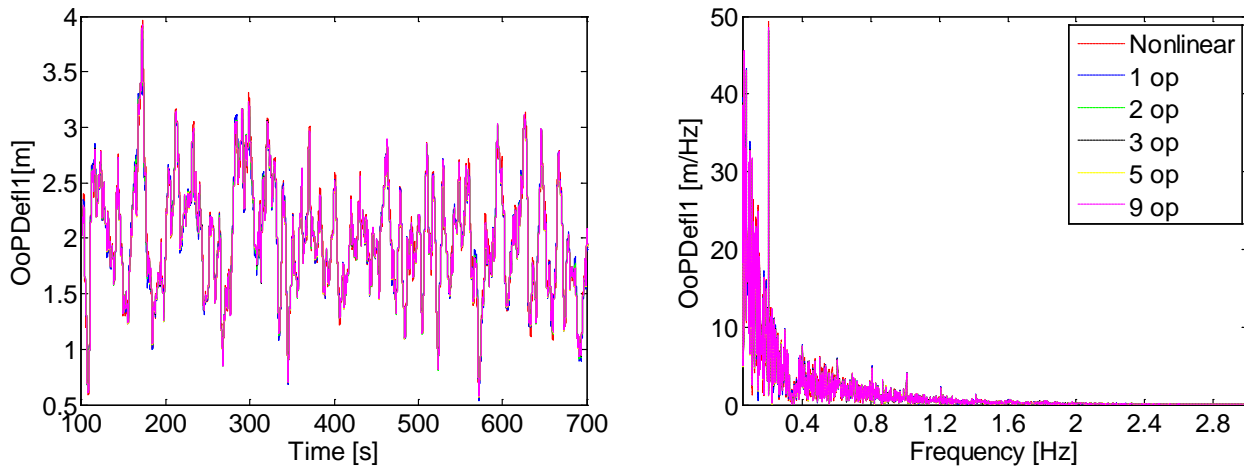
Figure 32 Time series and spectrum of blade out-of-plane deflection at different No. of OP

5.1.3 Tower properties

Figure 34 shows the L_2 error of tower properties under different No. of OP. In terms of tower top bending moment, increasing the number of operation points will increase the L_2 error. For tower top fore-aft and side-side bending moment, the L_2 error increases dramatically to more than 30%. Therefore if the tower top bending moment is set as criterions, only one OP can be used to minimize the error due to linearization. The linearization error at 1 OP should be compared with error due to DOFs to see which one is dominant. It can be seen that for, the error of tower top side-side bending moment (YawBrMxp), the error of DOFs is much larger at about 1.7% than that of linearization. While for the other bending moment, the error due to DOFs is larger than that of linearization.

This increase of L_2 error seems to be out of expectation and one possible explanation for this behavior can be found in Chapter 4. As discussed in Figure 22, Figure 23 and Figure 24, the tower properties have

high peaks in high frequency modes which are related to structure oscillations. This indicates that these responds can be very sensitive to even small variations in input. When more than one OP is used, the interpolated state values actually offset from each OP, which means noise will be involved for the input of the next time step. This noise then leads to significant error in the prediction of structure oscillation, and thus the large L_2 errors. Figure 33 shows the time series and spectrum, and it can be seen clearly that the errors concentrate around the oscillation related modes, which agrees with the previous explanation. It should be noted that linearization based on more than one OPs always introduce some noise due to its slightly nonlinear feature. However, for the power production and blade properties, they mainly respond directly to the instantaneous input. Thus the L_2 errors of them decrease when use more OP for linearization.
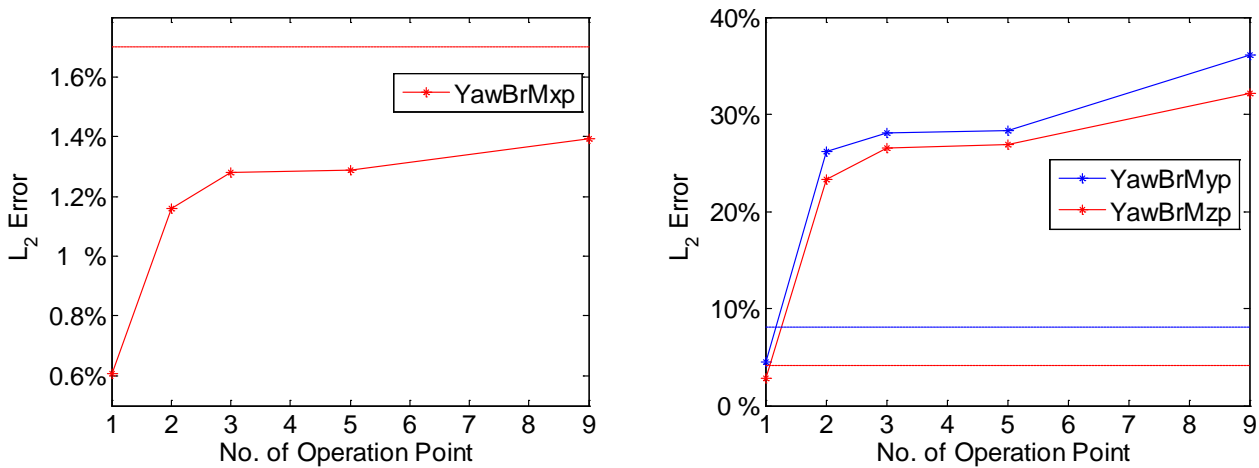
Figure 34 L_2 error of tower properties under different No. of OP
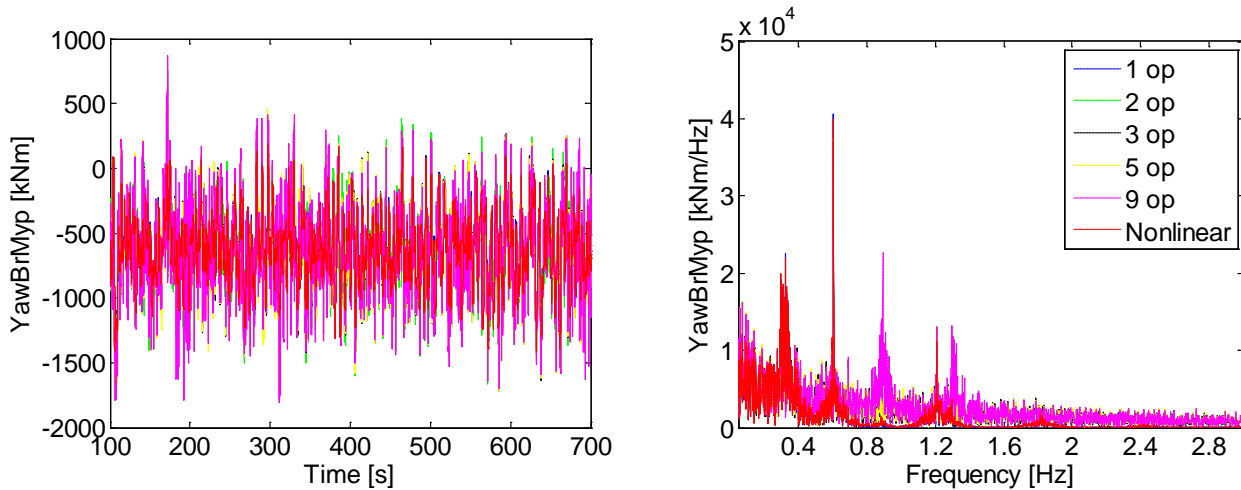
Figure 35 Time series and spectrum of tower top fore-aft bending moment at different No. of OP

5.2 Interpolation method

Besides the No. of OP, the interpolation method is also important, since higher order interpolation method may mitigate the oscillation when wind speed change rapidly. Therefore it is meaningful to find a balance between interpolation method and the accuracy. All the cases in this section use 9 operation points, and the DOF case is DOF_6. That is to say a relatively accurate linearization model has been applied. The only difference is the interpolation methods. Three methods are used, which are zero order, first order and spline, illustrated in Figure 36.
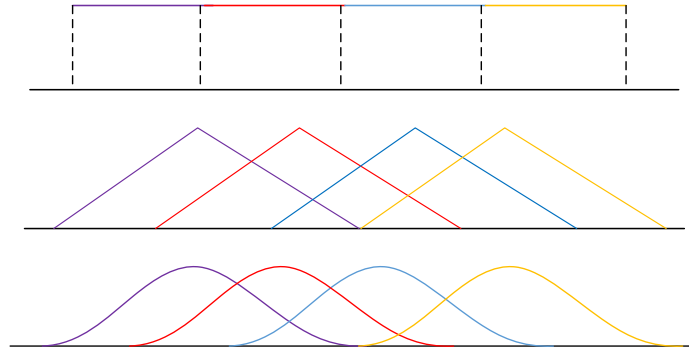
Figure 36 Illustration of interpolation method: Zero order (top) 1st order (middle) 2nd order (bottom)

The L_2 error of different quantities can be clarified into 3 groups according to the changing trend. The first group includes power and rotor speed, which are shown in Figure 37 (left). It can be seen that the higher order interpolation method does increase the accuracy. Theoretically the L_2 error can approach zero as the interpolation order becomes higher, while the computation time also increase. Moderate order of interpolation method, such as 1st order, is very accurate. For the second group shown in Figure 37 (right), the L_2 error almost stays constant under different interpolation method. As a result there is no benefit to use higher order interpolation method.
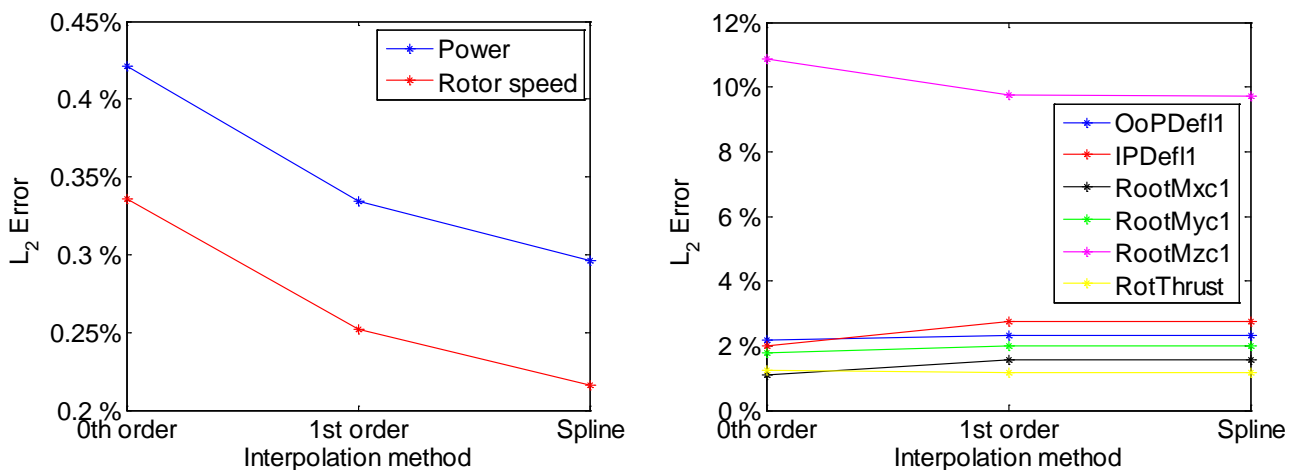
Figure 37 L_2 error of group 1 (left) and group 2 (right) under different interpolation methods

Group 3 includes the tower bending moment in three directions. Figure 38 displays the L_2 error under different interpolation methods. For zero order interpolation the L_2 error is much larger than 1st and spline methods. The reason is that shifting of operation points induces large unstable oscillation. However if linear interpolation method is applied, the shift is more smooth. Figure 39 (left) displays the time series of tower top fore-aft bending moment of zero order results comparing with nonlinear results. It can be seen clearly that there are very large oscillations at some time segments. The time series of 1st order interpolation comparing the nonlinear result is shown in Figure 39 (right). Although the results are not accurate enough, the oscillations are much smaller than zero order. For the purpose of optimizing interpolation methods and accuracy, the 1st order interpolation methods is the best choice for group 3.
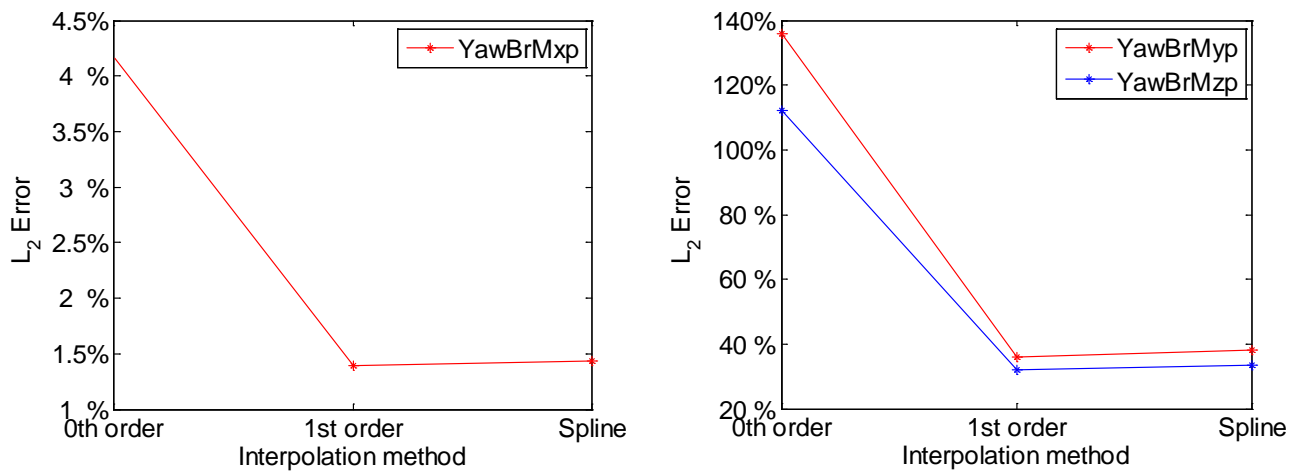
Figure 38 L_2 error of group 3 under different interpolation methods
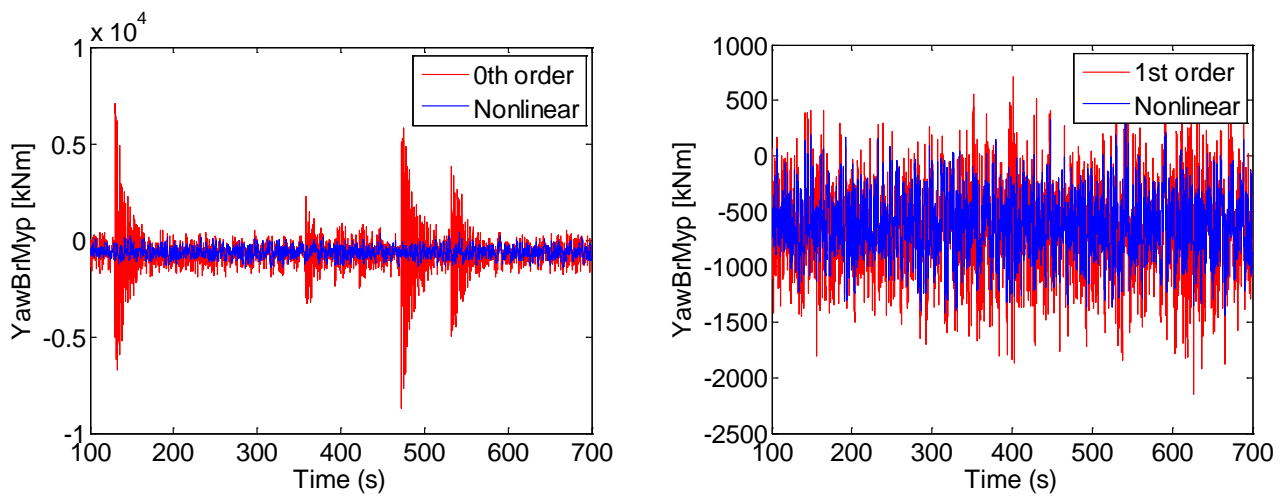
Figure 39 Time series of group 3 under different interpolation methods

55

5.3 Summary

According to the previous results and analysis, for some quantities there exists an optimum choice for the number of OP and interpolation method. These optimum choices are listed in Table 20. For the power production properties, the more OP and higher order interpolation method will decrease the modeling error.

Table 20 The optimum No. of OP and interpolation method

	Optimum No. of OP	Interpolation method
Power production properties	The more the better	The higher the better
Blade properties	2	Linear
Tower properties	1	Linear

Chapter 6 Total modeling error

The total modeling error is the difference between linear model with part DOFs and the nonlinear model with full DOFs. The total modeling error is a combination of error due to DOFs and linearization; however the relationship is not simply summation. In order to have an insight into the influence of DOFs and linearization to total modeling error, simulations are carried out for all the possible combinations of 6 different DOF cases as shown in Table 7, and 5 OP cases shown in Table 19.

The benefits of analyzing the influence of DOFs and linearization to total modeling error are three-fold. Firstly, the influence of DOF and OP can be compared directly and show the total error under different combinations. The results can provide guidelines for WT modeling and simulation with respect to different quantities. Secondly, according to the different influence of DOFs and OP, the most efficient direction to further improve the accuracy can be pointed out. Finally, the total modeling error determined in this chapter will be used as the basis to estimate the reliability of the ice-detection methods in following chapters.

According to the analysis in Chapter 4 & 5, the WT related quantities can be classified into three groups, which are quantities related to power production, blade properties and tower properties respectively. These three groups will be analyzed individually in the following sections, and it will be shown that the quantities within the same group have similar behaviors with respect to DOF & OP.

6.1 Power production properties

From analysis in Chapter 4, including more DOFs can decrease the error in power production variables due to DOFs. Moreover, in Chapter 5, it can be concluded that increasing the number of OP also decreases linearization error to some extent. Then an interesting question would be which factor dominates the total modeling error.

Figure 40 displays the total modeling error of power and rotor speed. The contours are made with respect to different combinations of DOFs and OP. It can be seen that for both power and rotor speed, although the DOFs have a mild influence, the OP dominates the total modeling error. The results demonstrate that power and rotor speed are almost linearly related with the inputs.

Note that, we can achieve a 0.5% error even with 1 DOF, if a proper OP method is applied. Thus for power and rotor speed, it would be accurate enough if we use the 1 DOF, and to improve the accuracy, the most efficient way is to increase the number of OP.
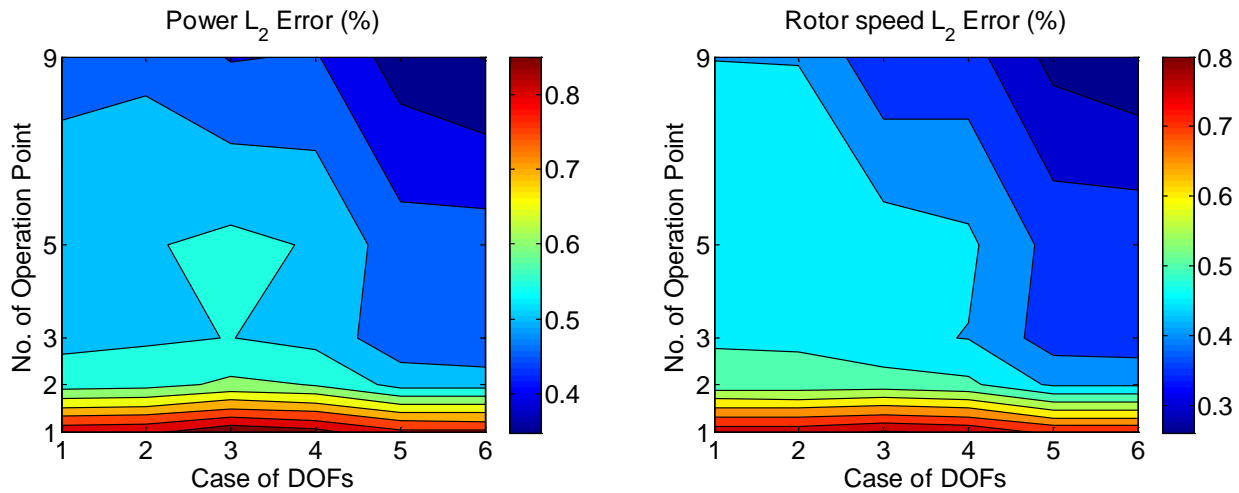
Figure 40 Total error of power (left) and rotor speed (right) at different combinations of DOF &OP

6.2 Blade properties

From analysis in Chapter 4, for blade out-of-plane deflections, including more DOFs can decrease the error due to DOFs. Moreover, in Chapter 5, it can be concluded that if the number of OP is more than 2, the linearization error will not decrease any more. The results from previous chapters may not work for the total modeling error, therefore we have to conduct detailed investigation into the total modeling error contours shown in Figure 41.

The contours are made with respect to different combinations of DOFs and OP. From the left figure it can be seen that there is a dramatic drop of errors from DOF case 2 to case 3. That means we must include the blade flapwise DOF to achieve a reliable result. For DOF cases 4, 5 and 6, we plot a separate contour to look into details, as shown in the right figure. The range of error is from 7% to 8%, which means there is not much improvement. The case with only 1 OP and DOF 4 has about 8% error, and the dominant factor is still DOFs.
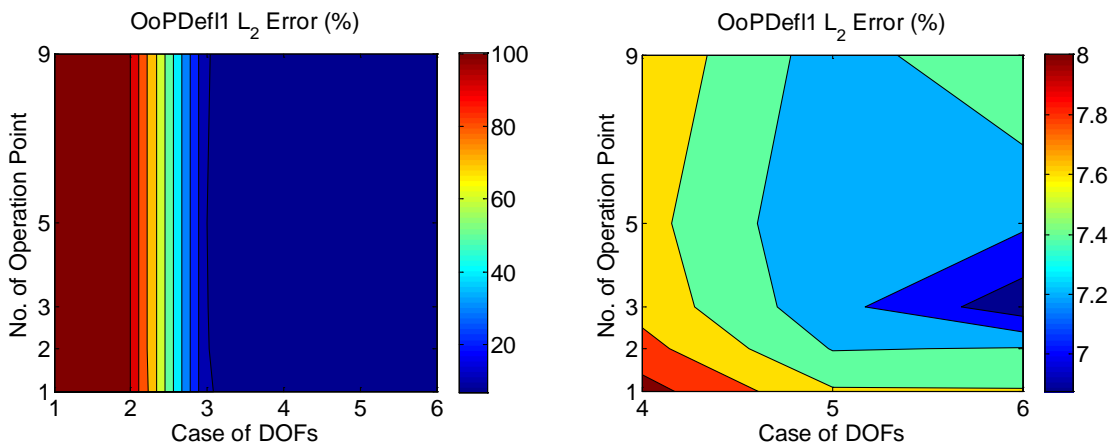
Figure 41 Total error of blade out-of-plane deflection at different combinations of DOF & OP

From analysis in Chapter 4 and 5, the blade in-plane deflection accuracy is mainly influence by the number of DOFs and will become stable if more than 2 OP for linearization is used.

The contours in Figure 42 are made with respect to different combinations of DOFs and OP. The patterns are similar to those of the out-of-plane deflections. There is a dramatic drop in error from DOF case 2 to case 4, which means both the blade flapwise DOF and blade edgewise DOF to achieve a reliable result. This finding agrees with that of Chapter 4. A detailed local contour is shown in the right figure for the DOF cases 4, 5 and 6. It can be seen that the contour is also similar to Figure 41(right). Although there is improvement by increasing the number of OP, the range of error is from about 6% to 7%, which means there is not much improvement.
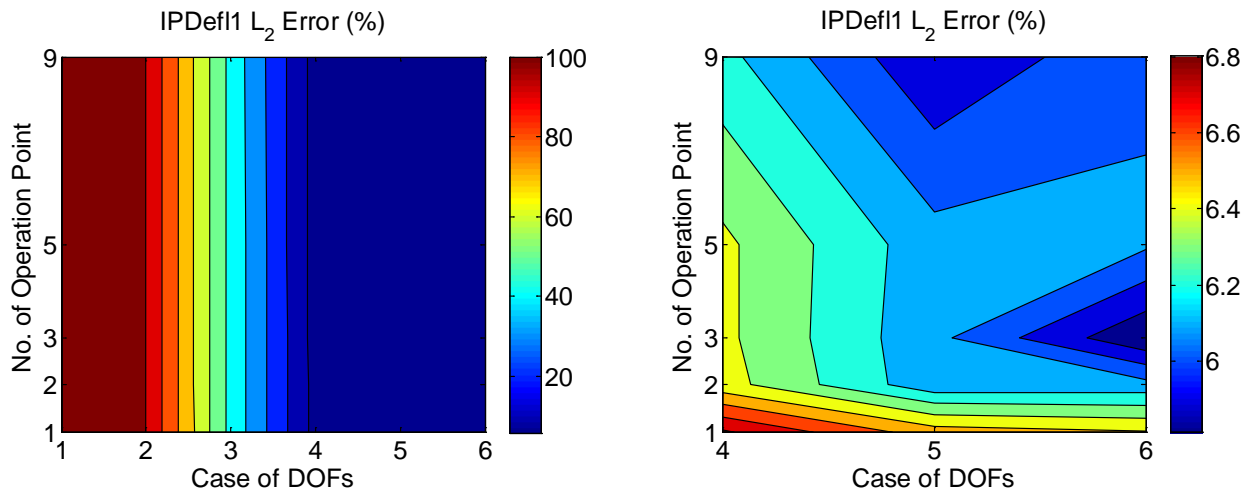
Figure 42 Total error of blade in-plane deflection at different combinations of DOF &OP

From analysis in Chapter 4 and 5, the dominant factor of blade in-plane bending moment is the number of DOFs, and the optimized number of OP is 2. The contours are made with respect to different combinations of DOFs and OP as shown in Figure 43. From the left figure it can be seen that the dominant factor is DOFs and the threshold of No. of DOFs is from case 3 to 4. That indicates the blade flapwise and blade edgewise DOFs are very important, which coincides with results in Chapter 4. For DOF cases 4, 5 and 6, we plot a separate contour to look into more details as shown in the right figure. The range of error is from about 1.6% to 1.9%, which means there is almost no improvement. Therefore, it has little meaning to include more than 4 DOFs and more than 2 OPs.
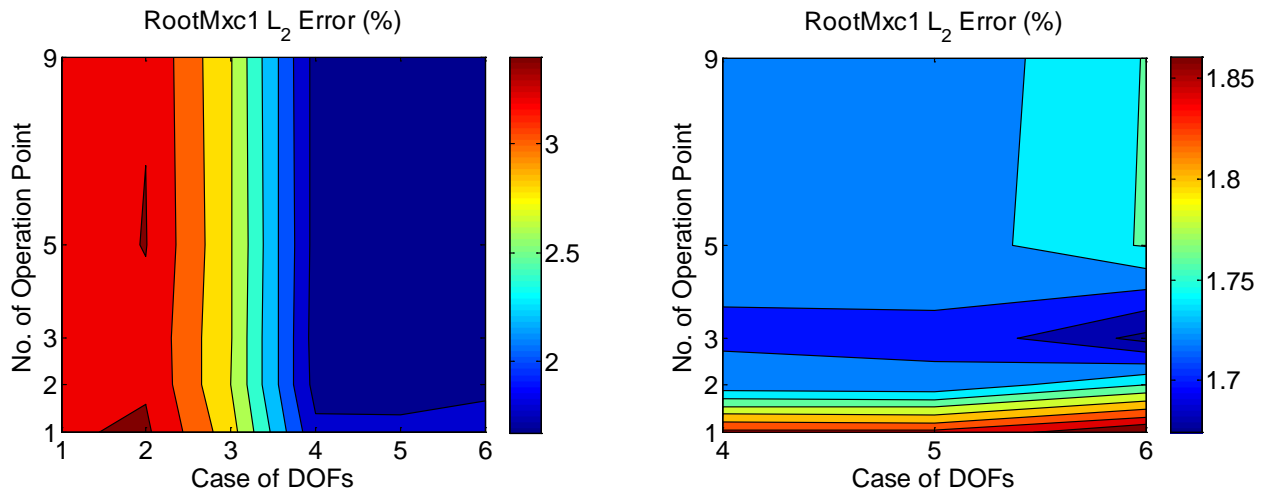
Figure 43 Total error of blade in-plane bending moment at different combinations of DOF &OP

Figure 44 shows contours with respect to different combinations of DOFs and OP. From the left figure it can be seen that the dominant factor is DOFs and threshold of No. of DOFs is from case 2 to 3, with the blade flapwise DOF considered. That means blade flapwise DOF is the most important DOF, which agrees with results in Chapter 4. For DOF cases 4, 5 and 6, a separate contour is plotted to look into more details. As shown in Figure 44 (right), the range of error changes from about 2.4% to 3.6%, which means there is some improvement. The dominant factor is still the number of DOFs. What's more there is no need to apply No. of OP larger than 2 and no need to apply DOF case 6, since there is no improvement in that area.

Figure 44 Total error of blade out-of-plane bending moment at different combinations of DOF &OP

Figure 45 shows the total modeling error of blade torsional moment at different combinations of DOFs & OP. From the left figure it can be seen that the dominant factor is DOFs and threshold of No. of DOFs is from case 3 to 4. That means the blade edgewise DOF should be considered to achieve an accurate result. For DOF cases 4, 5 and 6, a separate contour is shown in Figure 45 (right) to look into more

60

details. It can be seen that the range of error is from about 9.6% to 11%, and the dominant factor is still the number of DOFs. What's more there is no need to apply No. of OP larger than 2 and no need to apply DOF more than 5, since there is no improvement in that area.
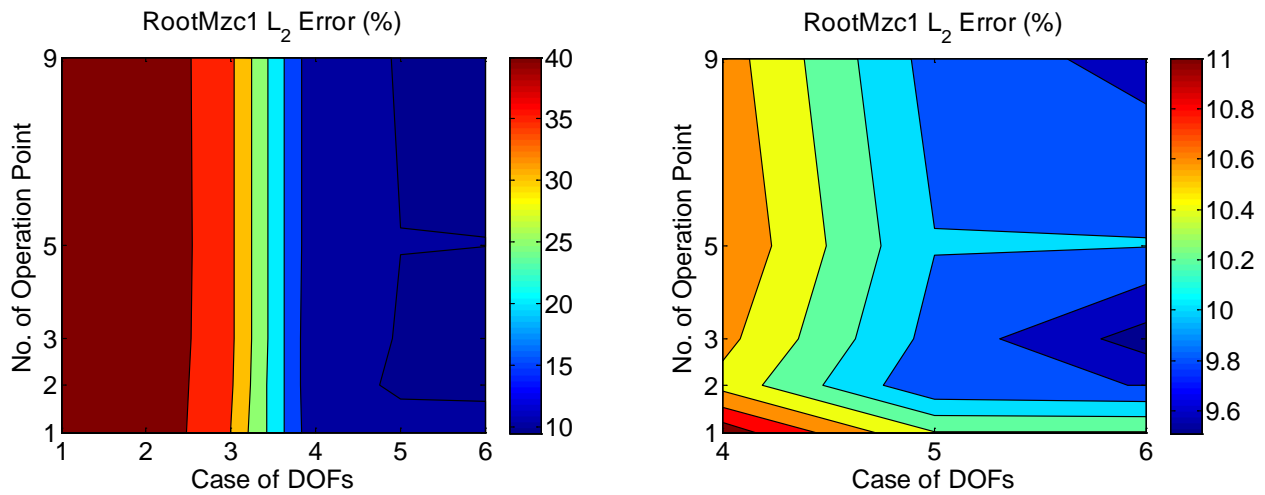
Figure 45 Total error of blade torsional moment at different combinations of DOF &OP

6.3 Tower properties

Figure 46 displays the total modeling error of thrust force at different combinations of DOF and OP. It can be seen clearly that the dominant factor is the number of DOFs, while the number of OP almost has no influence. That indicates the most efficient way to decrease total modeling error is to increase the number of DOFs. The range of error is from about 2% to 7%, which means there is much improvement by increasing DOFs. There are two threshold of DOF case 3 and case 5, which means the blade flapwise DOF and tower fore-aft DOF should be included to get an accurate result, which agrees with the results in Chapter 4. It can be conclude that with 1 OP and DOF case 5, the error is very small and more OP and DOFs do not increase the accuracy.
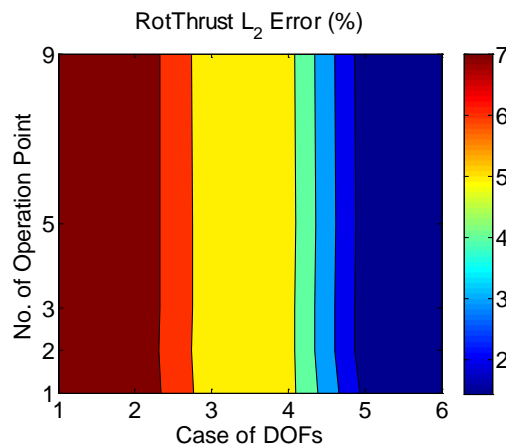
Figure 46 Total error of thrust force at different combinations of DOF & OP

61

From analysis in Chapter 4, for tower top side-side bending moment, including more DOFs can decrease the DOFs error. Moreover, in Chapter 5, it can be concluded that best choice for the number of OP is 1, since the linearization error will become larger as the number of OP increasing.

Figure 47 displays the total modeling error of tower top side-side bending moment at different combinations of DOF and OP. It can be seen clearly that increasing the number of OP does not decrease the error. What's more the error becomes even larger as the number of OP increase. The smallest error occurs when OP is 1 and DOF case 6. The optimized number of operation point is 1. And the DOF case must larger than 3. Note that there is relatively large error at DOF case 2, which means the drivetrain flexible DOF increase the error. Therefore it is better to not include the drivetrain DOF.
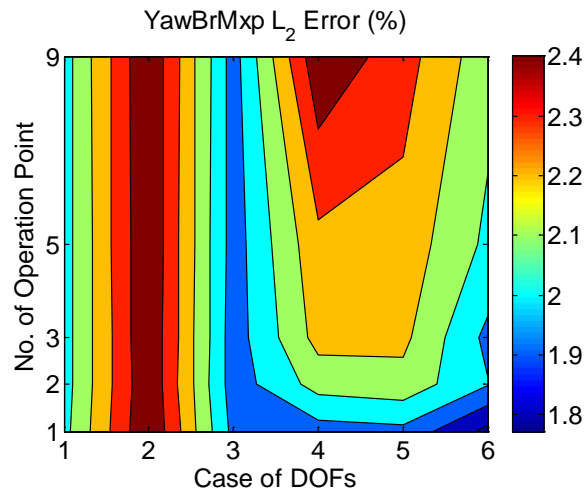
Figure 47 Total error of tower top side-side bending moment at different combinations of DOF &OP

Figure 48 displays the total modeling error of tower top fore-aft bending moment at different combinations of DOF and OP. Similar to the total modeling error of tower top side-side bending moment, increasing the number of OP does not decrease the error. What's more the error becomes even larger as the number of OP increase. The largest error occurs at 9 OP. The optimized number of OP is 1, which coincides with the results in Chapter 5. If the number of OP 1 is chosen, the more DOFs are included the smaller the errors are.
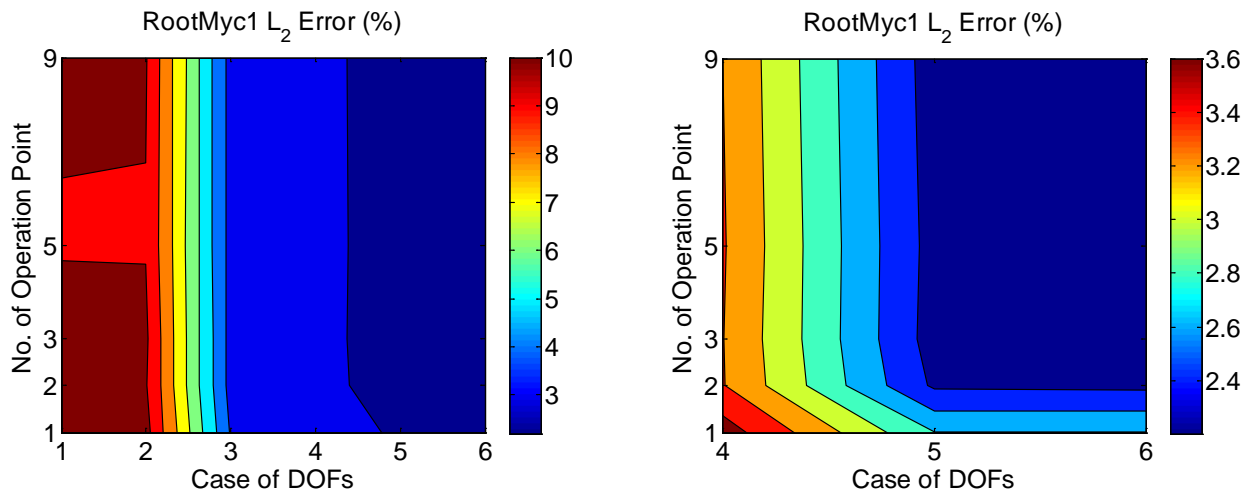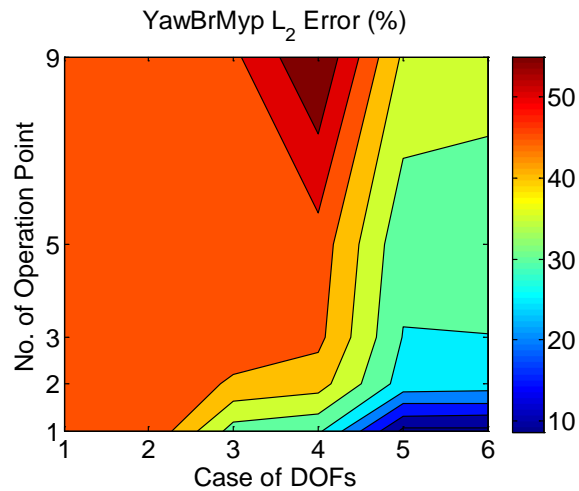
Figure 48 Total error of tower top fore-aft bending moment at different combinations of DOF &OP

Figure 49 displays the total modeling error of tower top torsional moment at different combinations of DOF and OP. It can be seen clearly that increasing the number of OP does not decrease the modeling error. What's more, the error becomes even larger as the number of OP increases. The largest error occurs at 9 OP, which coincide with the results of chapter 5. The optimized number of operation point is 1. If the number of OP 1 is chosen, the more DOFs are included the smaller the errors are.
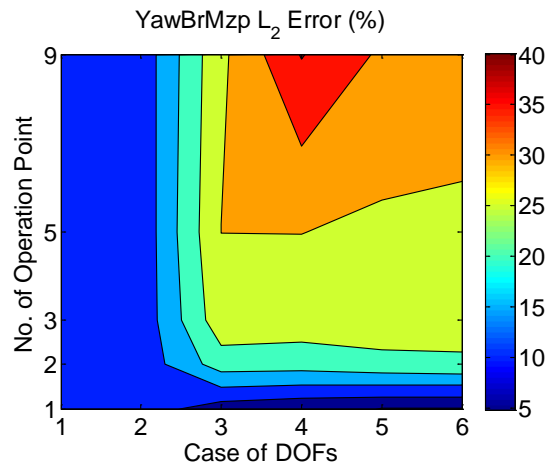
Figure 49 Total error of tower top torsional moment at different combinations of DOF & OP

6.4 Summary

According to the above analysis, the relative importance of DOF and OP is revealed and listed in Table 21 for different quantities. For power production properties, the dominant factor is the No. of OP, which means the most efficient way to increase modeling accuracy is to increase the No. of OP. For blade and tower properties, the dominant factor is the No. of DOFs. Noted that the No. of OP of tower properties should not be larger than 1.

Table 21 Dominant factors for different properties

	Dominant factor
Power production properties	OP
Blade properties	DOFs
Tower properties	DOFs (OP must be 1)

Chapter 7 Ice on Blade Influence and Detection

7.1 Ice on blade influence

Wind power in cold climate regions is attractive due to relatively high wind speed and low population density. However, ice on wind turbine blades remains one of the main challenges and becomes more significant when turbine size has increased (Laakso T et al. 2003). As for the operation of wind turbines, icing of blades mainly affects wind turbine in two ways: aerodynamics and additional mass to the blades.

The effect on aerodynamics should be considered since change in aerodynamic properties may decrease power output and increase thrust loads. Moreover, it also affects the performance of the controller as well. Additional mass on the blade due to icing yields higher inertia forces on the rotor and may change the natural frequencies of the blade, influencing the fatigue life time.

There are some additional challenges for wind turbines operating under icing condition that need accurate simulation tools. These include ice accretion simulation and estimation of rotor aerodynamics after icing. The most common approach for icing simulations is to couple meteorological information with an ice accretion model. Today, there exist three different types of ice accretion models:

The first approach is to do experiments. There is a limited amount of detailed information available for ice effects on wind-turbine-specific airfoil aerodynamics and associated ice mass effects. Almost of the studies are performed in icing and/or wind tunnels with two dimensional aircraft airfoils (Simo et al., 2016). The most extensive study made at NASA focused on detailed ice accretion effects of three typical aviation airfoils for various atmospheric conditions in two separate wind tunnels. With this extensive study (Addy, 2000), some first statistics for nearly 200 individual icing cases and their effects on airfoil penalties can be summarized.

The second method is numerical simulation by a computational fluid dynamics (CFD) code. Some of the most common models in this category are FENSAP-ICE (Habashi et al., 2004), TURBICE (Makkonen et al., 2001), and LEWICE (Wright, 2002). FENSAP-ICE is a 3D CFD solver that accounts for all ice processes. TURBICE and LEWICE are 2D models designed for the study of ice growth on airfoil cross-sections. These models have been shown to provide reasonable lift and drag responses to icing on wind turbine blade airfoils (Homola et al., 2010 a,b; Virk et al., 2010).

A third approach to modeling icing lies in between these two methods is represented by models such as the Makkonen model (Makkonen,2000), which is part of the ISO standard, and the OMNICYL model (Finstad,1986). These models use empirical relationships to estimate the percentage of incoming particles (collision efficiency) that would impact the cylinder as a function of the wind speed, cylinder diameter, and droplet size distribution. The empirical relationship has been evaluated using wind tunnel

data (Makkonen and Stallabrass, 1987), and was shown to provide a reasonable estimate for the collision efficiency.

In this study the ice model from empirical method summarized from experimental results. The available information for ice effects on wind-turbine-specific airfoil aerodynamics and associated ice mass effects are very limited, especially experimental studies. To get reliable data on how ice on blades influence the aerodynamic coefficient for our NREL 5 MW wind turbine is a challenge. Simo Rissanen (Rissanen 2016) from VTT Technical Research Centre of Finland put a lot of effort on finding validated simulation parameters to represent realistic iced wind turbine behavior under normal power production operation. These parameters can be later used to define design load cases for other cold climate wind turbines.

Iced airfoils were visually divided into four categories (start, light, moderate and extreme icing) to ease comparison of results and derive statistics (Rissanen 2016). Figure 50 displays the ice accretion shapes from various icing categories. As shown in Figure 50 , there is a thin layer of ice on the blade surface in start of icing case, and the blade shape has little changing. For the light icing case, more ice accumulated in the lead edge. For moderate ice case, the airfoil shape changes dramatically. The flow field will be changed a lot. In the extreme icing case, there are several sharp corners in the leading edge and the lift and drag coefficient will change significantly. In total, eight different references are carefully studied in the research of Rissanen. Almost all studies examined are performed in icing and/or wind tunnels with typical two dimensional (2D) aircraft airfoils (Rissanen 2016). All the references are listed in Table 22.
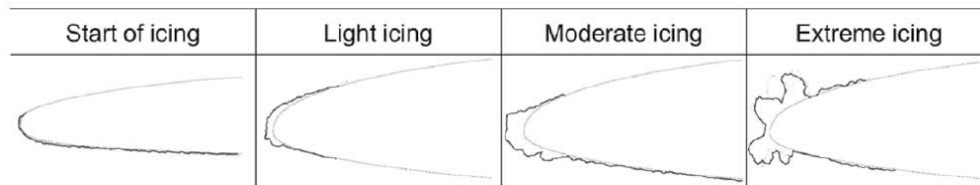
Figure 50 Ice accretion shapes from various icing categories

Table 22 Airfoil lift and drag coefficient measurement studies used in average lift and drag calculations (Simo Rissanen 2016)

	Reference	Case numbers from the references	
		CL	CD
Start	Addy (2000)	202, 225, 237, 128, 142	
	Hochart (2008)	601,621	1, 4
	Addy et al. (2003)	1, 4	202
	Broeren (2010)	202	1126, 1134
	Bragg et al. (2007)	1162, 1134	762
Light	Addy (2000)	607, 610, 622	
	Hochart (2008)	2	2
	Broeren (2010)	1162, 1125	1162, 1125
	Broeren (2002)	322	322
	Bragg et al. (2007)	730kc26	730, 730kc26
Moderate	Addy (2000)	628, 631, 646, 649	
	Tammelin et al. (1998)	B06	
	Hochart (2008)	5	3
	Addy et al. (2003)	212	212
	Broeren (2002)		290
Extreme	Addy (2000)	127, 145, 603, 608, 623, 661	
	Tammelin et al. (1998)	B22	
	Hochart (2008)	6	3, 6
	Addy et al. (2003)	944	944
	Broeren (2010)	1164	1164
	Busch et al. (2007)	horn	2Ds

Based on the eight airfoil icing references, lift and drag coefficients for clean and four types of iced airfoils were extracted. The relative change from clean to iced performance was investigated. We introduce the iced airfoil penalty factor, which is the relationship between clean and iced airfoil performance shown in equation(56).

$$P_L = \frac{C_{L\_ice}}{C_{L\_clean}}, \quad P_D = \frac{C_{D\_ice}}{C_{D\_clean}} \tag{56}$$

Where P_L and P_D are the penalty factor of lift and drag coefficient respectively, C_{L_ice} and C_{L_clean} are the lift coefficient of iced and clean blade respectively, C_{D_ice} and C_{D_clean} are the drag coefficient of iced and clean blade respectively.

The best-fit functions of penalties for both lift and drag coefficients curves are a function of airfoil angle of attack α as follows (Hugues-Salas 2017)

$$P_L(\alpha) = -A\alpha^2 - B\alpha + C$$
$$P_D(\alpha) = D\alpha + E \tag{57}$$

The lift penalty factor is a second order curve while drag penalty factor is a first order function. The detailed penalty factors of four categories of ice on blade are shown in Table 23.

Table 23 Iced penalty factor as function of angle of attack (Simo Rissanen 2016)

Ice category	CL penalty	CL R^2 correl.	CD penalty	CD R^2 correl.
Start	$y=-0.0016\times\alpha^2+0.0046\times\alpha+0.98$	0.97	$y=0.09\times\alpha+1.7$	0.73
Light	$y=-0.0018\times\alpha^2+0.0018\times\alpha+0.97$	0.96	$y=0.08\times\alpha+1.9$	0.87
Moderate	$y=-0.0012\times\alpha^2-0.0023\times\alpha+0.95$	0.98	$y=0.38\times\alpha+2.7$	0.53
Extreme	$y=-0.0008\times\alpha^2-0.0152\times\alpha+0.91$	0.91	$y=0.30\times\alpha+5.2$	0.52
Average of all	$y=-0.0014\times\alpha^2-0.0017\times\alpha+0.95$	0.99	$y=0.02\times\alpha+3.1$	0.02

For the NREL 5 MW wind turbine blade, 2 cylinders and 6 airfoil shapes are applied in different blade sections. The total length of blades is 64.5 m. The blade section shape and the corresponding (beginning) radius are listed in Table 24. For the iced condition, the penalty factors in Table 23 are applied on the 6 airfoil sections. We assumed that the aerodynamic properties of two cylinders are not influenced by ice, since the blade root position and blunt shape are less affected by ice.

Table 24 Airfoil schedule for NREL 5MW blade (Brian R. Resor 2013)

Blade Section Shape	(Beginning) Radius (m)
Cylinder 1	1.8
Cylinder 2	5.98
DU W-405	10.15
DU W-350	15.00
DU 97-W-300	20.49
DU 91-W2-250	26.79
DU 91-W-210	34.22
NACA 64-618	42.47

The feasibility of the above empirical method for the current study can be discussed as follows:

(1) Firstly, the experimental data can be considered as reliable and typical. The experimental data for fitting the penalty factor are all from NACA wind tunnel experiments for investigating aircraft icing problem. The airfoils types in the experiments are typical. The experiments of Addy includes 3 kinds of airfoils, which are 36-inch chord two-dimensional commercial transport and business jet models, IRT general aviation model and LTPT general aviation model (Addy, 2000). The other references listed in

Table 22. All use the NACA airfoils as shown in Table 25. The experiments are done in hundreds cases not a single case, and the results are published in great detail, therefore, the data can be considered as reliable.

Table 25 Airfoil used in the experiments

Reference	Airfoil
Addy, 2000	Commercial transport and business jet models, IRT general aviation model, LTPT general aviation mode
Bragg, 2007 & Broeren, 2002,2010	NACA 23012
Busch, 2007	NACA 0012
Hochart, 2008	NACA 63 415
Tammelin, 1998	NACA 4415

(2) Secondly, the curve fit method is suitable for the model based ice detection. Researcher Simo Rissane, from the Technical Research Centre of Finland, applied a relatively uniform curve fit of all the experimental data of different airfoils. The goal was to find average airfoil properties that correspond with typical icing events and suggested the curve fit parameters can be later used to define design load cases for other cold climate wind turbines. Of course a general method does not perfectly suitable for one certain airfoil. However one specific example is not very persuasive. The influence of aerodynamic properties is very sensitive to the shape of ice accumulating on the blade leading edge. Moreover, the icing shape could be very different at different temperature, humidity rotation speed and icing time. Therefore the best choice would be using the curve fit of different kinds of ice on blade.

(3) Thirdly, the icing on blade does not uniformly distribute on all blade sections. In most cases, there is more ice on the blade tip than blade root. It is very difficult to estimate what is the ice difference on different blade sections. As a simplification, the penalty factor of all blade section is assumed the same. This approximation will induce some inaccuracy. However, the change of blade tip aerodynamic properties influences most comparing to the other sections. Therefore, the estimation of blade tip aerodynamic change is the most important. As introduced before, the estimation of the blade tip airfoil is relatively accurate.

Figure 51 displays the lift and drag coefficient of NREL 5 MW wind turbine blade tip section (NACA 64-618) at different angles of attack. The other 5 blade section aerodynamic coefficients of iced and clean blade cased are displayed in appendix A5.

As shown in Figure 51, lift coefficients decrease and drag coefficients increase for all the ice on blade cases comparing with the clean blade. A dramatic drop in lift coefficient occurs when the angle of attack

is larger than 10 degrees. Moreover the lift coefficient decreases more and more as more dramatic ice shapes accumulated. In terms of drag coefficient, significant increase occurs when the angle of attack is larger than 10 degrees. The drag coefficients of moderate ice case and extreme ice case are similar and increase much more start ice and light ice cases.
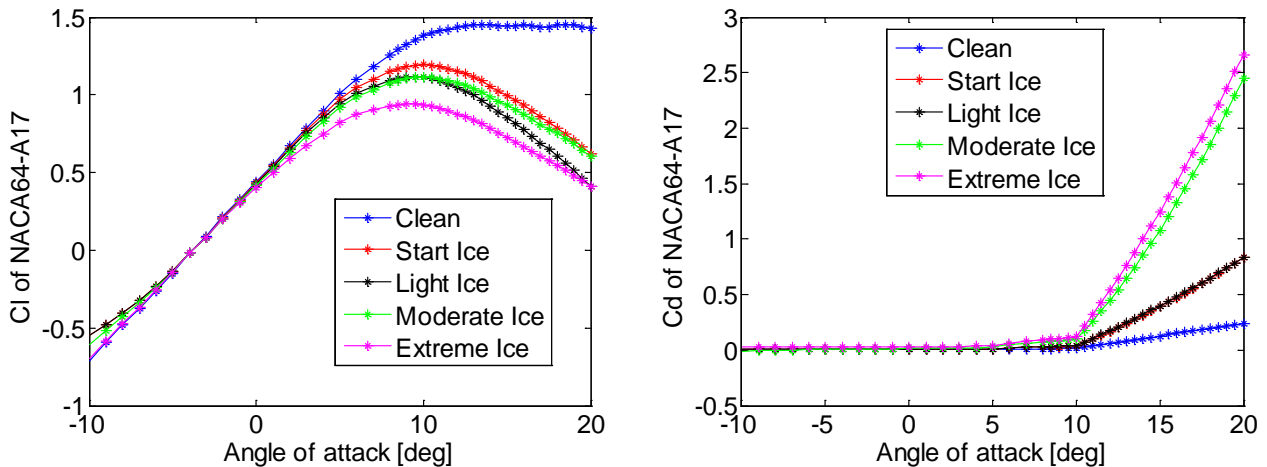
Figure 51 Lift (left) and drag (right) coefficient of NREL 5 MW blade tip section at different angle of attack

The explanation for lift decrease and drag increase is shown in Figure 52. The left figure shows flow around blade without ice, and the right figure shows flow around blade with ice. If there is ice on blade, the flow separation point is near the leading edge, and there is more turbulence on both below and above blade. The lift force is due to the pressure difference between the upper and lower side of blade. If there is ice on blade, there is turbulence on the lower side. Therefore, the pressure difference decreases and the lift force decreases. The drag force is induced by the pressure difference between the fore and aft of blade. If there is ice on blade, there is more turbulence on the aft side. Therefore, the pressure of blade aft part decreases. As a result, the drag force increases.
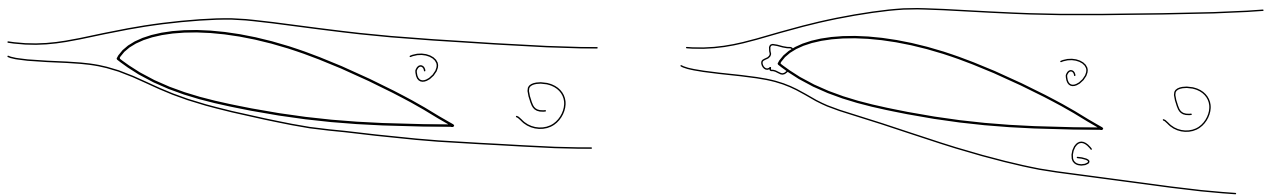
Figure 52 Illustration of flow without and with ice

Ice mass formation on the blades depends on parameters like wind velocity, ambient temperature, liquid water content, median volume diameter and duration of the icing event. All these parameters vary stochastically in space and time. The parameters on blade tip and root are quite different. Therefore ice

70

accumulation on the wind turbine blades is not uniform along the blade length. More ice accumulates away from the blade root as it sweeps through a larger area in rotation and collects more ice. In order to certify wind turbines and their components for the cold climate operation, GL (Germanischer Lloyd, 2010) proposed a guideline that defines the maximum ice mass distribution on the blade to calculate loads acting on the turbine in various design load cases. According to GL guidelines, the mass distribution shall be assumed at the leading edge. The ice mass distribution increases linearly from zero in the blade root to the value μ_E at half radius. Thereafter it remains constant up to the maximum value at the blade tip. The value μ_E is calculated as following

$$\mu_E = \rho_E \cdot k \cdot c_{min} \left(c_{max} + c_{min} \right) \tag{58}$$

Where μ_E is the mass distribution on the leading edge of the rotor blade at half the rotor radius [kg/m]. ρ_E is the ice density assumed as 700kg/m^3. Parameter k can be calculated as $0.00675 + 0.3\exp\left(-0.32R/R_1\right)$. R is rotor radius in meter and R_1 is 1 meter. c_{max} is the maximum chord length in meter and c_{min} is the chord length at the blade tip, linearly extrapolated from the blade contour in meter.

Figure 53 displays the ice mass on blade and blade mass distribution of NREL 5 MW wind turbine. Table 26 shows the ice mass of different cases and the percentage of ice mass compared to blade mass. As shown in the Figure 53, the ice accumulates much more on blade tip than blade root, and the ice accumulation of extreme ice case is significant. From the left figure, we can hardly identify the mass distribution difference between clean blade and iced blade of start, light and moderate ice cases. However the difference between clean blade and extreme iced blade is significant. As shown in Table 26, the total mass of clean blade is about 17613kg, and the accumulated ice of extreme ice case is about 10.66% of clean blade mass, which cannot be neglected. For the other cases, the ice mass is very small.
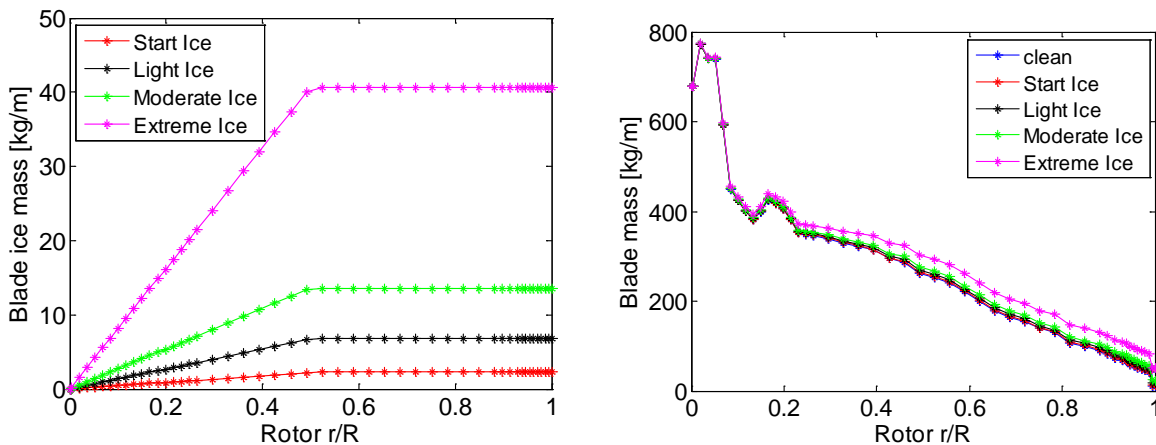
Figure 53 NREL 5 MW wind turbine blade ice mass (left) and blade mass (right) distribution

Table 26 Ice mass of different ice on blade cases

Case	Start	Light	Moderate	Extreme
Ice Mass [kg]	104.306	312.917	625.835	1877.5
Percentage	0.59%	1.78%	3.55%	10.66%

In terms of wind turbine operation, the changes in aerodynamics and blade mass will change the operational profile. Figure 55 and Figure 56 show the change of operational profile. The changes can be clarified into three aspects:

(1) Ice on the blade increases the rated wind speed. The rated wind speed has significant meaning for wind turbine operation. It defines the controller operation regions. At below rated wind speed, the pitch angle remains zero, and the generator torque and rotor speed increase with wind speed. At above rated wind speed, the torque and rotor speed is constant while pitch controller works as described in chapter 3. As shown in the Figure 55 and Figure 56, for clean blade case the rated wind speed is 11.4 m/s. For start ice and light ice cases the rated wind speed increase a little to about 12 m/s. The change of rated wind speed for moderate ice and extreme ice are significant to around14 m/s and 17 m/s respectively.

The reason for this phenomenon is illustrated in Figure 54. The lift force of iced blade L_{ice} is smaller than clean blade L_{clean}, while the drag force of iced blade D_{ice} is larger than clean blade D_{clean}. As a result the rotor torque of iced blade Tq_{ice} is also smaller than that of clean blade Tq_{clean}. If the aerodynamic torque is smaller, the generator power is also smaller than it should be. Furthermore, to make the ice mass rotate with blade also consumes some energy. Therefore the rated power of 5 MW can be reached at a relatively higher rated wind speed.
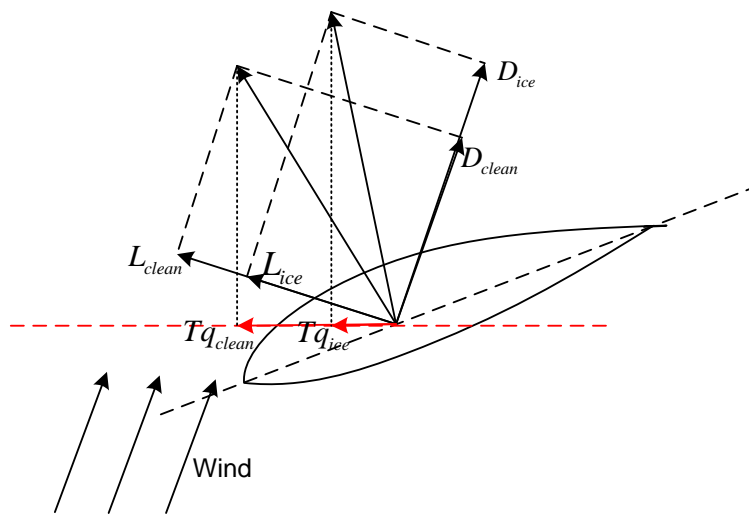
Figure 54 Illustration of torque force change

(2) For above rated wind speed condition, torque, rotor speed and power remain to their rated values. However pitch angle of iced blade is smaller than clean one under same wind speed. For variable speed pitch regulated wind turbines, the pitch controller is designed on the basis of the power curve for a clean blade to adjust the pitch angle in high wind speeds to maintain constant power production. Due to the change of lift and drag force, the pitch angle should be adjusted. The overall trend of pitch angle at above rated wind speed is similar, and the angles of iced blade are smaller than that of cleaned one. Table 27 shows the pitch angles of iced blade and clean blade at wind speed of 18 m/s.

Table 27 Pitch angle at wind speed 18 m/s

Case	clean	Start	Light	Moderate	Extreme
Pitch Angle[deg]	14.93	14.50	14.31	13.75	12.69

(3) For below rated wind speed condition, the torque controller works while pitch controller does not work. As a result the pitch angle remains zero. For torque, rotor speed and power, values of iced cases are smaller than that of clean blade. The reason for this phenomenon has been shown in Figure 54. The torque decreases due to the decrease of lift force and increase of drag force, as well as the extra ice mass. Therefore the power production becomes small.

From the power production point of view, ice on blade decreases the power production at below rated wind speed and has little influence on above rated wind speed (adjusted). Therefore it is meaningful to detect and remove ice and to maximum the power production.
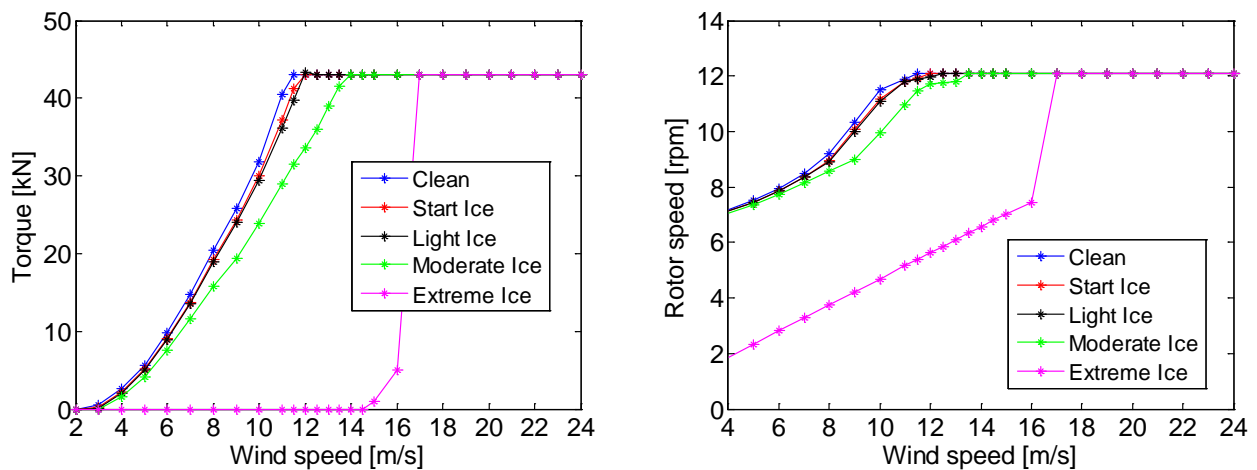
Figure 55 Generator torque (left) and rotor speed (right) at different wind speed
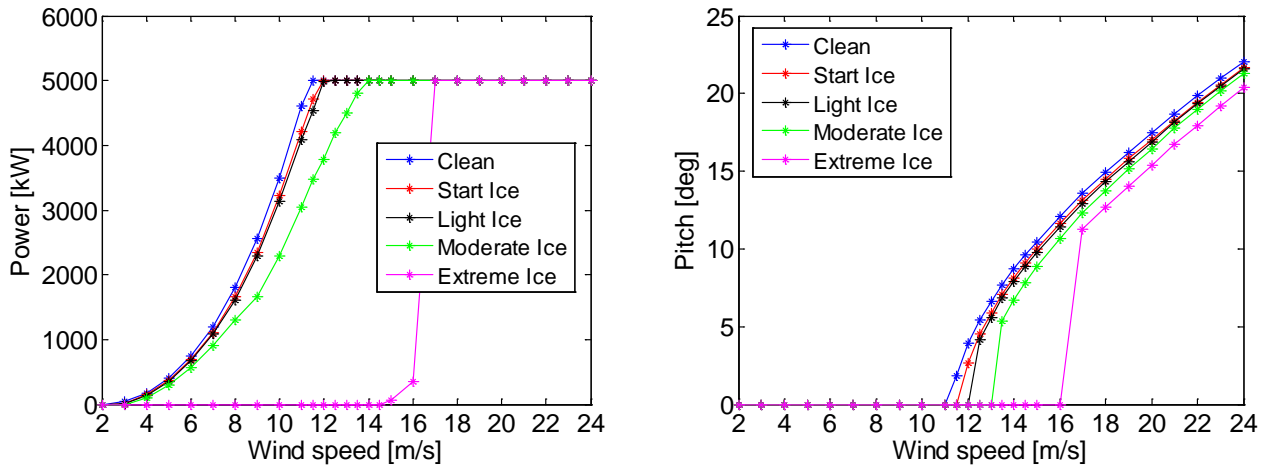
Figure 56 Power (left) and pitch angle (right) at different wind speed

Noted that in steady state condition, the power, torque and rotor speed remain constant at above rated wind speed condition. However if the wind speed is not constant, the quantities mentioned before have slight differences between iced blade and cleaned blade. Figure 57 displays the power output for different cases under varying above rated wind speed and the difference of power between iced blade case and clean blade case. The difference is partly due to dynamic effect that the iced case can not follow clean blade case well. At above rated wind speed, the pitch regulator is PI controller. The parameters P and I of clean blade case cannot perform well in ice on blade cases.
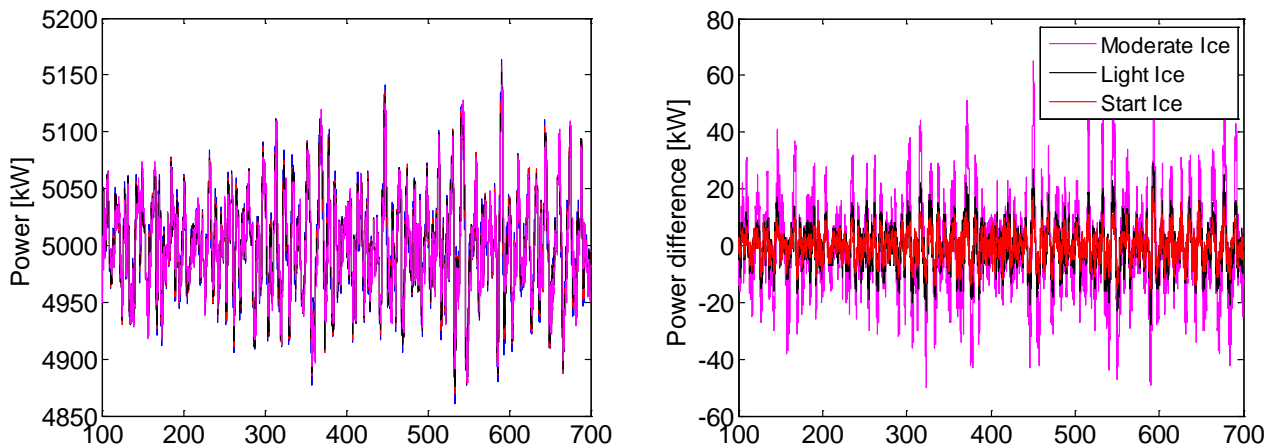
Figure 57 Power (left) and power difference (right) under variable wind speed

Figure 58 and Figure 59 display the influence of ice on blade for quantities related with loads and deflection. The thrust force and tower top side-side bending moment are two representative load examples. At below rated wind speed, the thrust force of iced case is smaller than that of clean blade case, while at above rated wind speed the thrust force of iced case is larger. Large thrust force will induce serious fatigue issues, which is the main harm for ice on blade at above rated wind speed

74

condition. For the tower top side-side bending moment, the value of iced case is no larger than cleaned one. The trend is similar to the torque moment shown in Figure 55 as it is induced by torque. For the blade deflections shown in Figure 59, at below rated wind speed, both out-of-plane and in-plane deflections of iced case are slightly smaller than that of clean one, but become larger in the above-rated wind speed range. The maximum values of iced cases are larger than that of clean case. Therefore it is necessary to detect and remove ice to reduce fatigue damage to the structure.
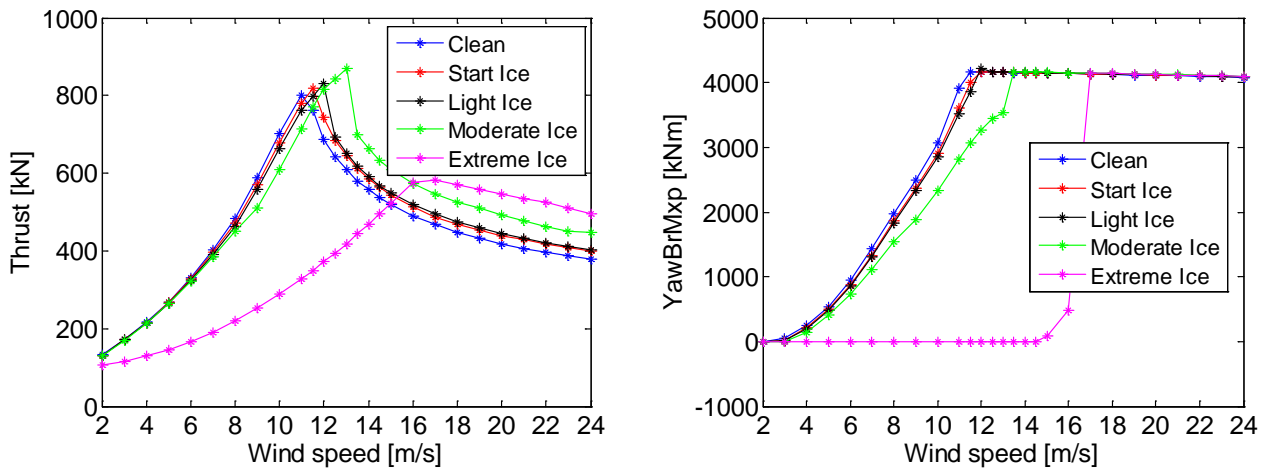
Figure 58 Thrust (left) and tower top side-side bending moment (right) at different wind speed
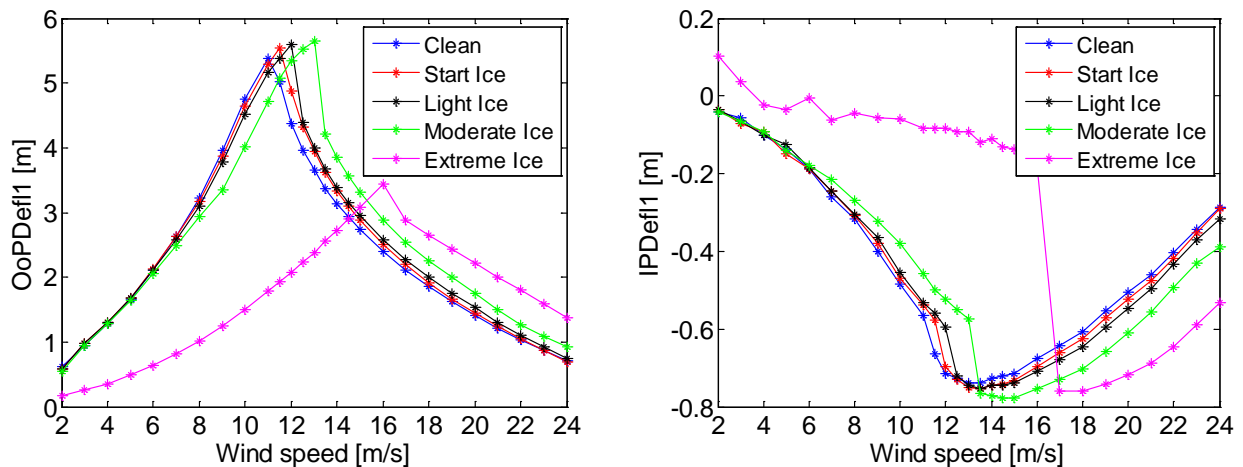
Figure 59 Blade out-of-plane (left) and in-plane (right) deflection at different wind speed

Overall it can be seen from all the figures that the start ice and light ice case cause slight changes for all the wind turbine properties, which means they would be difficult to detect. For moderate ice case, the change is more significant. However for extreme case, there are large changes. We do not focus on the extreme case, since it is very easy to detect. The detection is focus on the other three cases.

7.2 Ice on blade detection

In this thesis, a model-based detection method for wind turbine blade icing is developed. There are three main advantages of the method. Firstly the model-based ice-detection method is based on the measurements that already exist. By applying the wind turbine model, almost any kind of quantities can be determined including displacements, moments, loads and power production related quantities. Therefore the quantities with measurement value can be selected to detect ice without additional measurements. Secondly, the detection method can be implemented for any kind of blade aerodynamic changes, not only ice on blade. Any aerodynamic change will induce the change of output comparing with healthy system, therefore aerodynamic change like blade damage and pitch faults can be detected. Thirdly, the linearized healthy wind turbine model can also be applied for design of controllers and state estimators.

The concept of model-based ice-detection is as follows: Firstly ice on blade changes the aerodynamics, such as lift and drag coefficient. The blade mass increases as well. Therefore it can be considered as one wind turbine system changed to a different system. That means the outputs of the two systems, with ice and without ice, are different, even if the inputs are exactly the same. From the ice-detection point of view, if the difference of outputs between iced system and cleaned one is much larger than modeling error, ice on blade can be detected.

The flowchart shows the detection steps, where we neglect the measurement error**.** The measurement error is considered separately in section 7.3. In the ice on blade fault detection, there are two models. One is nonlinear iced model with full DOFs to simulate the real wind turbine with different kinds of ice on blade. The other is linear model with clean blade that represents for the model-based estimator. The input for nonlinear model is wind speed only, while the input for linear model is wind speed from measurement and pitch and torque from the nonlinear model outputs, which are also measurements in reality. It is obviously that there must be some difference between outputs from linear and nonlinear model. This difference is estimation difference, which is a combination of error due to ice on blade and modeling error in my study. If the estimation difference is much larger than the linear modeling error and measurement error, we are sure that the wind turbine is in fault condition.
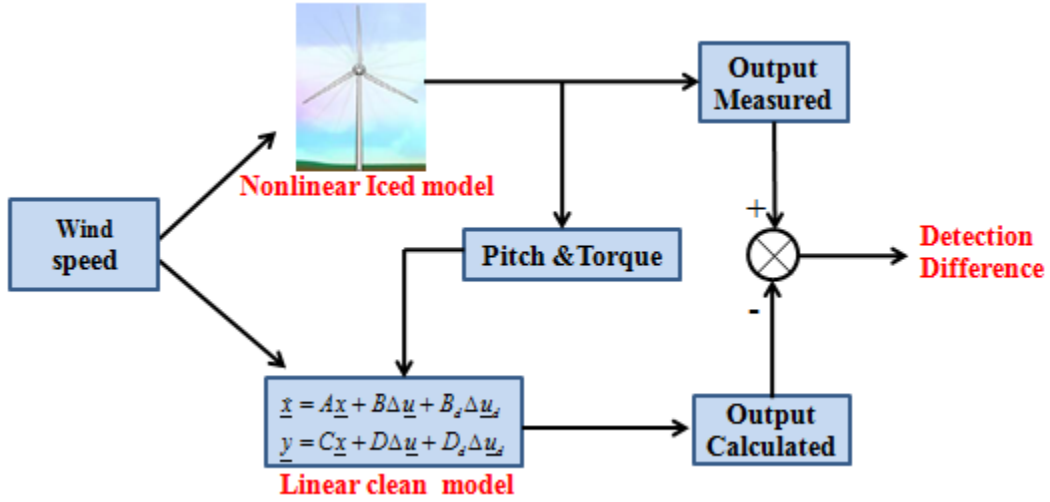
Figure 60 Flow chart of ice-detection concept

Here we introduce a parameter to describe the estimation difference compare with modeling error. The parameter is called normalized ice-detection error, which can be expressed as

$$Capability = D_{est} / E_{model} \tag{59}$$

where D_{est} is the estimation difference and E_{model} is the modeling error. The larger the capability value, the better performance in ice-detection. It should be noted that there is no measurement error included in (59). In an ideal case that the inputs and outputs are accurate, the capability should be larger than 1 to detect the ice on blade. In reality, there can be different sources of uncertainties, e.g. measurement errors. In this case, the capability should be sufficiently large to ensure successful ice-detection. This will be discussed in the next section.

7.3 Measurement for ice-detection

In the above analysis, inputs and outputs are considered as accurate. In reality, there can be errors in the measurements depending on the accuracy of equipment. The influence of measurements error behaves differently depending on whether they are in inputs or outputs. In the following, three cases will be introduced and they will be compared to define the ice-detection capability with measurement error considered.

Figure 61 shows the case that there is no measurement error at all. The difference between output of linear system without ice and nonlinear system without ice is the modeling error E_1. The difference between output of linear system without ice and nonlinear system with ice is the estimation difference D_{est1}. In this condition the ice-detection capability can be defined as

$$Capability = D_{est1} / E_1 \tag{60}$$

77

Figure 61 Definition of modeling error and estimation difference without measurement error

As described before, the inputs of linear system are the wind speed, generator torque and blade pitch. These quantities are from measurement in reality. If the inputs of the linear system are measurements, the outputs are also different from those without any measurement error. That means the measurement error will influence both the modeling error E_2 and estimation difference D_{est2} as shown in Figure 62. In this condition the ice-detection capability can be defined as

$$Capability = D_{est2} / E_2 \qquad (61)$$

Figure 62 Definition of modeling error and estimation difference with measurement error in inputs

Besides input quantities, the outputs of nonlinear system should include measurement error as shown in Figure 63. In that condition, the error due to both modeling and measurement can be expressed as E_3 and the estimation difference is D_{est3}. In this condition the ice-detection capability can be defined as

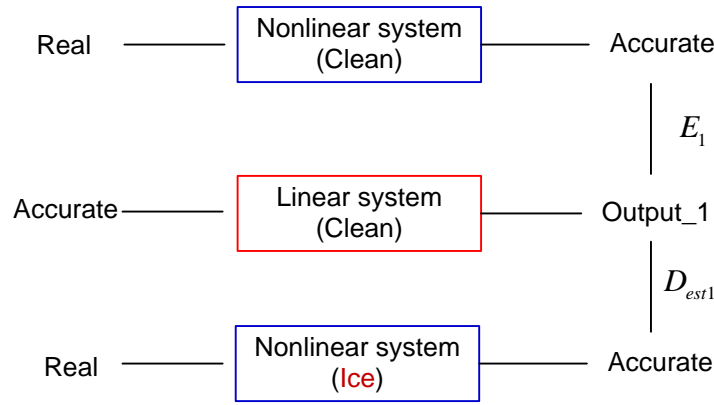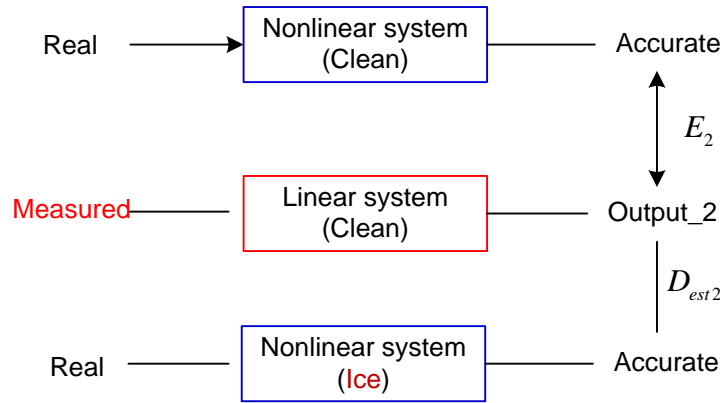$$Capability = D_{est3} / E_3 \qquad (62)$$
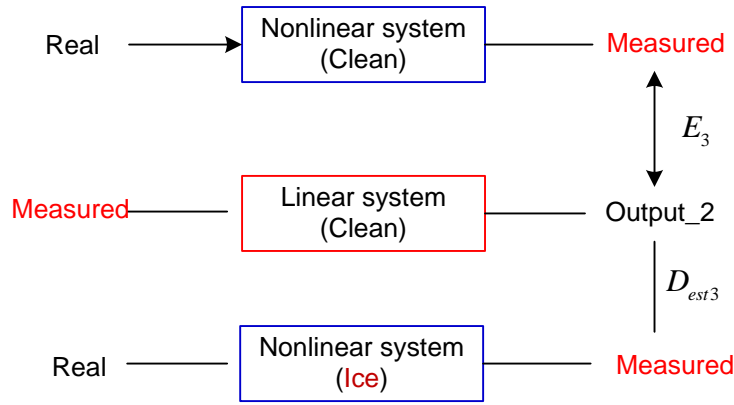
Figure 63 Definition of modeling error and estimation difference with measurement error in inputs and outputs

The measurement error largely depends on the instrument accuracy which varies from case to case. This indicates that the estimation difference and modeling error have to be determined again if the capability defined in (61) or (62) is used directly. A more efficient way is to consider the errors due to modeling and measurement separately. In this study, the measurement errors will be quantified by introducing uncertainty factors as follows

$$\mu' = \frac{D_{est1} / E_1}{D_{est2} / E_2}, \qquad \mu'' = \frac{D_{est2} / E_2}{D_{est3} / E_3} \tag{63}$$

The uncertainty factor μ' reflects the influence of input measurement error on the ice-detection capability. Similarly, the uncertainty factor μ'' reflects the influence of output measurement error on the ice-detection capability. The total uncertainty factor can be determined as

$$\mu = \mu' \cdot \mu'' \tag{64}$$

To have sufficient ice-detection capability, the value defined in (60) should be larger than the total uncertainty factor μ. In practice, the uncertainty factors depend on the sensors in use and should be empirically determined.

Table 28 shows a summary of measurement sensors for different quantities and some comments. The detailed explanations are as follows:

Measurement of wind speed: Wind speed should be measured, since it is an important input of wind turbine system. Anemometers are widely used for measuring wind speed. There are many types of anemometers, such as cup, vane, hot-wire and laser anemometer. According to the International Standard IEC 61400-12, if the anemometer is installed at flat terrain, the accuracy is recommended to be of class 1.7 or better. That means the measurement error should be smaller than 1.7%. If the anemometer

79

is used on nacelle, it will be influenced by the blade rotating. Therefore, the accuracy will be reduced. The recommended accuracy is class 2.5 or better, which means error smaller than 2.5%.

Measurement of power: The electric power of the wind turbine should be measured applying a power measurement device and be based on measurements of current and voltage on each phase. The class of the current transformers shall meet the requirements of IEC 60044-1 and the class of the voltage transformers shall meet the requirements of IEC 60186. The current and voltage can be measured accurately. The error should be less than 0.5%.

Measurement of rotor speed: The variable rotor speed should be measured, as it is an important quantity for motor control and monitoring the wind turbine. Typically, devices widely used are shaft encoders, photoelectric sensors and magnetic rotational speed sensors. All of these sensors send speed data in the form of electrical pulses. Most of these sensors provide simple, reliable and very accurate transducers for revolutions-per-minute (RPM) measurement applications. There is no accuracy requirement in the international standard for wind turbines.

Measurement of deflection: The deflection of wind turbine blade can be measured by position transducers for low frequency, velocity sensors for medium frequency, and accelerometers for high frequency. The accuracy is largely depended on the sensors, and there is no accuracy requirement in the international standard for wind turbines.

Measurement of moment: Currently, most common used moment seniors are the strain gauge and optic fiber optic sensor technologies (Kim, S.-W. 2013). However, sensor technologies currently used in wind turbine blades lack capabilities to measure deflection reliably (Shuai Zhang, 2015). The accuracy largely depends on the measurement method. Fiber optic sensors are more accurate and very expensive. Large amount of calibration is need. And there are no regulations for the moment measurement accuracy in the international standard for wind turbines.

Table 28 Measurement sensors and comments

Quantities	Sensors	Comments
Wind speed	Anemometers (Cup, Vane, Hot-wire)	Error<1% in flat terrain, influenced by blades
Power	Measured current and voltage	Very accurate, error<0.5%
Rotor speed	Shaft, photoelectric, magnetic type encoders	Very accurate
Deflection	Position transducers, velocity sensors, accelerometers	Relatively accurate, depending on the sensors
Moment	Strain gauges, fiber optic sensors	Accuracy depend on sensors, drift occurs

Chapter 8 Ice on Blade Detection一Above Rated Wind Speed

In this chapter we will introduce how to implement the model-based ice-detection method introduced in chapter 7 under above rated wind speed condition. The wind speed time series is the same as that of previous chapters shown in Figure 26 with mean wind speed 18 m/s.

In this chapter, first we will show how to detect ice on blade according to the difference between measurement values and estimated values, as well as how much ice on blade can be detected. Secondly we will show the normalized ice-detection error of different quantities under different DOFs, number of OP and ice categories. The modeling error determined in chapter 6 is a basis for ice-detection.

8.1 Ice-detection for an example case

In this section, a representative above rated wind speed example of ice-detection is studied. The wind speed shown in Figure 26 is applied. A relatively accurate linearized estimation model is used. The case of DOF is DOF 6 with generator mode, drivetrain mode and all the 1st order blade and tower deflection modes. The number of operation points is 9.

8.1.1 Power production properties

Figure 64 shows the estimation difference and modeling error of power and rotor speed at different ice on blade categories. The solid lines are the estimation difference of power and rotor speed and the dashed lines are the modeling error. The trend of estimation difference of power and rotor speed is similar. Therefore we will take the power as an example and describe in detail. For power at start ice case, the estimation difference (3.51%) is more than ten times larger than modeling error (0.35%). From the time series of estimated and measured power of start ice case shown in Figure 65, it can be seen that the measurement value is around 500 kW, while the estimated power at start ice case (blue line) is about 200 kW larger than the measurement. This large difference agrees with the error value shown in Figure 64. The reason can be explained refers to Figure 54. The lift coefficient of clean blade is larger than that iced blade, and the lift force is also larger. Therefore the torque and power of blade without ice are larger as well.

Next let's study the influence of ice categories. As shown in Figure 64 the estimation difference increases as more ice accumulates on the blade (Moderate > Light > Start). This can be verified from the time series of power. The measurement power of start, light and moderate cases are quite close, as the aim of controller is to keep a constant power production at above rated wind speed. While for the estimated values, more ice on blade induces larger power estimation. That means power estimation of moderate ice case is larger than light ice and larger than start ice case. Overall power and rotor speed are good criteria for ice-detection for above rated wind speed case.
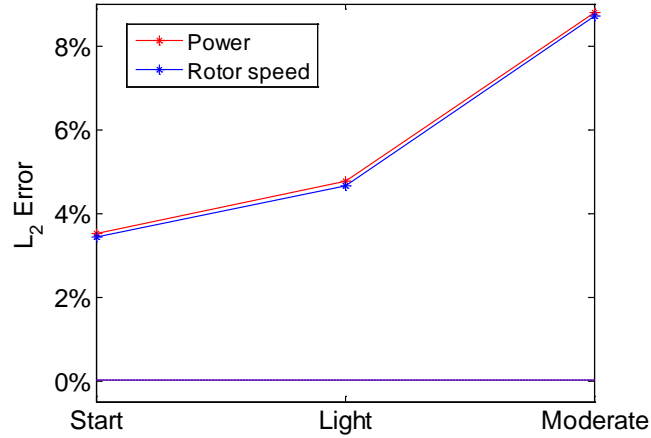
Figure 64 Estimation difference and modeling error of power and rotor speed at different ice on blade categories

Figure 65 Time series of measured power and estimate power under different ice categories

8.1.2 Blade properties

Figure 66 shows the estimation difference and modeling error of blade deflections at different ice on blade categories. The solid lines are the estimation difference of blade out-of-plane and in-plane deflections and the dashed lines are the modeling error. The trend of estimation difference of blade out-of-plane and in-plane deflections is similar. Therefore we will take the blade out-of-plane deflection as an example and describe in detail. For blade out-of-plane deflection at moderate ice case, the estimation difference (12.27%) is a little larger than modeling error (7.59%). From the time series of estimated and measured blade out-of-plane deflection of moderate ice case shown in Figure 67, it can be seen that the measurement value is smaller than the measurement. This large difference agrees with the error value shown in Figure 66.

Next let's study the influence of ice categories. As shown in Figure 66 the estimation difference increases as more ice accumulated on blade (Moderate > Light > Start). This can be verified from the time series of blade out-of-plane deflection. The estimated blade out-of-plane deflection of start, light and moderate cases are quite close. The measurement value of start and light ice cases are close to the estimated values. Only the measurement of moderate ice case is larger than the others.

We can conclude that the blade deflections are not influenced by the change of aerodynamics much. The reason maybe that the blade is twist, therefore lift force decrease and drag force increase results in a hardly changed blade deflections. Overall blade deflections are not criteria for ice-detection for above rated wind speed case.

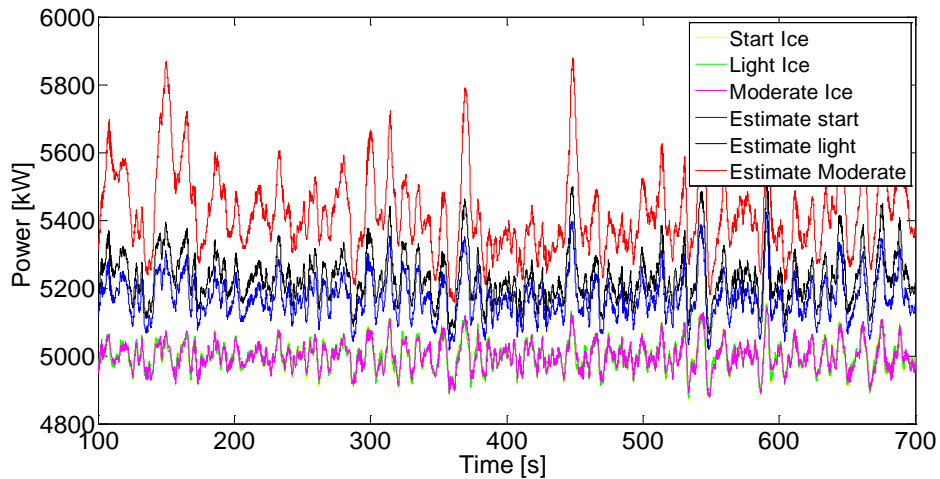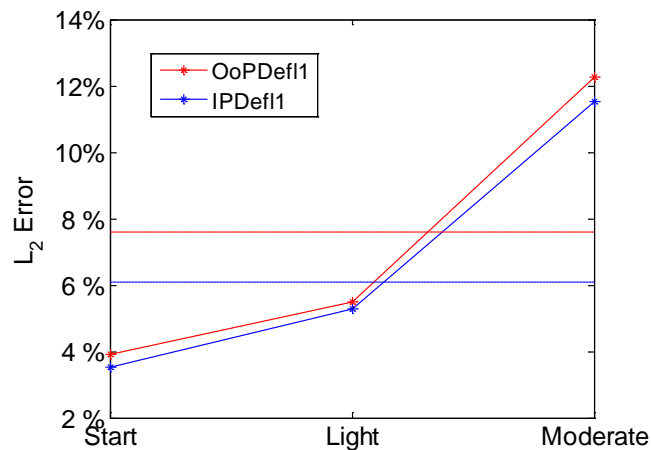Figure 66 Estimation difference and modeling error of blade deflections at different ice on blade categories

Figure 67 Time series (450s-500s) of measured blade deflections under different ice categories

83

Figure 68 shows the estimation difference and modeling error of blade root bending moment at different ice on blade categories. We will take the blade root torsional moment as an example and describe in detail. For blade root torsional moment at start ice case, the estimation difference (20.6%) is much larger than modeling error (9.73%). From the time series of estimated and measured blade root torsional moment of start ice case shown in Figure 69, it can be seen that the measurement value and estimated value are quite different at peaks.

Next let's study the influence of ice categories. As shown in Figure 68 the estimation difference increases as more ice accumulates on the blade (Moderate > Light > Start). This can be verified from the time series of blade root torsional moment. The estimated blade root torsional moment of start, light and moderate cases are quite close. While for the measurement values, more ice on blade induces larger blade root torsional moment.

It is quite interesting that although the modeling error of blade root torsional moment is quite large, however the estimated error is much larger. That means quantities with large modeling error can be good criteria for ice-detection for above rated wind speed case.

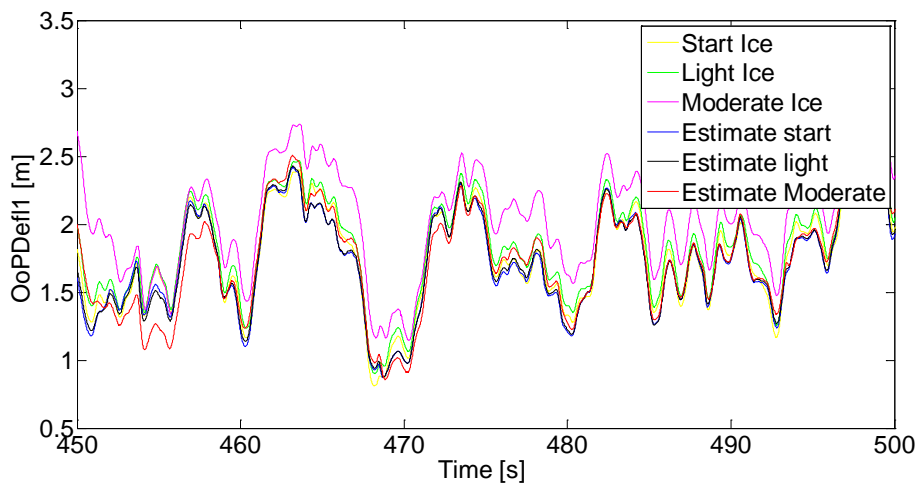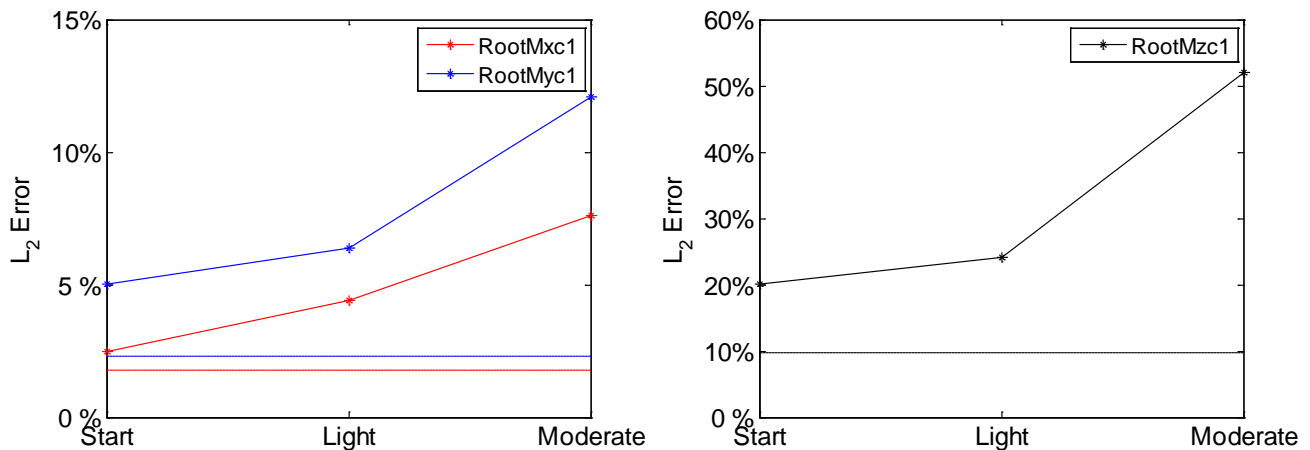Figure 68 Estimation difference and modeling error of blade root bending moment at different ice on blade categories
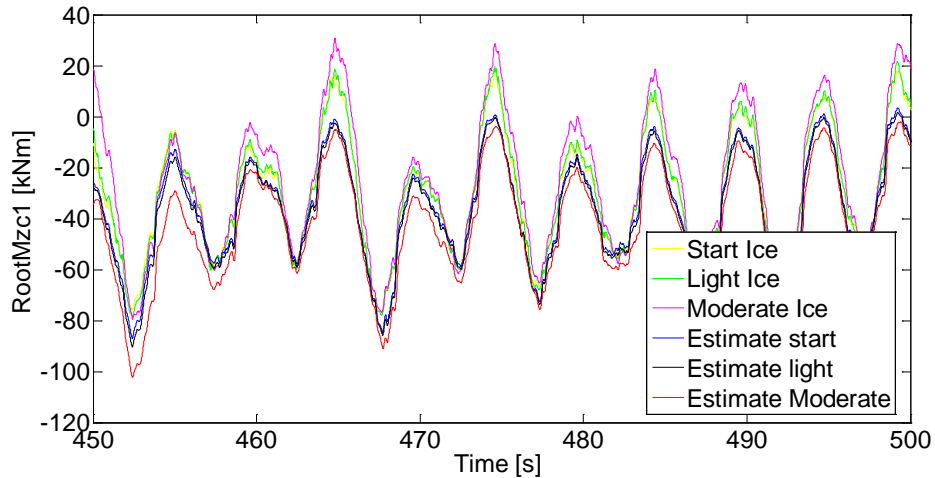
Figure 69 Time series (450s-500s) of measured blade root torsional moment under different ice categories

8.1.3 Tower properties

As shown in chapter 5, the modeling error is very large if the operation point is larger than 1. Therefore the calculation of tower top bending moment in this section is based on 1 OP and DOF case number 6.

Figure 70 shows the estimation difference and modeling error of tower root bending moment at different ice on blade categories. The solid lines are the estimation difference of tower top bending moment and the dash lines are the modeling error. The trend of estimation differences is similar. Therefore we will take the tower top fore-aft bending moment as an example and describe in detail. For tower top fore-aft bending moment at start ice case, the estimation difference (24.7%) is much larger than modeling error (8.67%). From the time series of estimated and measured tower top fore-aft bending moment of start ice case shown in Figure 71, it can be seen that the measurement value and estimated value are quite different.

Next let's study the influence of ice categories. As shown in Figure 70 the estimation difference increases as more ice accumulates on the blade (Moderate > Light > Start). This can be verified from the time series of tower top fore-aft bending moment. The measured tower top fore-aft bending moment of start, light and moderate cases are quite close. While for the estimated values, more ice on blade induces tower top fore-aft bending moment.

Comparing the three quantities, tower top fore-aft bending moment is a very good criterion for ice-detection for above rated wind speed case, followed by tower top torsional moment. While the tower top side-side bending moment is hardly to be used as a detection criteria, since the difference between the modeling error and estimation difference is very small.
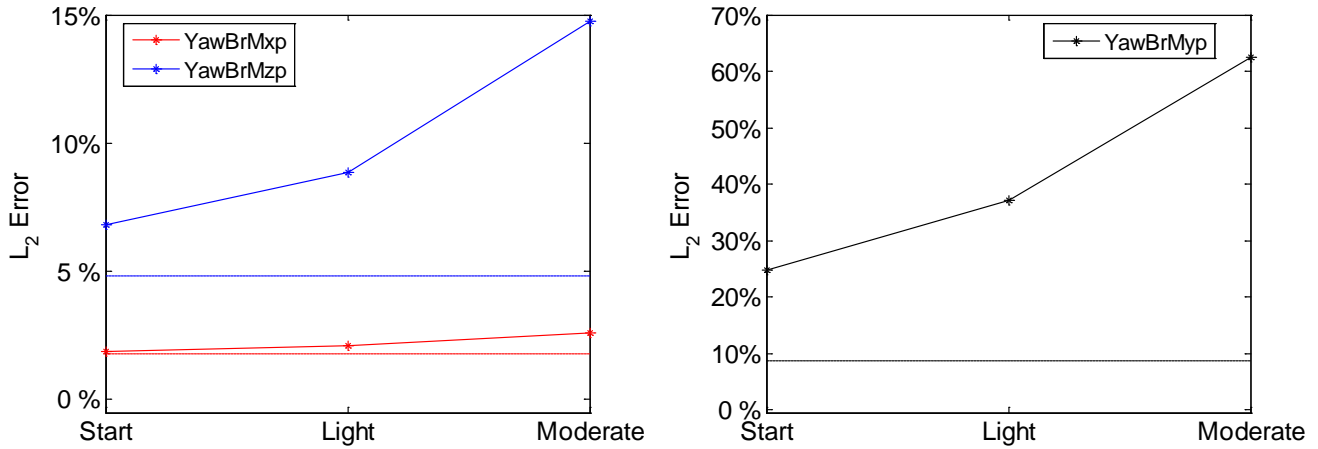
Figure 70 Estimation difference and modeling error of tower root bending moment at different ice on blade categories
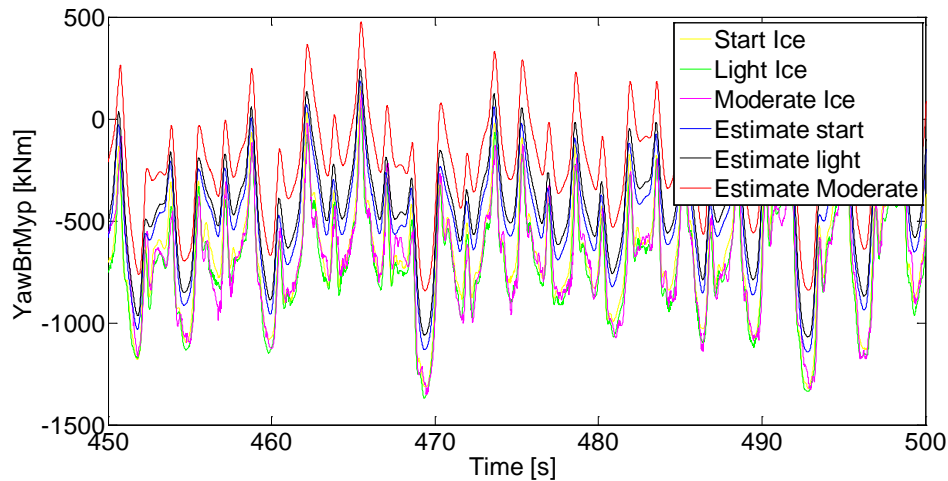
Figure 71 Time series (450s-500s) of measured tower top fore-aft bending moment under different ice categories

8.2 Ice-detection capability

As shown in the last section, the capability of ice-detection depends on the difference between estimation difference and modeling error. For a certain ice condition, a smaller modeling error can significantly improve ice-detection capability. Moreover, according to Chapter 6, there exist many approaches to achieve a better accuracy in linear wind turbine modeling, such as DOFs and OP. These facts inspire us to increase the ice-detection capability by using different modeling methods. Thus, in the following subsections, the influence of modeling methods on ice-detection will be analyzed for different quantities individually.

8.2.1 Power production properties

According to chapter 6, the most efficient way to decrease modeling error is to increase number of OP. The number of DOFs has little influence and 1 DOF is very accurate. Therefore the number of DOF of quantities related to power production is set to 1 (variable generator DOF), and the number of OP changes from 1 to 9. The contours of normalized power and rotor speed error at different No. of OP and ice conditions are shown in Figure 72. As the patterns of power and rotor speed error are similar, the power is analyzed in detail as an example, and the conclusions are also applicable for rotor speed.

The contour can be analysis in two aspects:

(1) For a certain OP model, the normalized ice-detection error, which represents the detection accuracy, can be predicted for a given ice condition. More ice on blade condition induces larger normalized error, therefore easier to be detected.

(2) For a certain ice-condition, more OP induces larger normalized error therefore larger ice-detection capability. For example from 1 OP to 2 OP, the ice-detection capability increases a lot especially for moderate ice case. Moreover, if the number of OP increases further, the capability changes less, although there is still benefit. The increase of OP has even better effects for more severe ice conditions, which indicates that increasing the No. of OP is a highly recommended method for power and rotor speed.
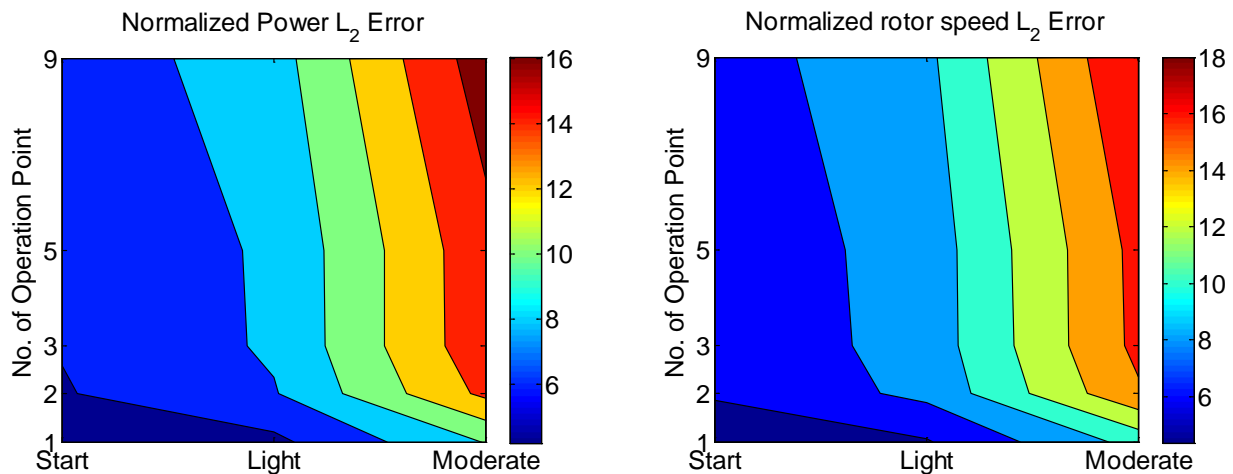
Figure 72 Normalized power (left) and rotor speed (right) error at different No. of OP and ice conditions

8.2.2 Blade properties

According to chapter 6, the most efficient way to decrease modeling error is to the increase number of DOFs. The number of OP has little influence and 3 OP the best choice. Therefore the number of OP of quantities related to blade properties is set to 3, and the number of DOF cases changes from 1 to 6. Figure 73 shows the contours of normalized blade deflection error at different DOF cases and ice

conditions. The patterns of blade deflections are similar, the in-plane deflection (left) is analyzed in detail as an example, and the conclusions are also applicable for the other.

The contour can be analyzed in two ways:

(1) For a certain DOF model, the normalized ice-detection error, which represents the detection accuracy, can be predicted for a given ice condition. More ice on blade condition has larger normalized error, therefore easier to be detected.

(2) For a certain ice-condition, increasing the number of DOF is helpful but limited. The ice estimation difference is no larger than twice the modeling error even in moderate ice condition. Therefore it is not recommended to use blade deflections as criteria for ice-detection.
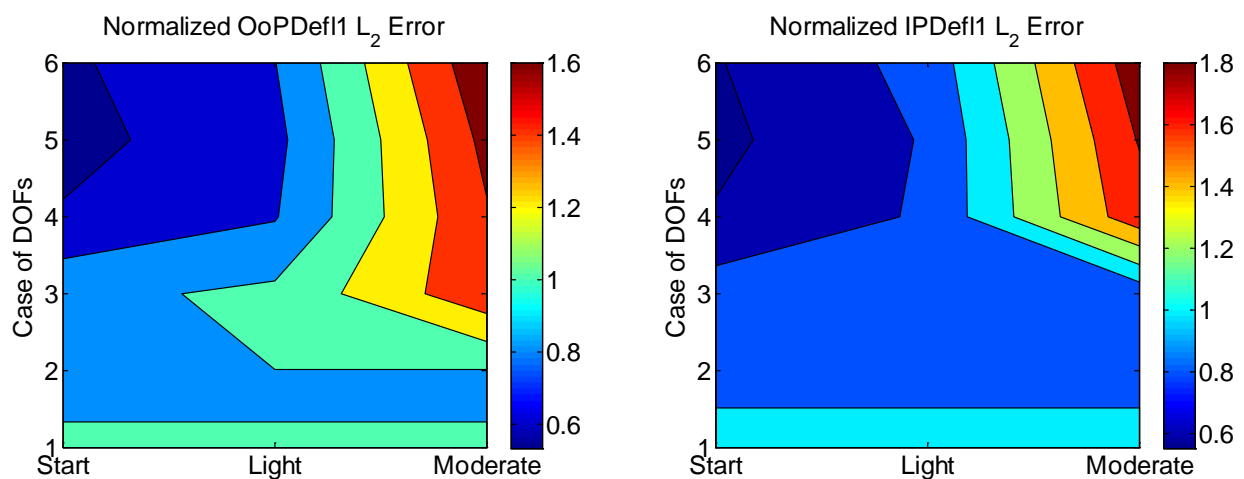
Figure 73 Normalized blade deflection error at different No. of OP and ice conditions

The normalized blade root bending moments are shown in Figure 74 and Figure 75. The patterns are similar:

(1) For a given DOF case, more ice on blade has larger normalized error, and is easier to be detected.

(2) For a certain ice-condition, more DOFs are very helpful for moderate ice-detection especially from 3 DOFs to 5 DOFs (around 4 DOFs), which agrees with chapter 6. Moreover, if the number of DOFs increases further, the capability changes less, although there is still benefit.

The normalized error is larger than 2 in most cases and can be as large as 5 at moderate ice condition. Therefore the blade root bending moment is recommended for ice-detection. For a demanded ice-detection capability, it is necessary to predict how many DOFs are needed. While for a general detection, there should be no less than 3 DOFs.

Figure 74 Normalized blade root in-plane (left) and out-of-plane (right) bending moment error at different No. of DOF and ice conditions
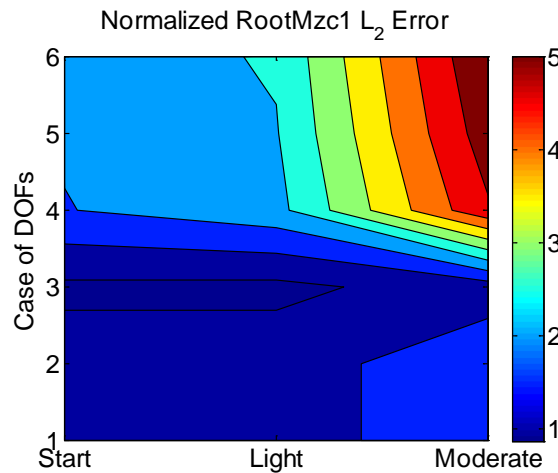
Figure 75 Normalized blade root torsional moment error at different No. of DOF and ice conditions

8.2.3 Tower properties

According to chapter 6, the most efficient way to decrease modeling error is to increase number of DOFs. The number of OP should be 1 since there will large error if more than 1 OP is selected. The number of DOF cases changes from 1 to 6. The contours of normalized tower top bending moment error at different DOF cases and ice conditions are shown in Figure 76 and Figure 77. The patterns of blade deflections are similar, but differ in detailed local regions. Thus the quantities should be analyzed individually.

For the tower top side-side moment shown in figure (left), the increase of DOF is helpful but limited. The value of normalized error is quite small, which means the difference between estimation difference and modeling error is small. Therefore it is not recommended to use tower side-side moment as ice-

detection criterion. For the tower top fore-aft moment shown in figure (right), at least 5 DOF are needed for ice-detection. There is little improvement if 6 DOFs are applied. It is suitable criteria for both light and moderate ice-detection. For the tower top torsional moment shown in Figure 77, increase of DOF is helpful to increase the ice-detection capability, especially from DOF 2 to DOF 3 and from DOF 4 to DOF 5. This quantity can be used as criteria for moderate ice-detection.
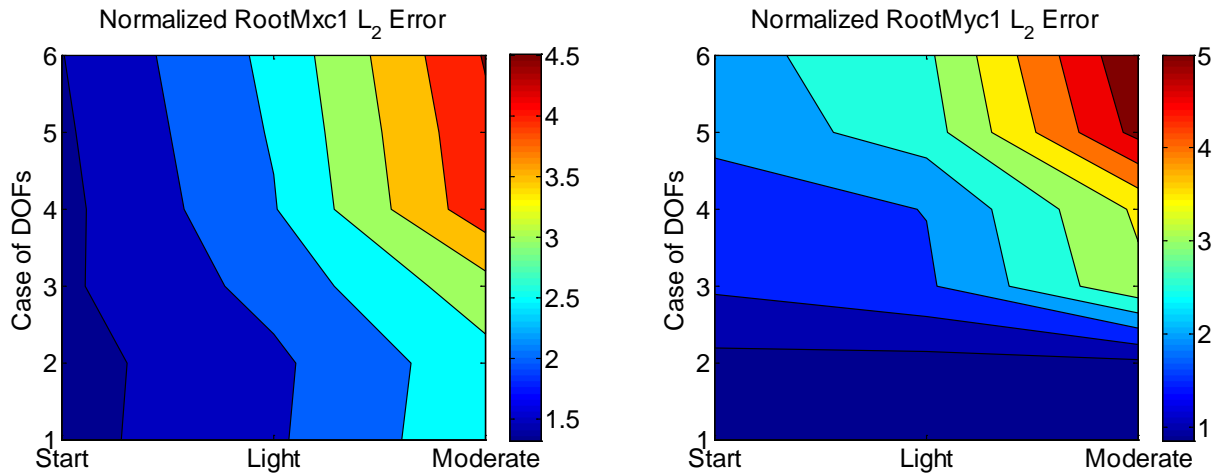

Figure 76 Normalized tower top side-side (left) and fore-aft (right) bending moment error at different No. of DOF and ice conditions
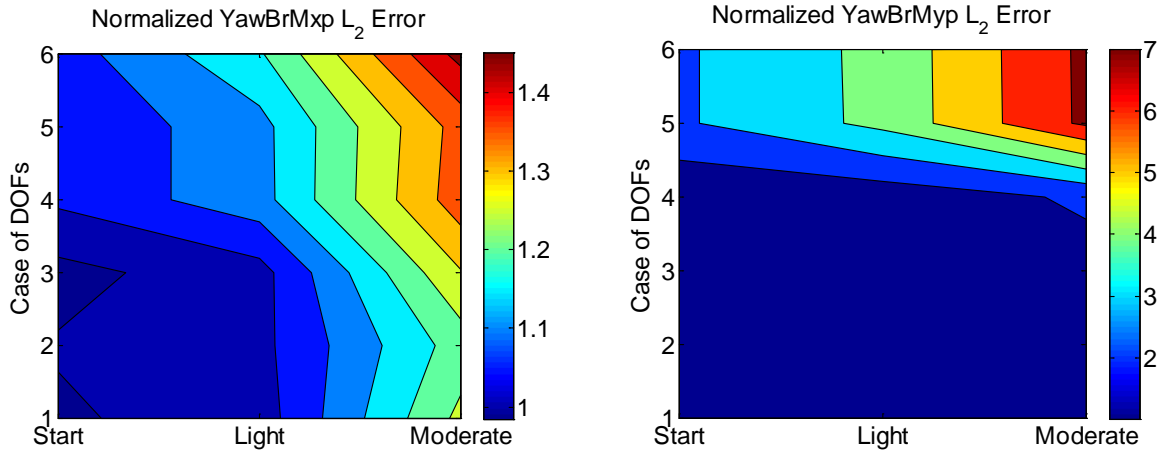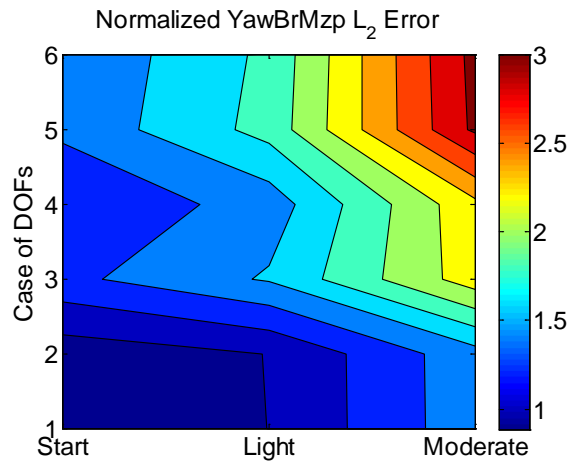

Figure 77 Normalized tower top torsional moment error at different No. of DOF and ice conditions

8.3 Ice-detection considering measurement errors

In the above analysis, all measurements are considered as accurate without measurement error. However in reality, there can be errors in the measurements depending on the accuracy of sensors as introduced in Section 7.3. In this section, the influence of input measurement error and output measurement error will be introduced.

8.3.1 Linear model input measurement error

The inputs of linearized system are wind speed, generator torque and blade pitch. Generator torque and blade pitch can usually be measured with high accuracy. However, the wind speed measurement may include some unavoidable noise. This influence strongly depends on the measuring equipment, which indicates that the impact can be different from case to case. In order to explain how to consider input measurement error and have more understanding about the influence of wind speed measurement error, a case study about different wind measurement error is conducted. It is assumed that the wind measurement error is random value with different error ranges.

Table 29 displays the wind speed measurement error range. As shown in Table 29, case WE_0 is the accurate wind speed, case WE_0.5 with measurement error varies from -0.5 m/s to 0.5 m/s randomly, case WE_1.0 with measurement error varies from -1.0 m/s to 1.0 m/s randomly, case WE_1.5 with measurement error varies from -1.5 m/s to 1.5 m/s randomly, and case WE_2.0 with measurement error varies from -2.0 m/s to 2.0 m/s randomly. Figure 78 shows part time series of different wind measurement with error comparing with accurate wind speed. In order to achieve reasonable results, here the number of OP is 9 for power and blade properties and 1 for tower properties, and the DOF case is 6. The ice condition is moderate ice.

Table 29 Wind speed measurement error

Case	WE_0	WE_0.5	WE_1.0	WE_1.5	WE_2.0
Error range (m/s)	[0, 0]	[-0.5, 0.5]	[-1.0, 1.0]	[-1.5, 1.5]	[-2.0, 2.0]
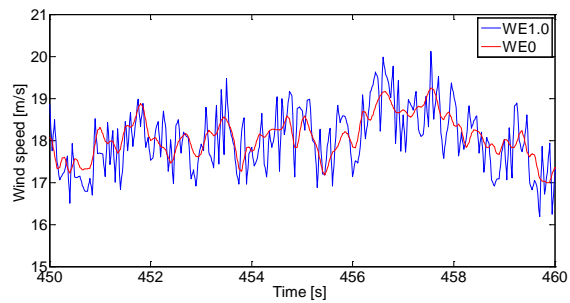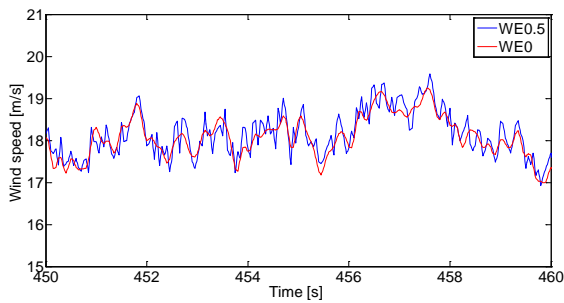
Figure 78 Time series (450s-460s) of wind speed with and without measurement errors

The input wind speed measurement error can influence not only the estimation difference, but also the modeling errors, which are shown in Table 30. The estimation difference does not increase much with the increase of measurement error. However, as wind speed measurement error increases, the modeling error increases a lot. That means the wind measurement error influences the ice-detection capability.
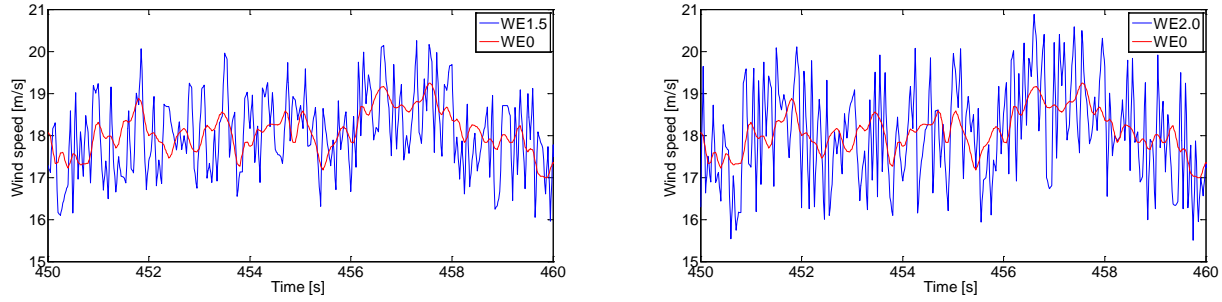
Table 30 Estimation difference and modeling error of different quantities

	Estimate Difference [%]					Modeling Error [%]				
	WE_0	WE_0.5	WE_1.0	WE_1.5	WE_2.0	WE_0	WE_0.5	WE_1.0	WE_1.5	WE_2.0
Gen Power	8.80	8.78	8.80	8.62	9.14	0.35	0.50	0.66	0.77	0.95
Rotor Speed	8.70	8.68	8.70	8.52	9.04	0.26	0.42	0.61	0.71	0.90
OoPDefl1	12.27	11.83	12.05	11.41	13.62	7.59	7.22	7.68	8.82	10.89
IpDefl1	11.52	11.26	11.44	11.21	12.73	6.08	5.93	6.54	7.66	9.49
RootMxc1	7.59	7.63	7.75	7.94	8.25	1.76	1.90	2.31	2.82	3.53
RootMyc1	12.06	11.76	11.96	11.55	13.24	2.28	2.86	4.14	5.34	6.81
RootMzc1	51.98	51.28	51.84	50.05	55.16	9.73	11.16	14.09	16.82	20.45
RotThrust	10.99	11.05	11.32	11.58	12.11	1.78	2.29	3.58	4.59	6.05
YawBrMxp	2.60	2.98	3.98	5.04	6.34	1.77	2.28	3.49	4.67	6.04
YawBrMyp	62.50	62.78	63.18	63.24	64.47	8.67	9.77	13.85	16.39	20.55
YawBrMzp	14.74	14.88	14.95	15.25	15.47	4.81	4.96	5.37	5.92	6.53

As defined in section 7.3, the ice-detection capability is the quotient between the estimation difference and the modeling error. Here the definition (61) will be used. The ice-detection capability is calculated for cases with different wind measurement error as shown in Table 31. It can be seen that the ice-detection capabilities decrease for all quantities when the range of measurement error increases. It should be noted that these capabilities all remain larger than 1, which means the ice can still be detected successfully. Moreover, the largest drop of capability happens in power and rotor speed. Although their capabilities drop to about one third of the original value, they are still sufficient for ice-detection.

92

Table 31 Ice-detection capability of different quantities considering wind speed measurement error

	WE_0	WE_0.5	WE_1.0	WE_1.5	WE_2.0
Gen Power	25.26	17.72	13.24	11.22	9.66
Rotor Speed	33.49	20.48	14.35	11.94	10.02
OoPDefl1	1.62	1.64	1.57	1.29	1.25
IpDefl1	1.90	1.90	1.75	1.46	1.34
RootMxc1	4.31	4.02	3.36	2.81	2.34
RootMyc1	5.28	4.12	2.89	2.16	1.95
RootMzc1	5.34	4.60	3.68	2.98	2.70
RotThrust	6.18	4.82	3.16	2.52	2.00
YawBrMxp	1.47	1.31	1.14	1.08	1.05
YawBrMyp	7.21	6.42	4.56	3.86	3.14
YawBrMzp	3.06	3.00	2.79	2.58	2.37

The uncertainty factor μ' defined in section 7.3 can be calculated. As shown in Figure 79 and Figure 80, the uncertainty factors increase as the wind measurement error increases, which agrees with the results shown in Table 31. The uncertainty factors of different quantities are quite different. For power, when wind speed measurement error is ±2 m/s, the uncertainty factor is more than 3. That means the capability defined by (60) should larger than 3 for successful ice-detection under that measurement error level. The impact of input measurement errors is different for different quantities. Based on the influence of measurement errors, the quantities can be approximately classified into two groups, highly influenced or slightly influenced. Power related properties, thrust and blade root bending moment in y direction are highly influenced, while the rest are slightly influenced by measurement error.
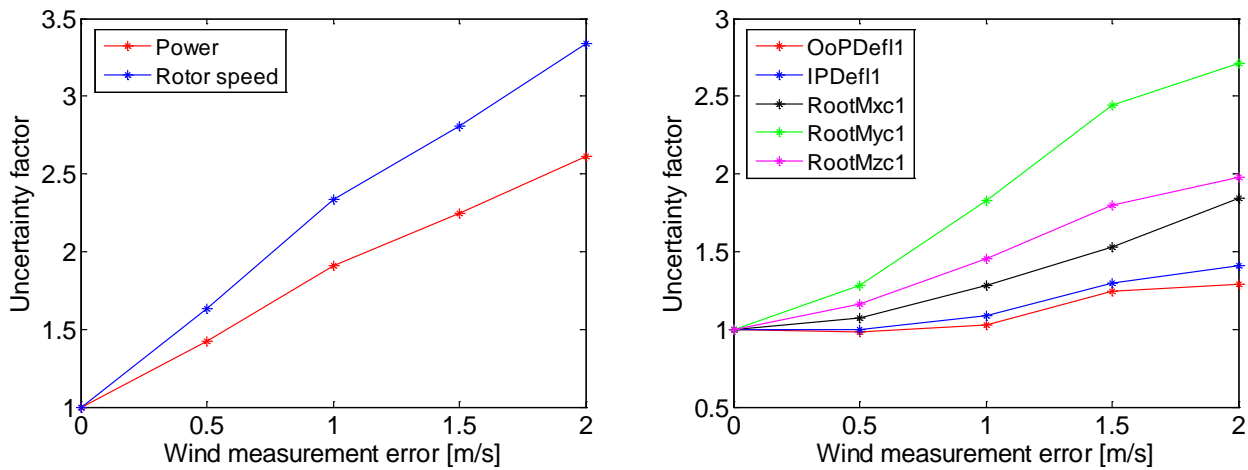
Figure 79 Uncertainty factor of power production and blade properties
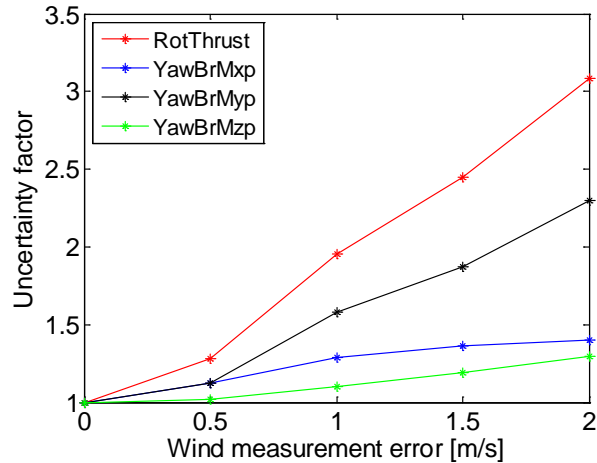
Figure 80 Uncertainty factor of tower properties

8.3.2 Nonlinear system output measurement error

In the previous study, the measurement noise in outputs is neglected. However, the output measurement may include some unavoidable noise. This influence strongly depends on the measuring equipment, which indicates that the impact can be different from case to case. In order to explain how to consider output measurement error and have a better understanding about the influence of output measurement error, a case study about different output measurement error is conducted. It is assumed that the output measurement error is random value with different error ranges.

Four levels of output measurement error are considered. Specifically, the upper and lower bound of the random error is the $\pm 2.5\%$, $\pm 5\%$, $\pm 7.5\%$, $\pm 10\%$ of the maximum of the absolute value of the corresponding output quantity. Figure 81 shows the time series of blade root out-of-plane bending moment with different measurement errors as an example.

94
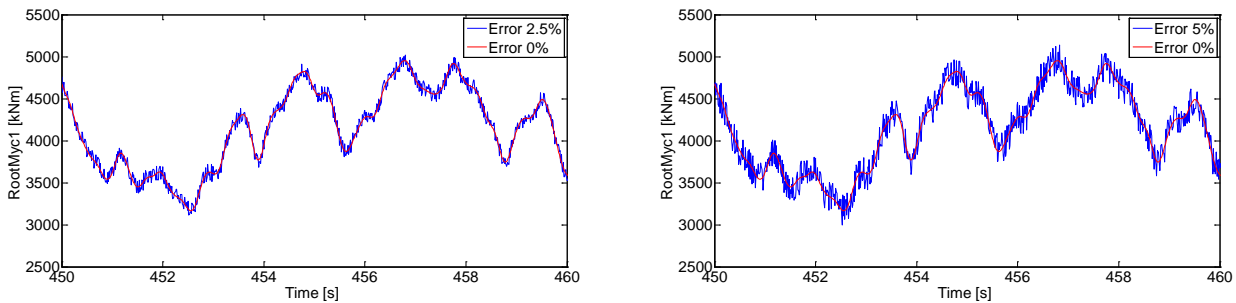
Figure 81 Time series (450s-460s) of blade root out-of-plane bending moment with and without measurement errors

Similar to section 8.3.1, the output measurement error can influence not only the estimation difference, but also the modeling error, which are shown in Table 32, where E_0, E_2.5, E_5, E_7.5, E_10 represent the upper and lower bound of the random error is $\pm 0\%$, $\pm 2.5\%$, $\pm 5\%$, $\pm 7.5\%$, $\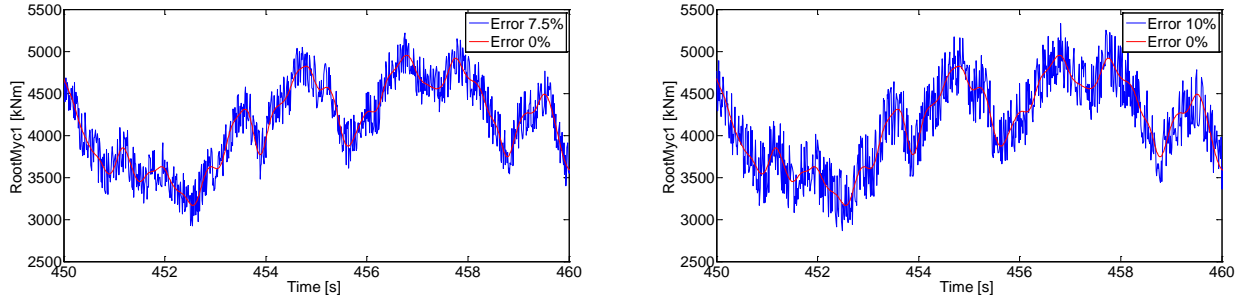pm 10\%$ of the maximum of the absolute value of the corresponding output quantity. The estimation difference does not increase much with the increase of measurement error. However, as output measurement increase, the modeling error increases a lot, especially for power and rotor speed. That means the output measurement error does influence the ice-detection capability.

(Note that what we call the modeling error is actually the combination of error due to modeling and error due to measurement)

Table 32 Estimation difference and modeling error of different quantities

	Estimate Difference [%]					Modeling Error [%]				
	E_0	E_2.5	E_5	E_7.5	E_10	E_0	E_2.5	E_5	E_7.5	E_10
Gen Power	8.74	8.77	8.86	9.02	9.23	0.83	1.12	1.71	2.38	3.10
Rotor Speed	8.64	8.68	8.79	8.98	9.22	0.77	1.10	1.77	2.52	3.30
OoPDefl1	13.09	13.18	13.45	13.88	14.47	8.64	8.77	9.15	9.77	10.55
IpDefl1	12.28	12.37	12.59	12.98	13.53	7.32	7.47	7.90	8.58	9.44
RootMxc1	7.66	7.77	8.09	8.63	9.30	2.31	2.67	3.48	4.56	5.75
RootMyc1	12.42	12.49	12.67	12.98	13.38	4.32	4.48	4.94	5.64	6.49
RootMzc1	53.41	53.43	53.54	53.71	53.97	14.80	14.89	15.19	15.64	16.29
RotThrust	11.32	11.38	11.53	11.81	12.17	3.58	3.76	4.23	4.92	5.74
YawBrMxp	3.98	4.07	4.33	4.71	5.22	3.49	3.59	3.87	4.29	4.83
YawBrMyp	63.18	63.20	63.23	63.31	63.46	13.85	13.93	14.17	14.54	15.06
YawBrMzp	14.95	15.00	15.20	15.48	15.88	5.37	5.48	5.80	6.32	6.95

As defined in section 7.3, the ice-detection capability is the quotient between the estimation difference and the modeling error. Here the definition (62) will be used. The ice-detection capability is calculated for cases with different levels of output measurement error as shown in Table 33. It can be seen that the ice-detection capabilities decrease for all quantities when the range of measurement error increases. It should be noted that these capabilities all remain larger than 1, which means the ice can still be detected successfully. Moreover, the largest drop of capability happens in power and rotor speed, and they are still sufficient for ice-detection.

Table 33 Ice-detection capability of different quantities considering wind speed measurement error

	E_0	E_2.5	E_5	E_7.5	E_10
Gen Power	10.54	7.85	5.19	3.79	2.98
Rotor Speed	11.28	7.86	4.97	3.57	2.80
OoPDefl1	1.51	1.50	1.47	1.42	1.37
IpDefl1	1.68	1.66	1.59	1.51	1.43
RootMxc1	3.32	2.91	2.33	1.89	1.62
RootMyc1	2.88	2.79	2.57	2.30	2.06
RootMzc1	3.61	3.59	3.52	3.43	3.31
RotThrust	3.16	3.03	2.73	2.40	2.12
YawBrMxp	1.14	1.13	1.12	1.10	1.08
YawBrMyp	4.56	4.54	4.46	4.36	4.21
YawBrMzp	2.79	2.74	2.62	2.45	2.29

The uncertainty factor μ'' defined in section 7.3 can be calculated. As shown in Figure 82 and Figure 83, the uncertainty factors increase as the output measurement error increases, which agree with the results shown in Table 33. For most quantities, the uncertainty factors are less than 1.5. While for power and rotor speed, when the measurement error is $\pm10\%$, the uncertainty factor is more than around 4. The impact of output measurement errors is different for different quantities. Based on the influence of measurement errors, the quantities can be approximately classified into two groups, highly influenced or slightly influenced. Power related properties are highly influenced, while the rest are slightly influenced by measurement error.
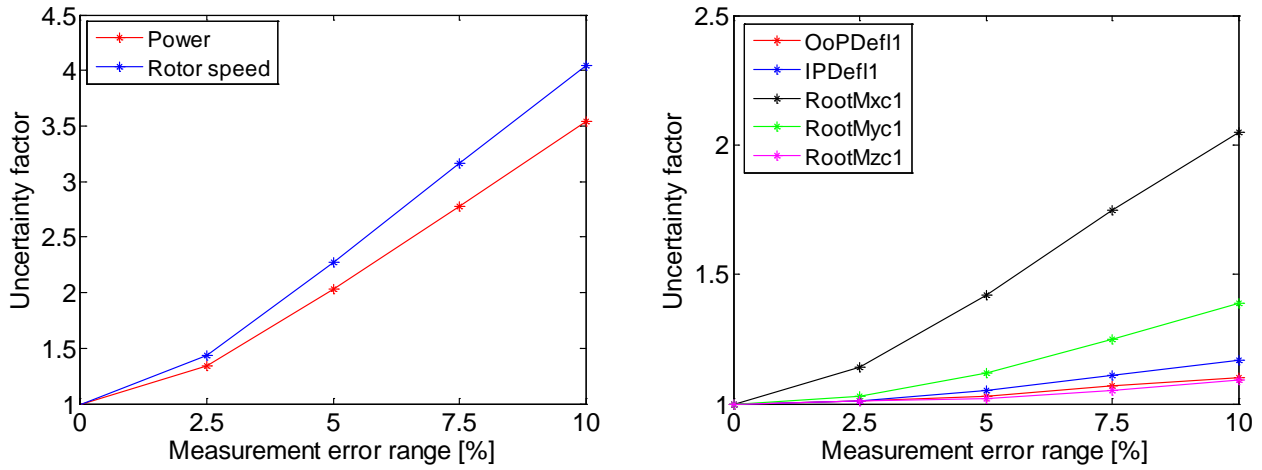
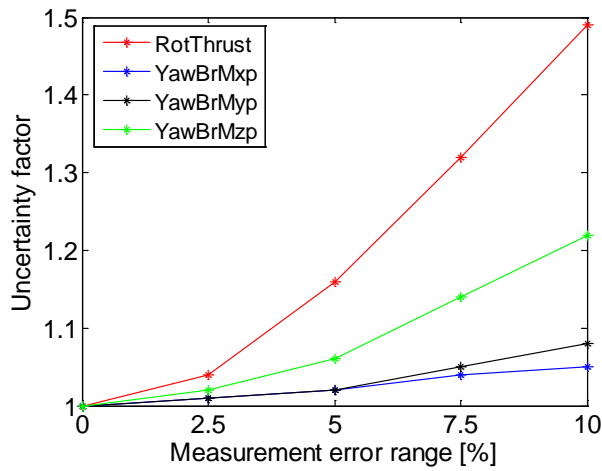Figure 82 Uncertainty factor μ'' of power production and blade properties

Figure 83 Uncertainty factor μ'' of tower properties

8.4 Influence of ice distribution on blade

In the previous study, the ice formed on the blade has been assumed with almost uniform distribution. However, in reality, there are more ice accumulates on blade tip than blade root. In this section, the influence of non-uniform ice distribution on the ice detection capability will be investigated. As shown in Table 34, three cases with different ice distribution are studied. Similarly as introduced in Chapter 7, the blade sections from top to bottom in the table are implemented from the blade root to tip. For case 1, all the blade sections are considered with moderate ice, which is the same situation as in previous sections. For case 2, only the blade tip is considered with moderate ice, and other blade parts are covered with light ice. For case 3, there is moderate ice on blade tip and no ice on the other blade sections. It should be noted that the part of blade with less ice distribution (light in case2, or no ice in case 3)

consists of more than 60% of the blade length. In reality, if the blade tip is covered with moderate ice, the ice conditions of other blade sections are probably between moderate ice and no ice. This indicates that case 1 and case 3 are two extremes cases, and case 2 can be regarded as what may really happen.

Table 34 Ice distribution cases

Blade Section	Case 1	Case 2	Case 3
DU W-405	Moderate	Light	No ice
DU W-350	Moderate	Light	No ice
DU 97-W-300	Moderate	Light	No ice
DU 91-W2-250	Moderate	Light	No ice
DU 91-W-210	Moderate	Moderate	Moderate
NACA 64-618	Moderate	Moderate	Moderate

Figure 84 and Figure 85 shows the ice detection capability of power, blade and tower related properties under different ice distribution conditions. The ice detection capability of most quantities reduced to some extent, except the blade in-plane moment and tower side-side moment. From case 1 to case 2, the detection capability reduces about 20%. And from case 2 to case 3, the detection capability also reduces about 20%. Although detection capabilities reduce, most of them are larger than 1, which means the blade icing can still be detected successfully. Moreover, the changing patterns of different quantities are similar. This means most of the conclusions in previous sections are still applicable.

For implementation in reality, it is necessary to use more detailed ice distribution to determine the ice-detection capability. The current study focus on the concept of the method and considering the conclusions for different ice-distributions are similar, the uniformly distributed ice condition will be used in the following Chapters.
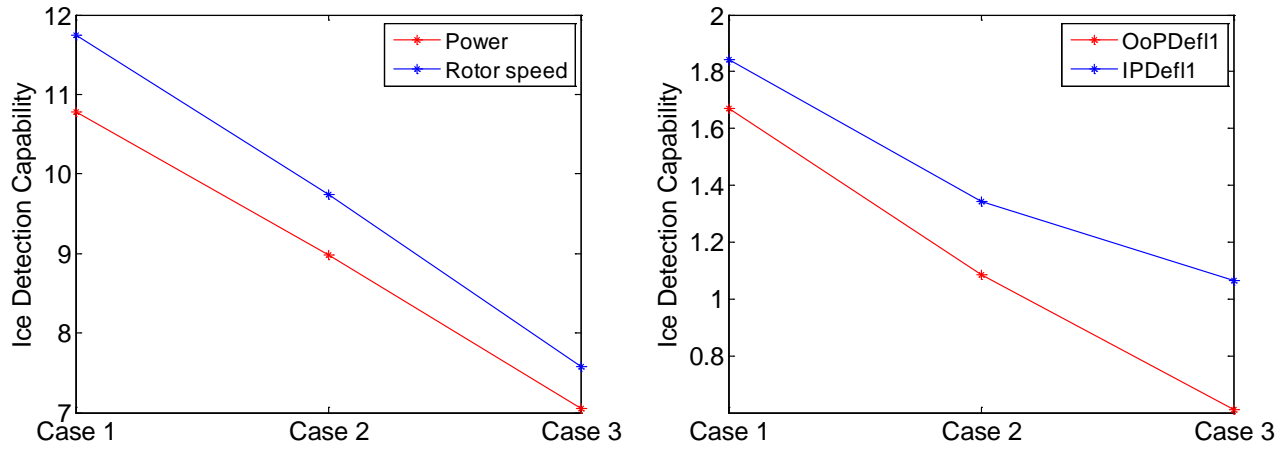
Figure 84 Ice detection capability of power related properties (left) and blade deflections (right) under different ice distribution
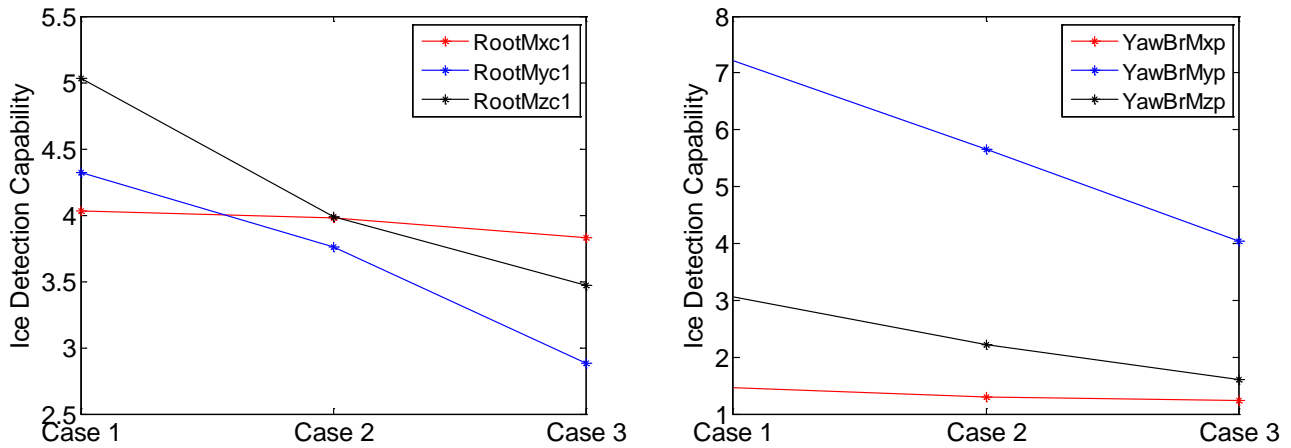

Figure 85 Ice detection capability of blade root bending moment (left) and tower top bending moment (right) under different ice distribution

8.5 Summary

The capabilities of ice-detection of different quantities are list in Table 35. The capability is defined to three levels. "Limited" represents the ice-detection capability is limited with the normalized error smaller than 2. "Moderate" means ice-detection capability is moderate and the normalized error is from 2 to around 6. "High" means the ice-detection capability is high and the normalized error is above 6. The above definitions are based on the survey in Section 7.3 for sensors capability and on the analysis in Section 8.3 for influence of measuring error. In reality, the sources of uncertainty can be complicated and the above definitions should be tuned accordingly. As shown in Table 35, power and rotor speed

have the best detection capability. The blade moments and tower moment in y direction can also be used for detection. However, the rest quantities have very limited detection capability. Therefore, they are not recommended for detection purpose.

Table 35 The ice-detection capability for above rated wind speed

	Start	Light	Moderate
Power	High	High	High
Rotor speed	High	High	High
OoPDefl1	Limited	Limited	Limited
IpDefl1	Limited	Limited	Limited
RootMxc1	Limited	Moderate	Moderate
RootMyc1	Limited	Moderate	Moderate
RootMzc1	Limited	Moderate	Moderate
YawBrMxp	Limited	Limited	Limited
YawBrMyp	Moderate	Moderate	High
YawBrMzp	Limited	Limited	Moderate

Chapter 9 Ice on Blade Detection—Below Rated Wind Speed

In the previous chapters, the above rated wind speed case was studied in great detail. Moreover, according to Chapter 3, the below rated wind speed should also be analyzed. In the below rated wind speed condition, the pitch angle is always zero and power production changes as wind speed change.

In this chapter, the modeling error for below rated will be analyzed first, in a similar way as in Chapter 6. The focus will be put on how DOFs and OP influence the modeling error of different quantities. Then, the model-based ice-detection method proposed in Chapter 7 will be applied to examine its capability in below rated wind conditions.

As an example, the calculations within this chapter will use the wind history as shown in Figure 86. The mean wind speed is 7 m/s, and oscillates between 3 m/s and 11 m/s. The Frequency profile is shown in Figure 86. This is a typical below rated wind speed case for the 5MW wind turbine, and the analysis for it should be applicable in general.
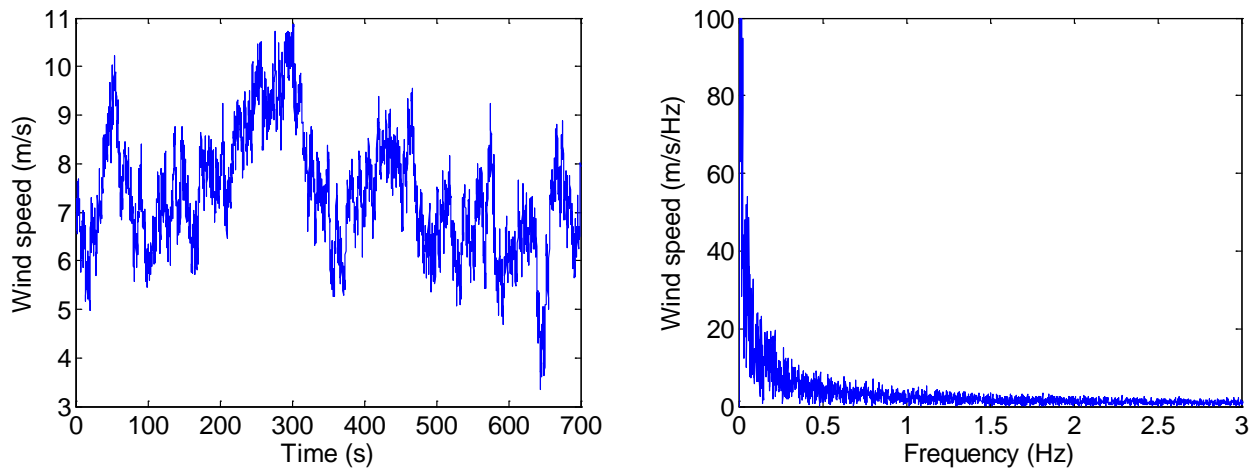

Figure 86 Wind speed time series (left) wind speed spectrum (right)

For DOFs, the choices are the same as in Chapter 6. And as for the OP, the similar strategies are applied, with wind speed in Table 36 used. For the same considerations in Chapter 6, the WT related quantities can be classified into three groups, which are quantities related to power production, blade properties and tower properties respectively. These three groups will be analyzed individually in the following sections, and it will be shown that the quantities within the same group have similar changing patterns with respect to DOF & OP.

Table 36 Details of operation points for below rated wind speed

No. of OP.	1	2	3	5	9
OP.[m/s]	7	6, 8	5, 7, 9	3, 5, 7, 9, 11	3, 4, 5, 6, 7, 8, 9, 10, 11

9.1 Total modeling error

9.1.1 Power production properties

The total modeling error of power and rotor speed is shown in Figure 87. The contours are made with respect to different combination of DOFs and OP. It can be seen that for both power and rotor speed, the DOFs have little influence, and the OP dominates the total modeling error. The results demonstrate that power and rotor speed are almost linearly related with the inputs.

It should be noted that the modeling errors in this below rated case are larger than that of above rated cases in Chapter 6. This is due to that the power and rotor speed in the below rated wind speed cases change along with wind speed, while they are controlled to be stable in the above rated wind speed cases.
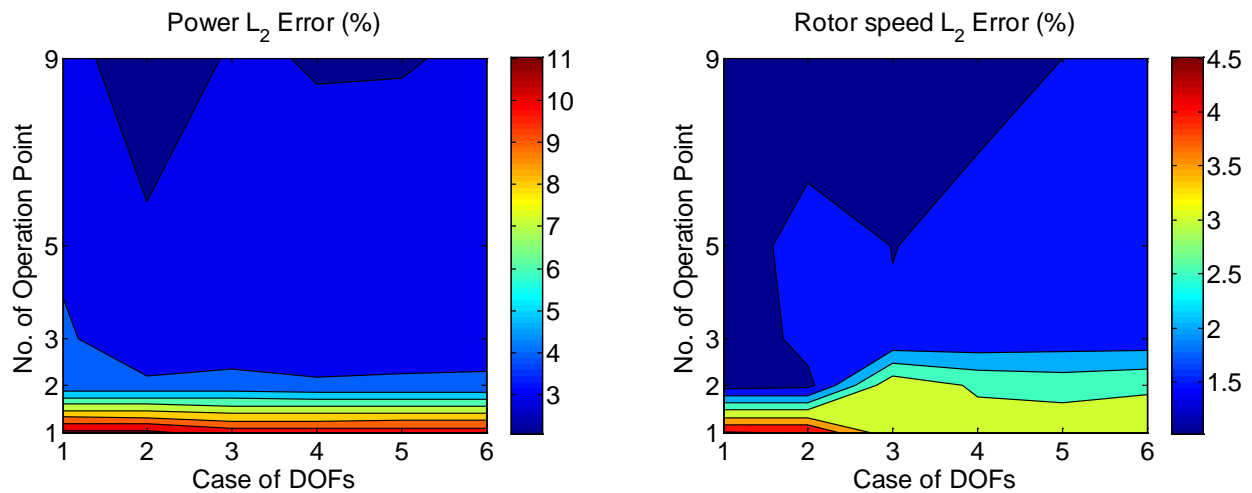

Figure 87 Total error of power (left) and rotor speed (right) for different combinations of DOF &OP

9.1.2 Blade properties

Figure 88 shows the total modeling error of blade out-of-plane deflection for different combinations of DOFs and OP. From the left figure it can be seen that there is dramatic drop of errors from DOF case 2 to case 3. That means we must include the blade flapwise DOF to achieve a reliable result. For DOF cases 4, 5 and 6, we plot a separate contour to look into details shown in the right figure. It can be seen that the No. of DOFs does not influence the error, while the number of OP matters especially from 1 OP to 2 OP. There is not much improvement when the No. of OP is larger than 2.
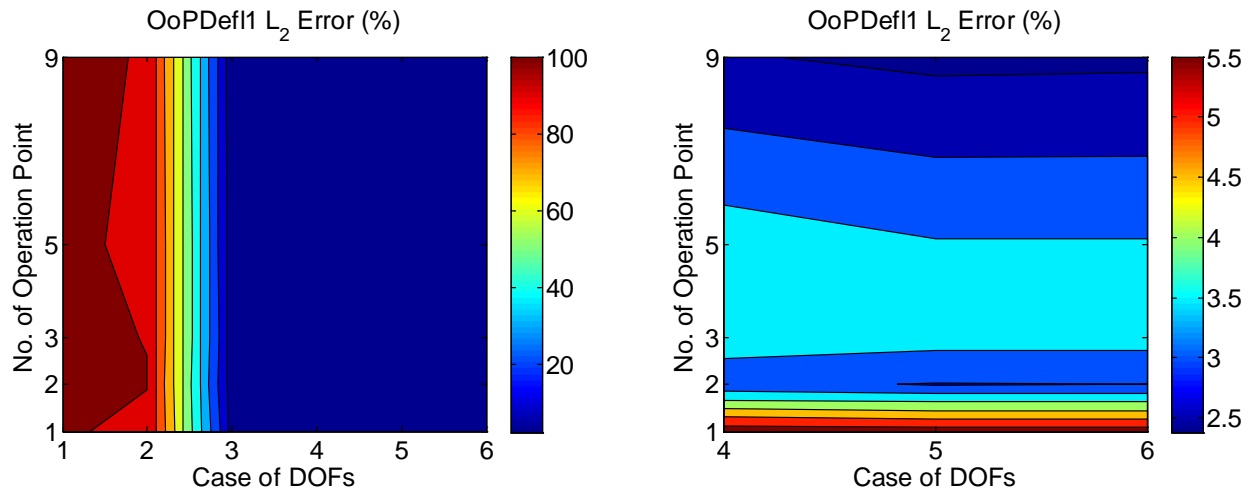
Figure 88 Total error of blade out-of-plane deflection at different combination of DOF & OP

Figure 89 shows the total modeling error of blade in-plane deflection at different combination of DOFs and OP. From the left figure it can be seen that there is dramatic drop of errors from DOF case 2 to case 4. That means we must include the blade flapwise DOF and blade edgewise DOF to achieve a reliable result. For DOF cases 4, 5 and 6, we plot a separate contour to look into more details as shown in the right figure. It can be seen that range of error from about 2% to 3%, which means there is not much improvement. Similar to out-of-plane deflection, the No. of DOFs does not influence the error, while the number of OP matters especially from 2 OP to 3 OP. There is not much improvement when the No. of OP is larger than 3.
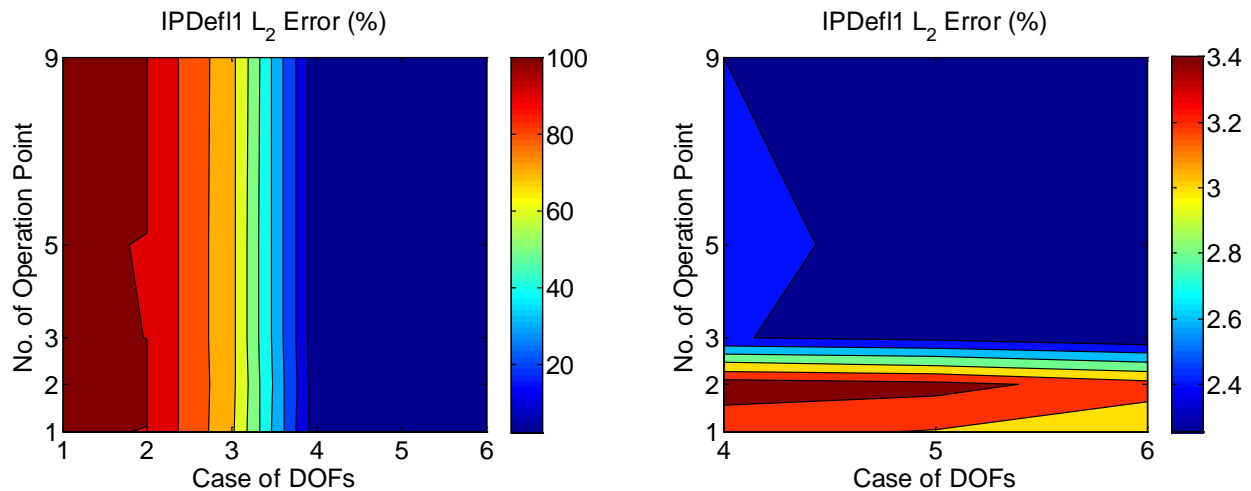

Figure 89 Total error of blade in-plane deflection at different combination of DOF &OP

The contour of blade in-plane bending moment is shown in Figure 90. It can be seen that the modeling error does not change much no matter what DOF or OP choices are implemented. Considering the model error is already small (about 2.5%), this non-decreasing error may due to some high order effects that have not been included in any models.
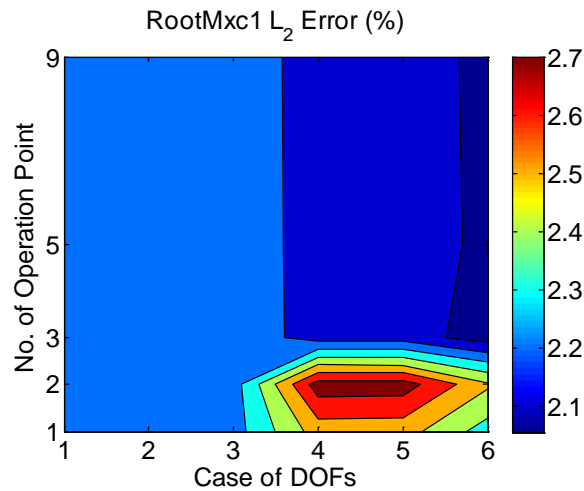
Figure 90 Total error of blade in-plane bending moment at different combination of DOF &OP

The modeling error for blade out-of-plane bending is contoured in Figure 91. Overall the error decreases as more DOFs are included and more OPs are applied. The error changes much from DOF number 2 to 3, that means the blade out-of-plane DOF must be include to achieve a better result. The threshold for number of OP is 2, that means the number of OP must larger than 2. The benefit of increasing DOFs and OP is limited when DOF is larger than 3 and OP is larger than 2.
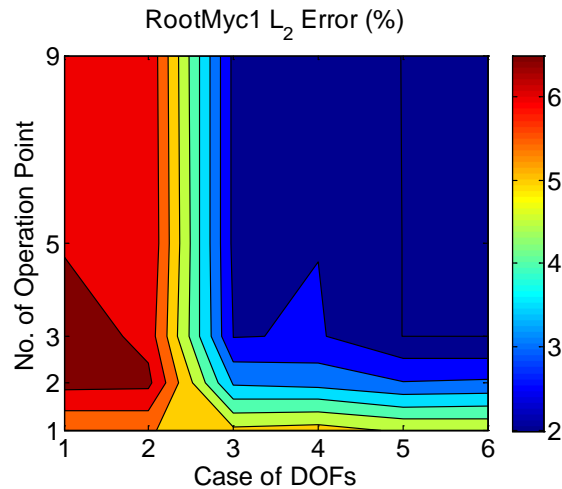

Figure 91 Total error of blade out-of-plane bending moment at different combination of DOF &OP

Figure 92 displays modeling error of blade torsional moment made with respect to different combinations of DOFs and OP. From the left figure it can be seen that the dominant factor is DOFs and threshold of No. of DOFs is case 2 to 4. That means we must include the blade flapwise and edgewise DOFs to achieve an accurate result. For DOF cases 4, 5 and 6, we plot a separate contour to look into more details as shown in the right figure. It can be seen that range of error from about 25% to 12%, which means there is much improvement. The dominant factor is the No. of OP. What's more there is no need to apply No. of OP larger than 3, since there is little improvement in that area.
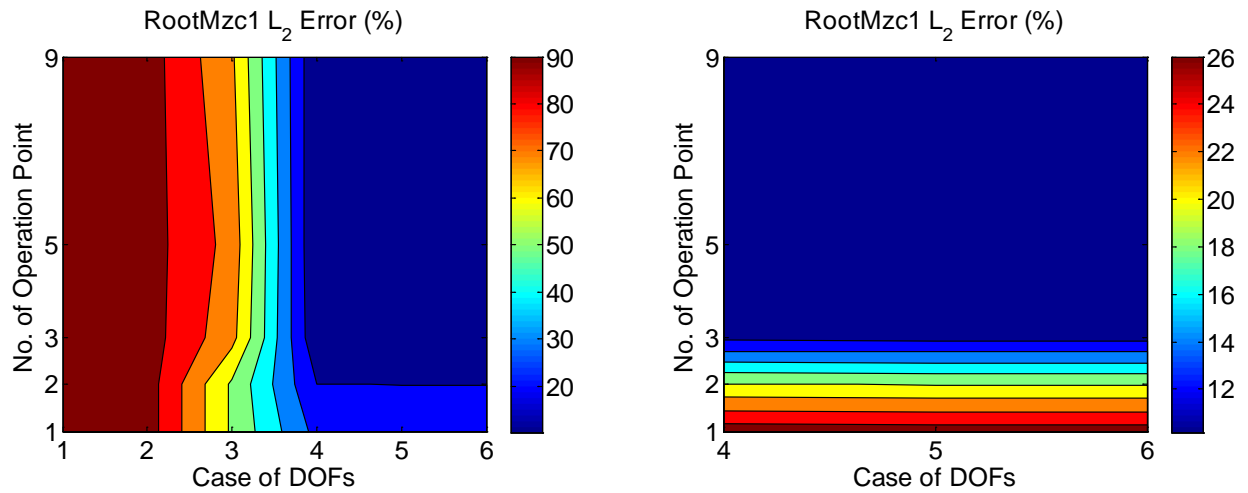
104

Figure 92 Total error of blade torsional moment at different combination of DOF &OP

9.1.3 Tower properties

Contour of modeling error of thrust is made with respect to different combination of DOFs and OP shown in Figure 93. It can be seen that the modeling error decrease with the increase of DOF. Especially, two thresholds can be found from DOF2 to DOF3 and from DOF 4 to DOF 5. The modeling error can be considerably lowered by using more than one OP. And it seems that no further benefits can be achieved if more than 3 OP is used.
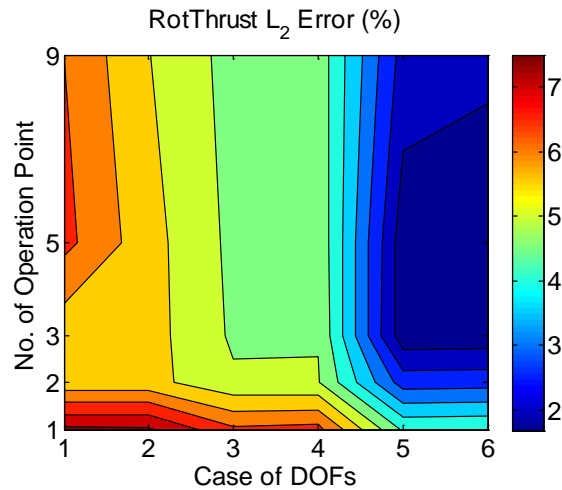
Figure 93 Total error of blade out-of-plane bending moment at different combination of DOF &OP

Contours of modeling error of tower top side-side, fore-aft and torsional moment are made with respect to different combination of DOFs and OP shown in Figure 94 and Figure 95. It can be seen that, if 1 or 2 DOFs are used, the modeling error remains small no matter how many OP is used. The reason is that in this case, there is little structure oscillation in the wind turbine model, thus the OP won't influence much. If DOF 3 or even higher DOF are used, the modeling error has a slight decrease if only one OP applied.

However, it will dramatically increase when more than one OP is used. One possible explanation for this phenomenon is that there will be structure oscillations, which will be amplified due to nonlinear effects. Therefore the number of DOFs and OP should be determined with special care.
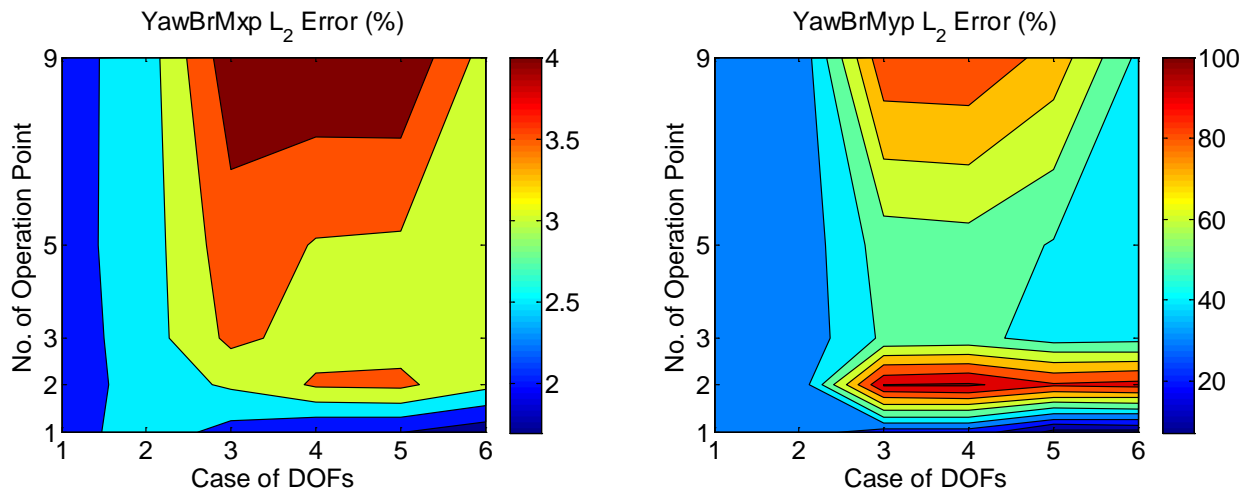

Figure 94 Total error of tower top side-side (left) and fore-aft (right) bending moment at different combination of DOF &OP
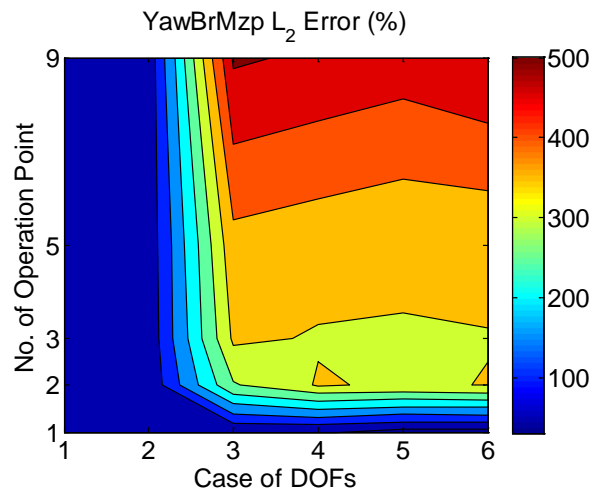
Figure 95 Total error of tower torsional moment at different combination of DOF &OP

9.2 Ice-detection capability

The capability of ice-detection depends on the difference between estimation difference and modeling error. According to section 9.1, there exist many approaches to achieve a better accuracy in linear wind turbine modeling, such as DOFs and OP. These facts inspire us to increase the ice-detection capability by using different modeling methods. Thus, in the following subsections, the influence of modeling methods on ice-detection will be analyzed for different quantities individually. The method used is the same as Chapter 8.

9.2.1 Power production properties

According to section 9.1.1, the most efficient way to decrease modeling error for power production is to increase number of OP. The number of DOFs has little influence and 1 DOF is accurate enough. Therefore the number of DOF of quantities related to power production is set to 1 (variable generator DOF), and the number of OP changes from 1 to 9. The contours of normalized power and rotor speed error at different No. of OP and ice conditions are shown in Figure 96. As the patterns of power and rotor speed error are similar, the power is analyzed in detail as an example, and the conclusions are also applicable for rotor speed.

The contour can be analysis in two aspects:

(1) For a certain OP model, the normalized ice-detection error, which represents the detection accuracy, can be predicted for a given ice condition. More ice on blade condition induces larger normalized error, therefore easier to be detected. The ice-detection capability for power in below rated wind speed case is much larger than that of above rated wind speed. The reason is that ice on blade has large influence on power at below rated wind speed, which is shown in Figure 56.

(2) For a certain ice-condition, more OP induces larger normalized error therefore larger ice-detection capability. For example from 5 OP to 9 OP, the ice-detection capability increases a lot especially for moderate ice case. The increase of OP has even better effects for more severe ice conditions, which indicates that OP methods is a highly recommended modeling method for power and rotor speed.
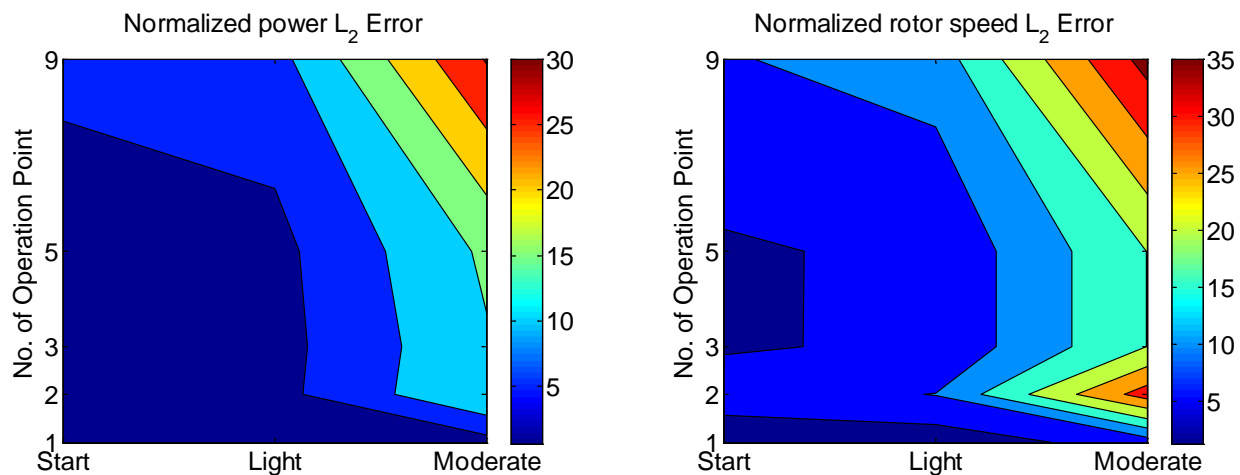
Figure 96 Normalized power (left) and rotor speed (right) error at different No. of OP and ice conditions

9.2.2 Blade properties

According to section 9.1, 3 OP the best choice and it would be helpful to investigate the influence of the number of DOFs. Therefore the number of OP of quantities related to blade properties is set to 3, and the number of DOFs changes from 1 to 6. Figure 97 shows the contours of normalized blade deflection error

at different DOF cases and ice conditions. The patterns of blade deflections are similar, the in-plane deflection (left) is analyzed in detail as an example, and the conclusions are also applicable for the other.

The contour can be analysis in two aspects:

(1) For a certain DOF model, the normalized ice-detection error, which represents the detection accuracy, can be predicted for a given ice condition. More ice on blade condition has larger normalized error, therefore easier to be detected. The ice-detection capability of blade deflection of below rated wind speed is much larger than that of above rated wind speed.

(2) For a certain ice-condition, increasing the number of DOF is helpful from DOF 2 to DOF 3 for blade out-of-plane deflection and from DOF 3 to DOF 4 for blade in-plane deflection. Moreover, if the number of DOF increases further, the capability changes less, although there is still benefit. The increase of DOF has even larger effects for more severe ice conditions. Overall the blade deflection is recommended for ice-detection.
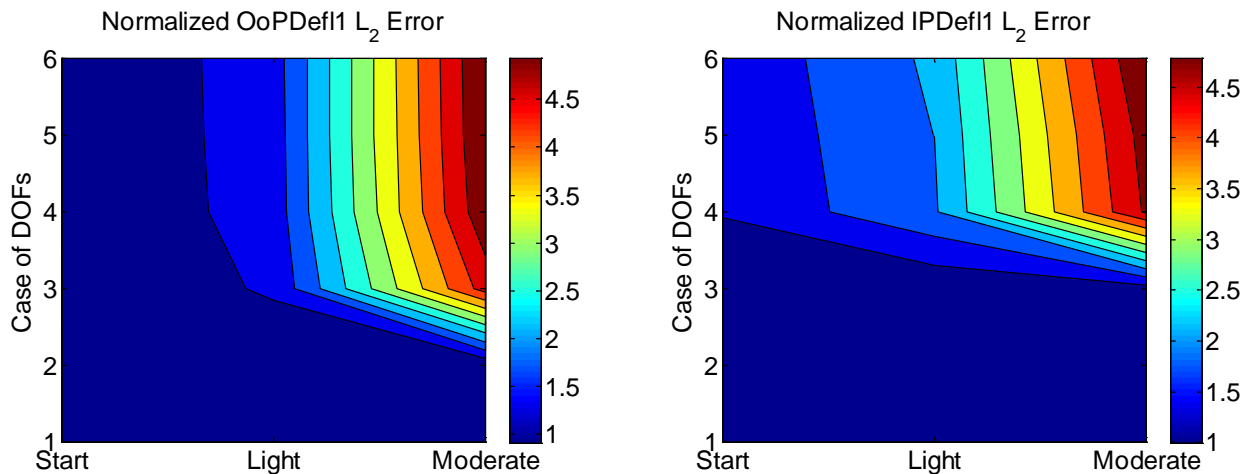

Figure 97 Normalized blade deflection error at different No. of DOF and ice conditions

The contours of normalized blade root bending moment error at different DOF cases and ice conditions are shown in Figure 98and Figure 99. They are different in the changing patterns, especially in detailed local regions. Thus the quantities should be analyzed individually. For the blade in-plane moment shown in Figure 98 (left), the changing pattern is quite different the others. More DOFs don't increase the ice-detection capability. 1 DOF is the best choice. For the blade out-of-plane moment shown in Figure 98 (right), ice-detection capability increase as the ice condition becomes severe from start to moderate. Increase the No. of DOFs does not improve the ice-detection capability. Overall it has relatively large ice-detection capability and is recommended for ice-detection. For the blade torsional moment shown in Figure 99, the ice-detection capability is relatively small for all No. of DOFs and ice conditions. Therefore it is not recommended for ice-detection.
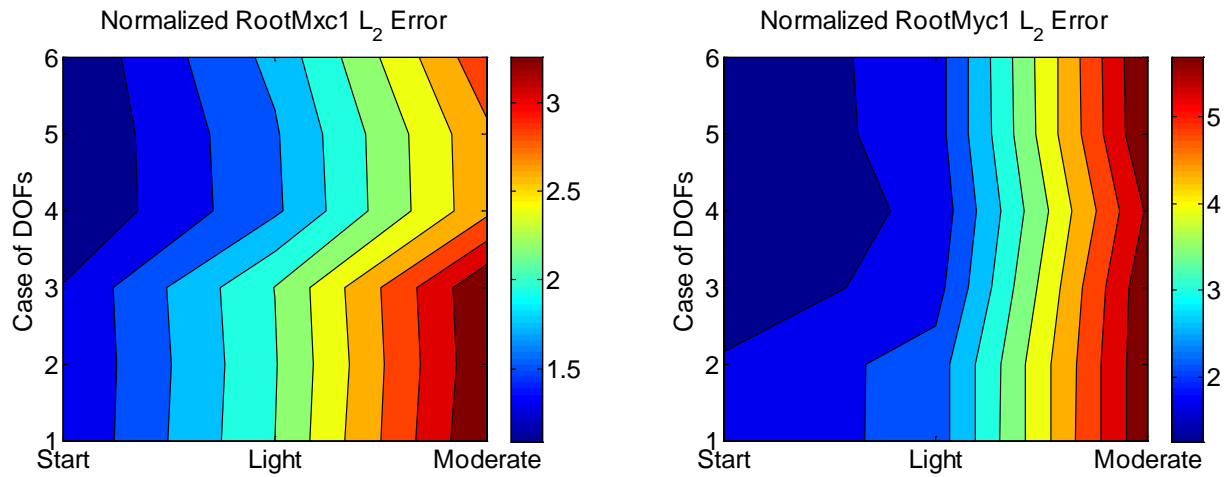
Figure 98 Normalized blade root in-plane (left) and out-of-plane (right) bending moment error at different No. of DOF and ice conditions
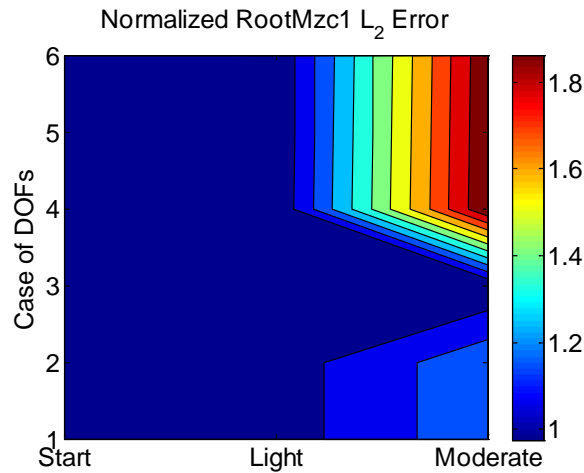

Figure 99 Normalized blade root torsional moment error at different No. of DOF and ice conditions

9.2.3 Tower properties

According to section 9.1, the most efficient way to decrease the modeling error is to increase the number of DOFs. The number of OPs is 1 and the number of DOF cases changes from 1 to 6. The contours of normalized tower top bending moment error at different DOF cases and ice conditions are shown in Figure 100 and Figure 101. They are different in the changing patterns, especially in detailed local regions. Thus the quantities should be analyzed individually.

For the tower top side-side moment shown in Figure 100(left), the increase of DOF is helpful but limited. The value of normalized error is quite small, which means ice-detection capability is small. Therefore it is not recommended to use tower side-side moment as ice-detection criteria. For the tower top fore-aft

moment shown in Figure 100(right), no matter how many DOFs are included and what ice conditions are, the ice-detection capability is very small. Therefore, it is not recommended for ice-detection. For the tower top torsional moment, increase of DOF is helpful to increase the ice-detection capability, especially from DOF 4 to DOF 5 and from DOF 2 to DOF 3. This quantity can be used as criteria for ice-detection.
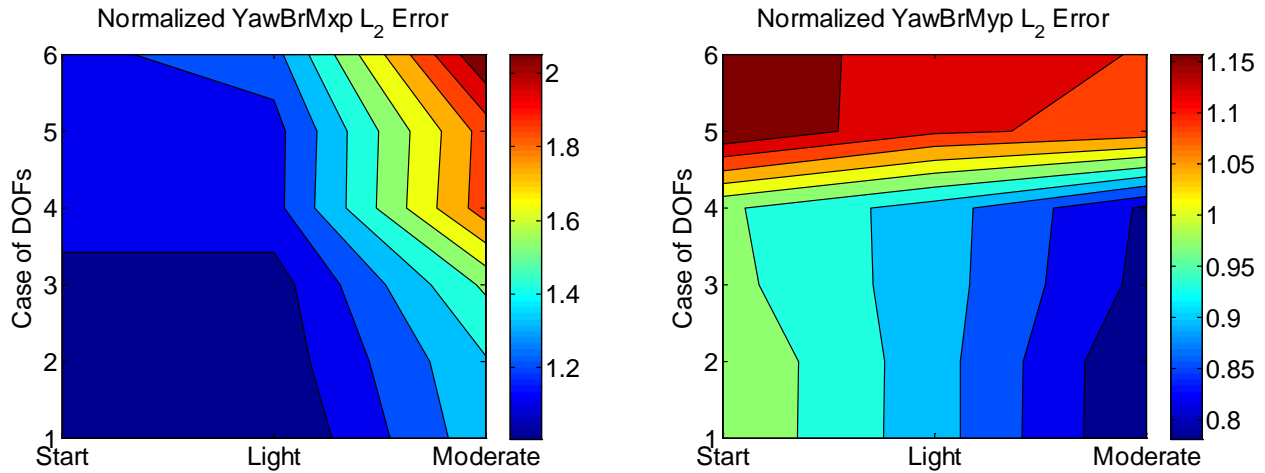

Figure 100 Normalized tower top side-side (left) and fore-aft (right) bending moment error at different No. of DOF and ice conditions
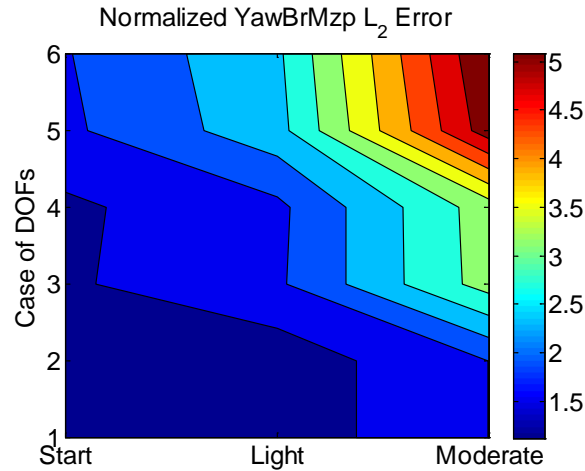

Figure 101 Normalized tower top torsional moment error at different No. of DOF and ice conditions

9.3 Summary

The capabilities of ice-detection of different quantities are list in Table 37. The capability is defined to three levels. The capability is defined to three levels. "Limited" represents the ice-detection capability is limited with the normalized error smaller than 2. "Moderate" means ice-detection capability is moderate and the normalized error is from 2 to around 6. "High" means the ice-detection capability is high and the normalized error is above 6. The base and limitation for the above definitions are similar to that discussed in Section 8.4. As shown in Table 37, the results are similar to above rated wind speed condition, but the detection capability is reduced in general. However, they are still sufficient for ice detection.

Table 37 The ice-detection capability for below rated wind speed

	Start	Light	Moderate
Power	Moderate	Moderate	High
Rotor speed	Moderate	High	High
OoPDefl1	Limited	Limited	Moderate
IpDefl1	Limited	Limited	Moderate
RootMxc1	Limited	Moderate	Moderate
RootMyc1	Limited	Moderate	Moderate
RootMzc1	Limited	Limited	Limited
YawBrMxp	Limited	Limited	Moderate
YawBrMyp	Limited	Limited	Limited
YawBrMzp	Limited	Moderate	Moderate

Chapter 10 Conclusions and Suggestions for Future Work

In this study, a model-based detection method has been developed for ice on wind turbine blades. The detection method has been systematically verified for a 5MW wind turbine. The main work and conclusions are summarized as follows.

(1) Development of a wind turbine model

The developments of a wind turbine model are in two steps. Firstly, the nonlinear model is established with Blade Element Method (BEM) for the aerodynamics and modal analysis method for structure dynamics. Then this nonlinear model is linearized for convenience in design and simulation. The linearization starts by determining the number of DOFs and OP. This model has been used for ice-detection in the later part of this study. Moreover, it can be used for other generous purposes like wind turbine control design.

(2) Analysis of the modeling errors

The total modeling error is the difference between linear model with part DOFs and the nonlinear model with full DOFs. The total modeling error is a combination of error due to DOFs and linearization. In order to have an insight into the influence of DOFs and linearization to total modeling error, simulations are carried out for all the possible combinations of 6 different DOFs cases and 5 OP cases. The relative importance of DOF and OP is revealed and suggestions are given for an optimum choice of DOFs and OP. This provides the foundation to improve the model-based ice-detection capability in the later study.

The main conclusions are as follows. Firstly, for the power related properties, the most important DOFs are blade flapwise and tower fore-aft DOFs. Since the modeling error decrease continuously as more OPs are used, there is no optimum No. of OPs. From the contours of total modeling error, it can be concluded that the dominant factor for power related properties is the number of OPs. That means the most efficient way to decrease the modeling error of power related properties is to increase the No. of OPs, rather than increase the No. of DOFs. Secondly, for the blade related properties, the most important DOFs are blade flapwise and edgewise DOFs. If the No. of OPs is larger than 2, the error due to linearization becomes stable. Therefore, the optimum number of OPs is 2 for blade related properties. Moreover, the dominant factor is the No. of DOFs. Thirdly, for the tower related properties, the most important DOFs are blade flapwise and tower fore-aft DOFs. And the optimum No. of OPs is 1. Under that condition, the No. of DOFs is the dominant factor for tower related properties.

(3) Development of a model-based ice-detection method

The influence of ice on blade is studied, which is the basis of ice on blade detection. Then a model-based ice-detection method is developed. The concept of model-based ice-detection is as follows: Firstly ice on blade changes the aerodynamics and the blade mass. Therefore it can be considered as one wind

turbine system changed to a different system. That means the outputs of the two systems, with ice and without ice, are different, even the inputs are exactly the same. From the ice-detection point of view, if the difference of outputs between iced system and cleaned one is much larger than modeling error, ice on blade can be detected. For possible measurement error in reality, they are efficiently considered by introducing uncertainty factors.

(4) Verification of the model-based ice-detection method

The ice-detection capability of different output quantities are studied, including the power production, blade and tower properties. Their behaviors are quite different in detection capability. For each quantity, detailed analysis has been carried out in the aim of improving the ice-detection capability. The implementation is based on the properties of the wind turbine modeling.

The uncertainty factors have been studies, in order to efficiently determine ice-detection capability considering measurement errors. With measurement error considered, a drop in the detection capability has been observed. Based on the influence of measurement errors, the quantities can be classified into two groups, highly influenced or slightly influenced. Power related properties are highly influenced, while blade and tower related properties are slightly influenced by measurement error.

The verification studies on detection capability have been performed for both above rated and below rated wind speed conditions. Suggestions have been given for how to choose output quantities according to the sensors and requirements in accuracy. The main conclusions and suggestions are as follows. Firstly, for the above rated wind speed, power and rotor speed have the best detection capability, and they are highly recommended to be used for ice detection. The blade root bending moment and tower top bending moment in y direction has moderate detection capability, and they can also be applied for ice detection. However, for the rest quantities, the detection capabilities are very limited. Therefore, they are not recommended for ice detection. Secondly, for the below rated wind speed condition, the conclusions are similar. Although the detection capability is reduced in general, they can still be used for ice detection. Overall, the ice-detection method is widely proved in different working conditions.

The influence of ice-distribution on the blade has also been studied. The blade root usually has less ice than the blade tip. Although this decrease in the icing amount can lead to lower ice-detection capabilities, most of the quantities are still feasible for detection. Moreover, the changing patterns of ice-detection capabilities remain the same, which means the previous conclusions still validate.

Suggestions for future work

Here are some suggestions for the future works. Firstly, more study is need for the measurement error, since the ice detection method is much influenced by measurement uncertainties. Specifically, the precision of the sensors should be studied in-depth. And conduct more investigation about on features of error, such as frequency of noise and the range of errors. Then based on the more reliable measurement

errors, the uncertainty factor can be estimated more properly. Secondly, wider implementation of the ice detection method is suggested to be studied. In this thesis, the method is applied on the NREL 5MW wind turbine. And it is also very interesting to study whether the method can be applied for other wind turbine designs, such as vertical axis wind turbine and smaller wind turbines. What's more, it is also meaningful to study whether this method is proper to be applied in floating wind turbines. As there are more DOFs in floating wind turbines, the complexity will increase. Finally, verifications based on real measurement data are important to judge whether the method work well in reality. Therefore, if measurement data is available, the verification work is strongly suggested.

Reference

Addy H (2000) NASA/TP-2000-210031, DOT/FAA/AR-99/89: Ice Accretions and Icing Effects for Modern Airfoils. Cleveland, OH: NASA.

Addy H, Broeren A, Zoeckler J, et al. (2003) NASA/TM – 2003-212124: A wind tunnel study of icing effects on a business jet airfoil. Prepared for the 41st aerospace sciences meeting and exhibit, Reno, NV, 6–9 January, AIAA-2003-0727. Reston, VA: AIAA.

Alan D. Wright, (2004): Modern Control Design for Flexible Wind Turbines. National Renewable Energy Laboratory report, 2004.

Bragg M, Broeren A, Addy H, et al. (2007) NASA/TM – 2008-214830: Airfoil ice-accretion aerodynamics simulation. Prepared for the 45th aerospace sciences meeting and exhibit, Reno, NV, 1–8 January, AIAA-2007-0085. Reston, VA: AIAA.

Brian R. Resor, (2013): Definition of a 5MW/61.5m Wind Turbine Blade Reference Model. Sandia National Laboratories, California, 2013.

Broeren A (2002) DOT/FAA/AR-02/68: Effect of Residual and Intercycle Ice Accretions on Airfoil Performance. Washington, DC: FAA.

Broeren A (2010) Effect of high-fidelity ice-accretion simulations on full-scale airfoil performance. Journal of Aircraft 47(1): 240–254.

Cattin, R. (2012): Icing of wind turbines: Vindforsk projects, a survey of the development and research needs, Elforsk report 12:13, 2012.

Cattin, R. et al. (2016) Evaluation of ice detection systems for wind turbines, Final Report, VGB Research Project No. 392, Available at: https://www.vgb.org/vgbmultimedia/392_Final+report-p-10476.pdf, 2016.

Etemaddar, M., Hansen, M. O. L. and Moan, T. (2014): Wind turbine aerodynamic response under atmospheric icing conditions, 25 Wind Energ., 17: 241–265, doi: 10.1002/we.1573, 2014.

Finstad, K.J., (1986): Numerical and Experimental Studies of Rime Ice Accretionon Cylinders and Airfoils. Doctor of philosophy, The University of Alberta, Edmonton, Alberta.

J.M. Jonkman, (2003): Modeling of the UAE Wind Turbine for Refinement of FAST_AD, National Renewable Energy Laboratory report, 2003. Available electronically at http://www.osti.gov/bridge.

Jonkman, J. M. and Buhl Jr., M. L, (2005): FAST User's Guide. NREL/EL-500-38230. Golden, CO: National Renewable Energy Laboratory, August 2005.

Lars Christian Henriksen, (2007): Model Predictive Control of a Wind Turbine. Master thesis, Technical University of Denmark, Kongens Lyngby, Denmark.

Jonkman, J., et al. (2009), Definition of a 5-MW Reference Wind Turbine for Offshore System Development. 2009, National Renewable Energy Laboratory.

Jonkman J M, (2013): The new modularization framework for the FAST wind turbine CAE tool 51st AIAA Aerospace Sciences Meeting including the New Horizons Forum and Aerospace Exposition, 7–10 January 2013, Grapevine (Dallas/Ft. Worth Region), TX.

Jason Jonkman and Bonnie Jonkman, (2016) FAST Modularization Framework for Wind Turbine Simulation: Full-System Linearization. Conference of the Science of Making Torque from Wind, Munich, Germany, 2016.

Habashi, W. G., M.Aubé, G. Baruzzi, F. Morency, P. Tran, and J. C. Narramore, (2004): FENSAP-ICE: A FULLY 3D IN-FLIGHT ICING SIMULATION SYSTEM FOR AIRCRAFT , ROTORCRAFT AND UAVS. 24th International Congress of the Aeronautical Sciences, Yokohama, Japan.

Hochart C (2008) Wind turbine performance under icing conditions. Wiley Wind Energy 11(4): 319–333.

Homola, M. C., T. Wallenius, L. Makkonen, P. J. Nicklasson, and P. A. Sundsbø, (2010a): The relationship between chord length and rime icing on wind turbines. Wind Energy, 13 (7), 627–632.

IEA Wind Task 19 Group (2011) IEA Wind Recommended Practices 13: Wind energy projects in cold climate.

International Standard IEC 61400-12, Wind turbine generator systems – Part 12: Wind turbine power performance testing.

International Standard IEC 60044-1, Instrument transformers – Part 1: Current transformers.

ISO 12494, 2001. Atmospheric Icing of structures. ISO copyright office, Geneva, Switzerland.

Kim, S.-W.; Kang, W.-R.; Jeong, M.-S.; Lee, I.; Kwon, I.-B. Deflection Estimation of a Wind Turbine Blade Using FBG Sensors Embedded in the Blade Bonding Line. Smart Mater. Struct. 2013, 22, 125004-1–125004-11.

Laakso T, Holttinen H, Ronsten G, Tallhaug L, Horbaty R, Baring-Gould I, Lacroix A, Peltola E, Tammelin B. (2003) Stateof- the-art of wind energy in cold climates. IEA R&D Wind, Wind Energy in Cold Climates, April 2003; 33.

Lehtomäki V and Wallenius T (2015) Overview of cold climate wind energy: Challenges, solution and future needs. Wiley Interdisciplinary Reviews: Energy and Environment. Epub ahead of print 18 March.

Makkonen, L. and J. R. Stallabrass, (1987): Experiments on the Cloud Droplet Collision Efficiency of Cylinders. Journal of Climate and Applied Meteorology, 26 (10), 1406–1411.

Makkonen, L., (2000): Models for the growth of rime, glaze, icicles and wet snow on structures. Philosophical Transactions of the Royal Society A: Mathematical, Physical and Engineering Sciences, 358 (1776), 2913–2939.

Makkonen, L., T. Laakso, M. Marjaniemi, and K. J. Finstad, (2001): Modelling and prevention of ice accretion on wind turbines. Wind Engineering, 25 (1), 3–21.

Matthew C. Homola, Per J. Nicklasson, Per A. Sundsbø, 2006: Ice sensors for wind turbines. Cold Regions Science and Technology 46 (2006) 125-131.

Navigant Research (2013) World Market Update 2012. Copenhagen: Navigant Research.

R.E. Wilson, S.N. Walker, and P. Heh, 1999: TECHNICAL AND USER'S MANUAL FOR THE FAST_AD ADVANCED DYNAMICS CODE, National Renewable Energy Laboratory report, 1999.

Shuai Zhang, Tobias Lindstrøm Jensen, et al. (2015) UWB Wind Turbine Blade Deflection Sensing for Wind Energy Cost Reduction. Sensors 2015, 15, 19768-19782.

Tammelin Bt, Cavaliere M, Holttinen H, et al. (1998) Wind Energy Production in Cold Climate (WECO). EU-JOULE3, JOR3-CT95-0014. EU.

Wright, W., (2002): User Manual for the NASA Glenn Ice Accretion Code LEWICE Version 2.2.2. Tech. rep., National Aeronautics and Space Administration, Cleveland, Ohio.

Appendix

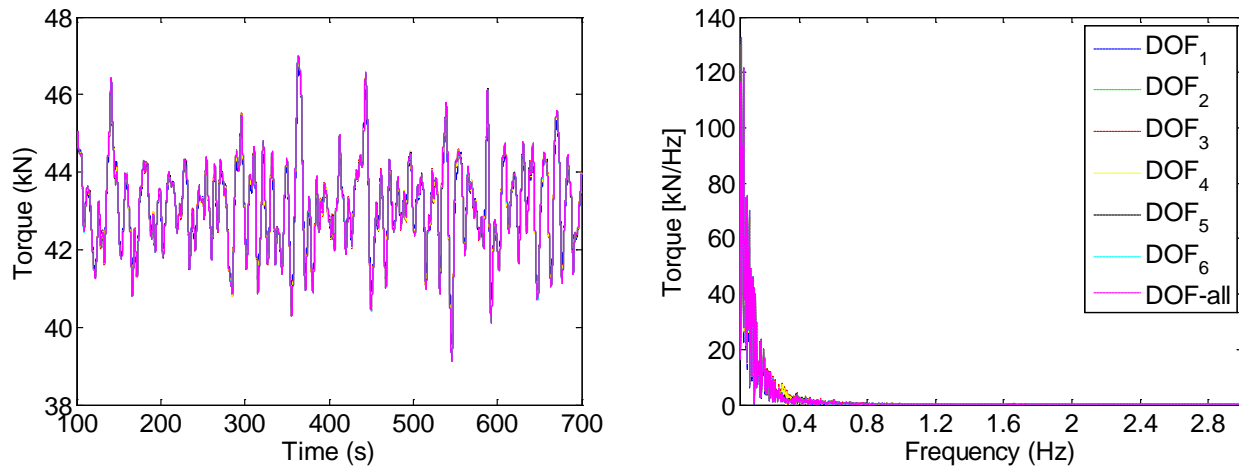## A1. Figure for error due to limited No. of DOFs

Figure 1 Time series (left) and spectrum (right) of torque under different DOFs
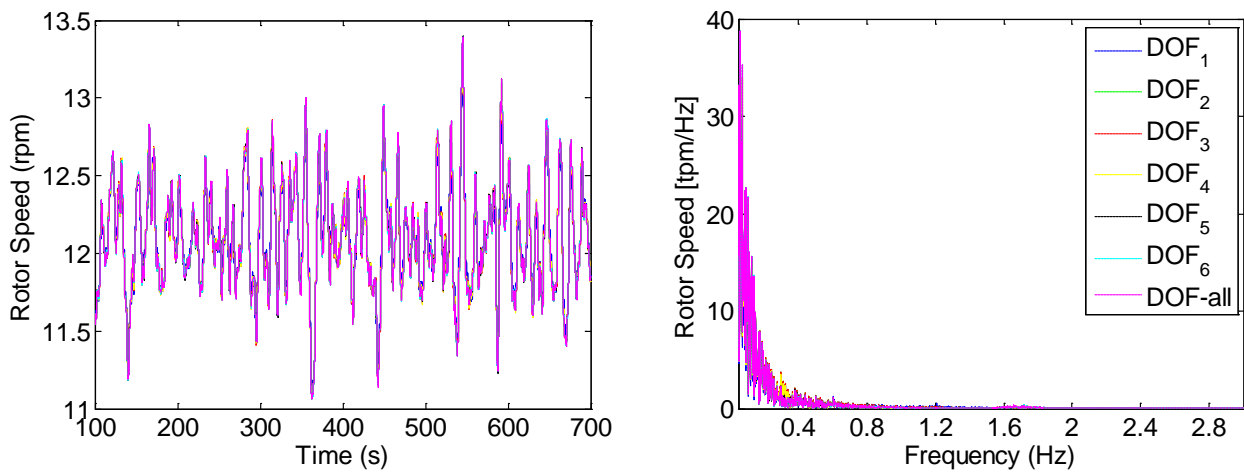

Figure 2 Time series (left) and spectrum (right) of rotor speed under different DOFs
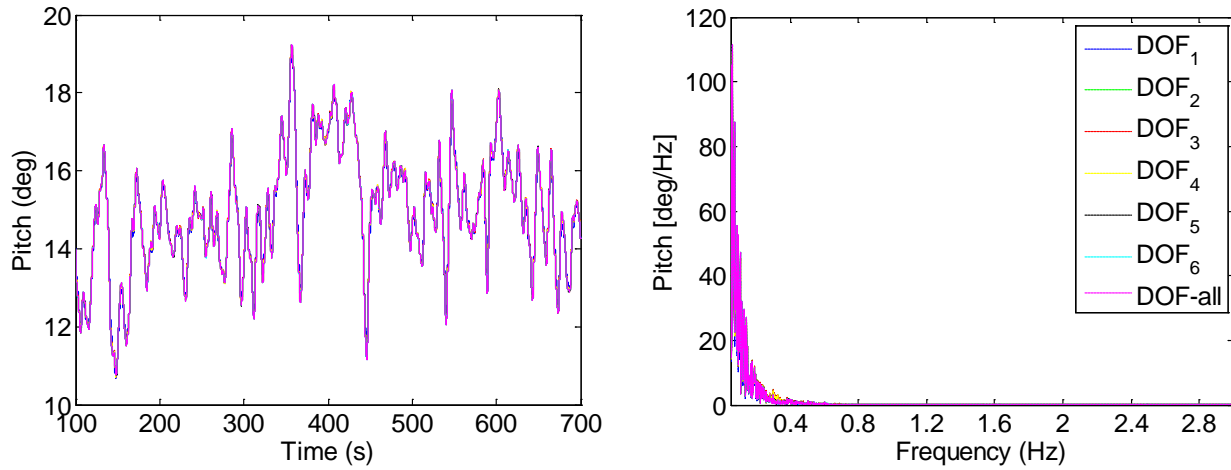
Figure 3 Time series (left) and spectrum (right) of pitch under different DOFs

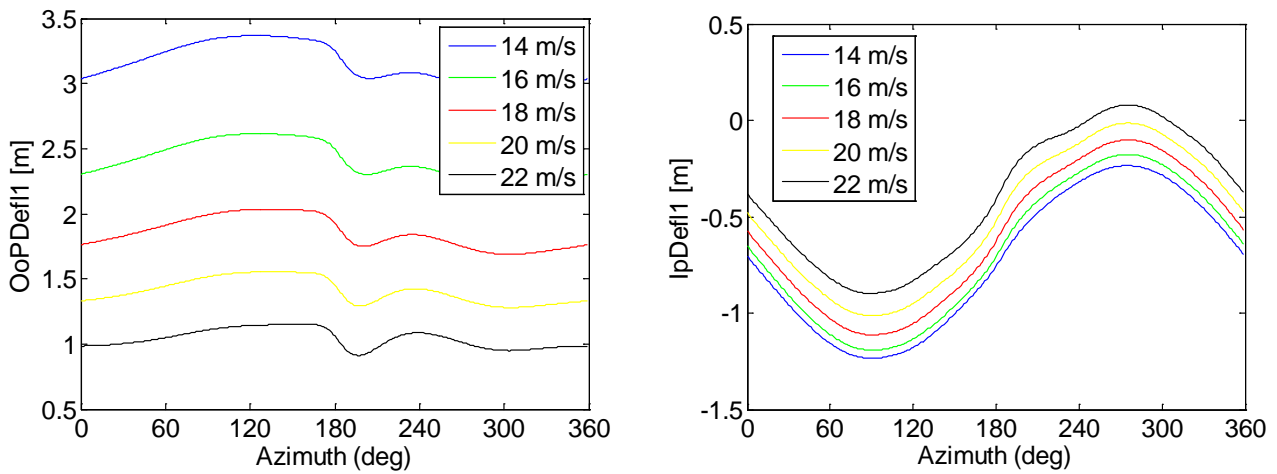## A2. Figure for OP. at different azimuth

Figure 4 Blade out-of-plane OP (left) and in-plane OP (right) deflections of different azimuth angle and wind speed
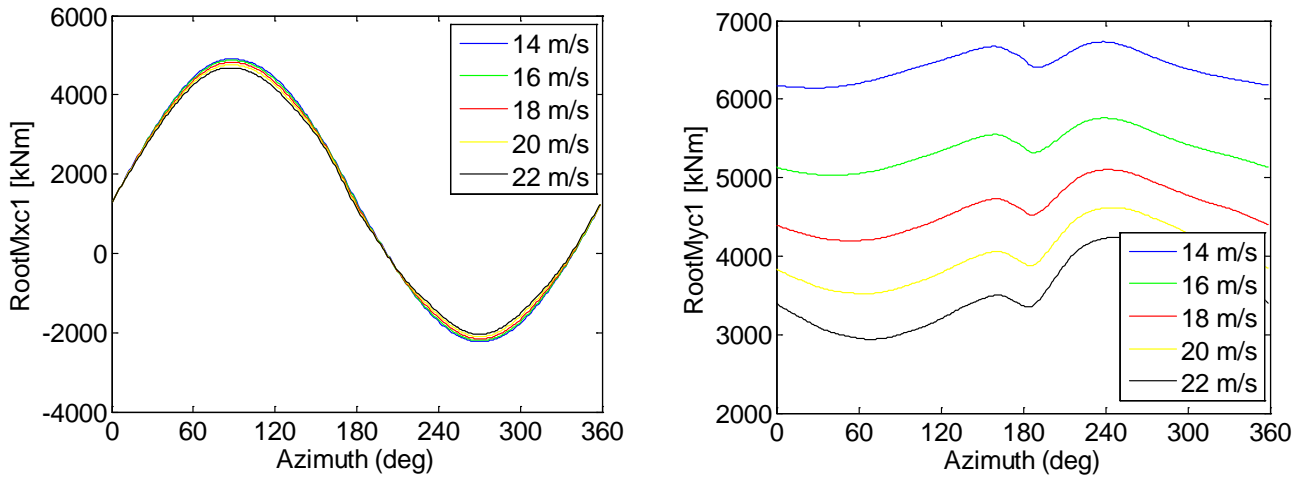
Figure 5 Blade in-plane OP (left) and out-of-plane OP (right) bending moment of different azimuth angle and wind speed
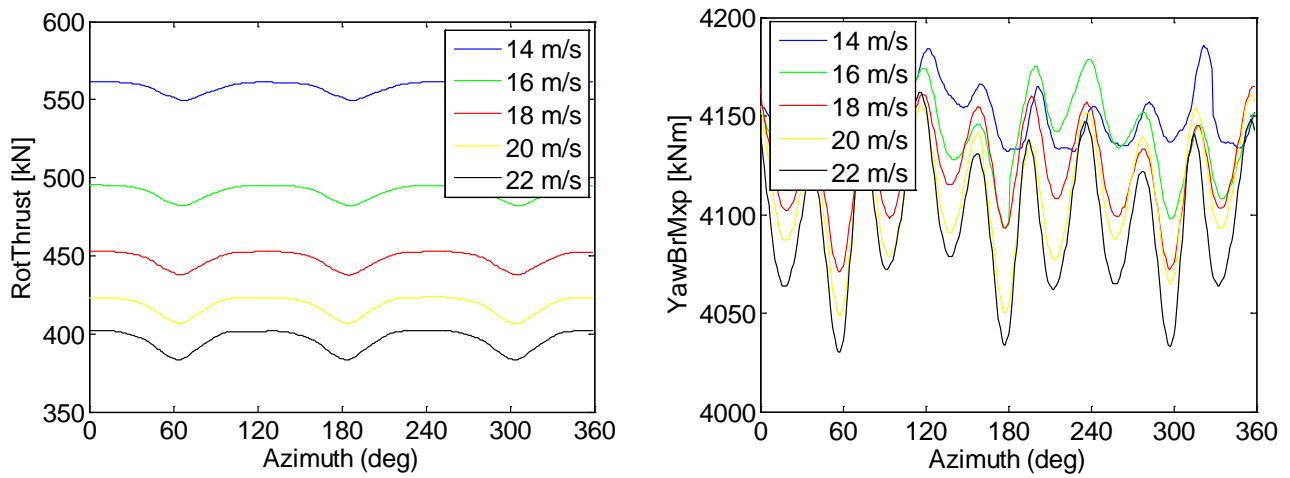

Figure 6 Rotor thrust OP (left) and tower side-side bending moment OP (right) of different azimuth angle and wind speed
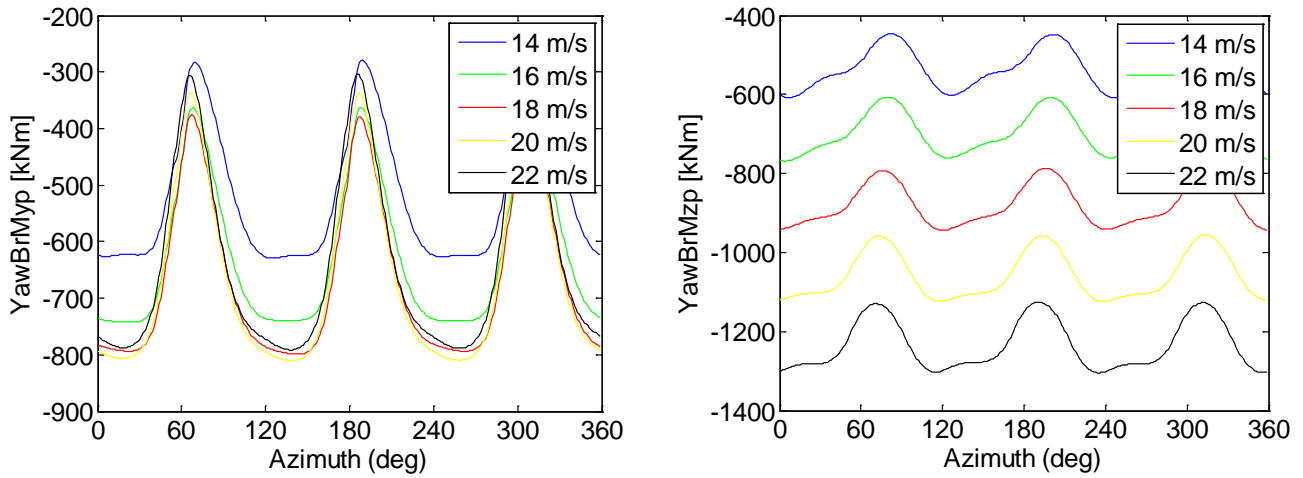
Figure 7 Tower fore-aft OP (left) and tower side-side OP (right) bending moment of different azimuth angle and wind speed
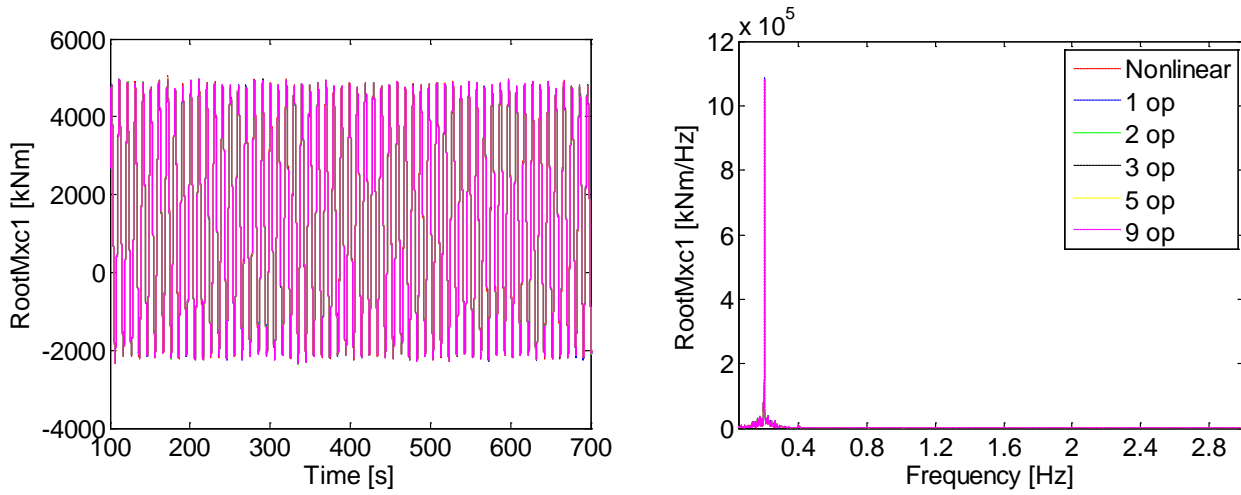
A3. Figure for error due to linearization (OP)

Figure 8 Blade root in-plane bending moment time series (left) and spectrum (right) at different OP
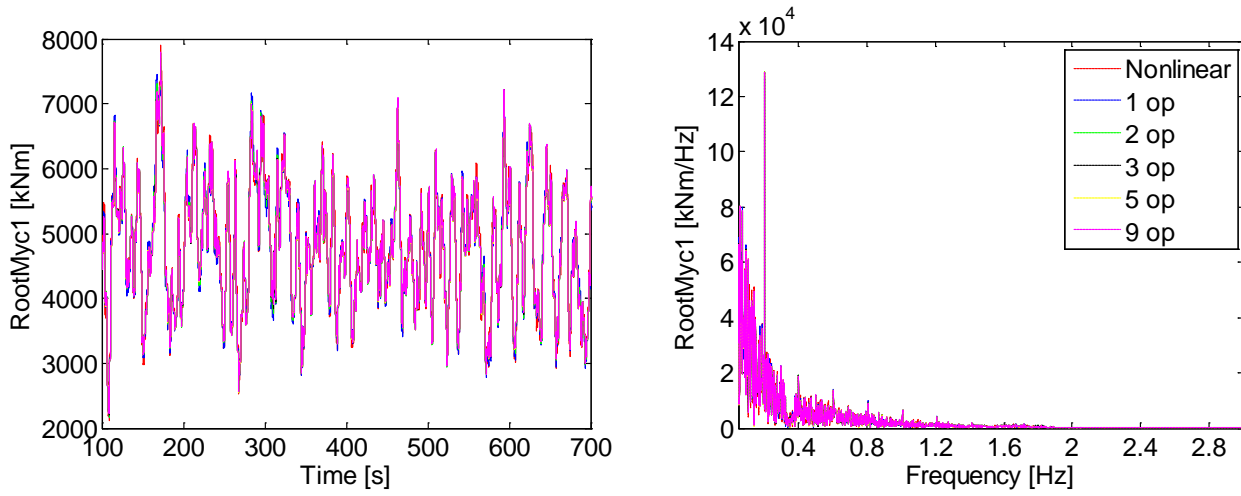
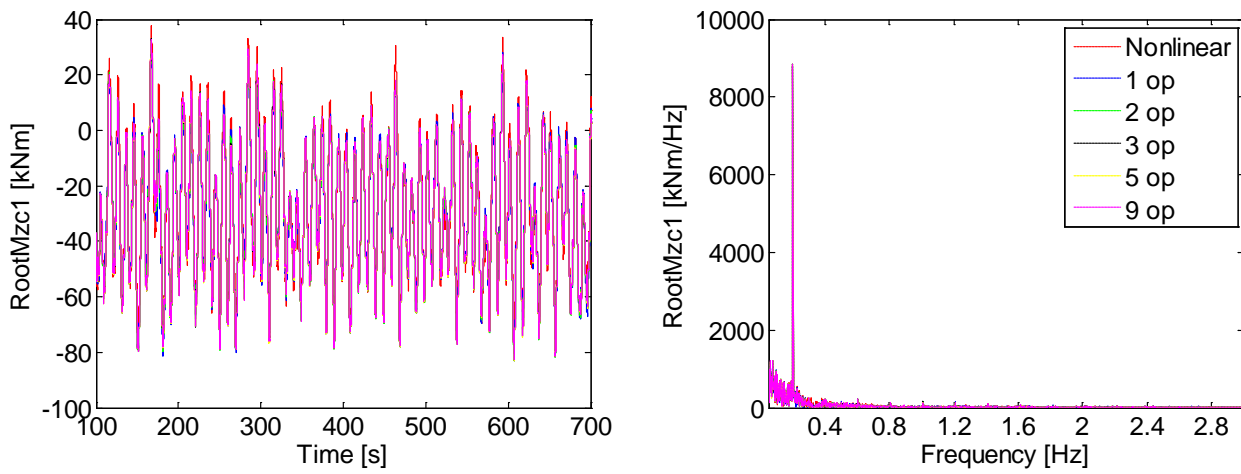Figure 9 Blade root out-of-plane bending moment time series (left) and spectrum (right) at different OP

Figure 10 Blade root torsional moment time series (left) and spectrum (right) at different OP

125

A4. Table for total modeling error contour plot

Table 1 Total modeling error of different quantities and DOFs

	DOF_1 [%]					DOF_1 [%]				
No. of OP	1	2	3	5	9	1	2	3	5	9
Gen Power	0.83	0.58	0.54	0.54	0.48	0.84	0.58	0.54	0.55	0.49
Rotor Speed	0.78	0.52	0.49	0.49	0.45	0.78	0.52	0.49	0.49	0.45
OoPDefl1	100.00	100.00	100.00	100.00	100.00	100.00	100.00	100.00	100.00	100.00
IpDefl1	100.00	100.00	100.00	100.00	100.00	100.00	100.00	100.00	100.00	100.00
RootMxc1	3.37	3.31	3.30	3.34	3.33	3.43	3.38	3.37	3.40	3.39
RootMyc1	10.30	10.10	10.12	9.98	10.05	10.29	10.09	10.12	9.97	10.04
RootMzc1	44.60	44.49	44.36	44.59	44.39	44.59	44.48	44.36	44.58	44.39
RotThrust	7.82	7.76	7.76	7.79	7.78	7.81	7.75	7.75	7.78	7.77
YawBrMxp	2.07	2.05	2.06	2.05	2.06	2.50	2.49	2.49	2.49	2.50
YawBrMyp	49.50	49.34	49.36	49.35	49.35	49.50	49.34	49.36	49.35	49.35
YawBrMzp	11.89	11.64	11.63	11.59	11.62	11.92	11.68	11.67	11.63	11.66

Table 1 Total modeling error of different quantities and DOFs (continue)

	DOF_3 [%]					DOF_4 [%]				
No. of OP	1	2	3	5	9	1	2	3	5	1
Gen Power	0.89	0.61	0.55	0.56	0.45	0.87	0.60	0.53	0.55	0.87
Rotor Speed	0.81	0.52	0.46	0.48	0.36	0.79	0.51	0.45	0.46	0.79
OoPDefl1	10.18	10.05	10.02	10.00	10.09	8.08	7.87	7.73	7.67	8.08
IpDefl1	47.12	46.96	46.94	46.91	46.83	6.82	6.44	6.42	6.42	6.82

RootMxc1	2.89	2.80	2.81	2.82	2.81	1.84	1.72	1.72	1.72	1.84
RootMyc1	3.93	3.64	3.62	3.63	3.62	3.71	3.42	3.41	3.42	3.71
RootMzc1	34.96	35.68	36.13	36.09	36.13	11.12	10.53	10.66	10.78	11.12
RotThrust	5.44	5.38	5.40	5.41	5.38	5.36	5.30	5.34	5.35	5.36
YawBrMxp	1.97	1.95	1.95	1.95	1.95	1.96	2.14	2.24	2.27	1.96
YawBrMyp	33.04	44.22	48.26	49.81	48.95	31.08	42.18	46.28	48.05	31.08
YawBrMzp	7.78	22.64	28.08	30.04	29.00	6.35	22.18	27.89	30.07	6.35

Table 1 Total modeling error of different quantities and DOFs (continue)

|	DOF_5 [%]					DOF_6 [%]				
No. of OP	1	2	3	5	9	1	2	3	5	9
Gen Power	0.81	0.53	0.47	0.47	0.38	0.81	0.53	0.45	0.47	0.35
Rotor Speed	0.74	0.44	0.38	0.38	0.29	0.74	0.44	0.37	0.39	0.26
OoPDefl1	7.62	7.39	7.27	7.23	7.30	7.61	7.41	6.87	7.24	7.59
IpDefl1	6.55	6.13	6.13	6.14	5.91	6.51	6.14	5.81	6.12	6.08
RootMxc1	1.84	1.72	1.72	1.73	1.72	1.88	1.76	1.67	1.76	1.76
RootMyc1	2.81	2.37	2.31	2.32	2.30	2.80	2.36	2.20	2.32	2.28
RootMzc1	10.41	9.83	9.93	10.01	9.92	10.41	9.80	9.51	10.01	9.73
RotThrust	1.78	1.51	1.51	1.52	1.51	1.78	1.51	1.44	1.52	1.49
YawBrMxp	1.97	2.17	2.22	2.26	2.35	1.77	2.00	1.98	2.08	2.13
YawBrMyp	8.84	27.99	29.80	31.49	39.17	8.67	27.88	29.95	31.52	37.58
YawBrMzp	4.89	23.86	27.29	29.11	34.17	4.81	24.01	27.46	28.91	32.76

A5. Plot for lift and drag coefficient
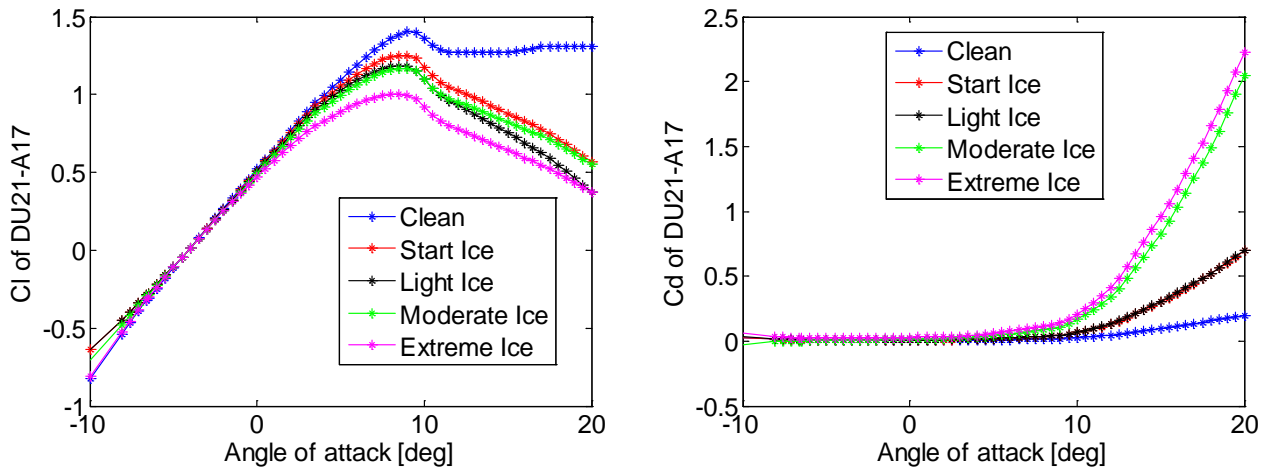
Figure 11 Lift (left) and drag (right) coefficient of NREL 5 MW blade section DU21-A17 at different angle of attack
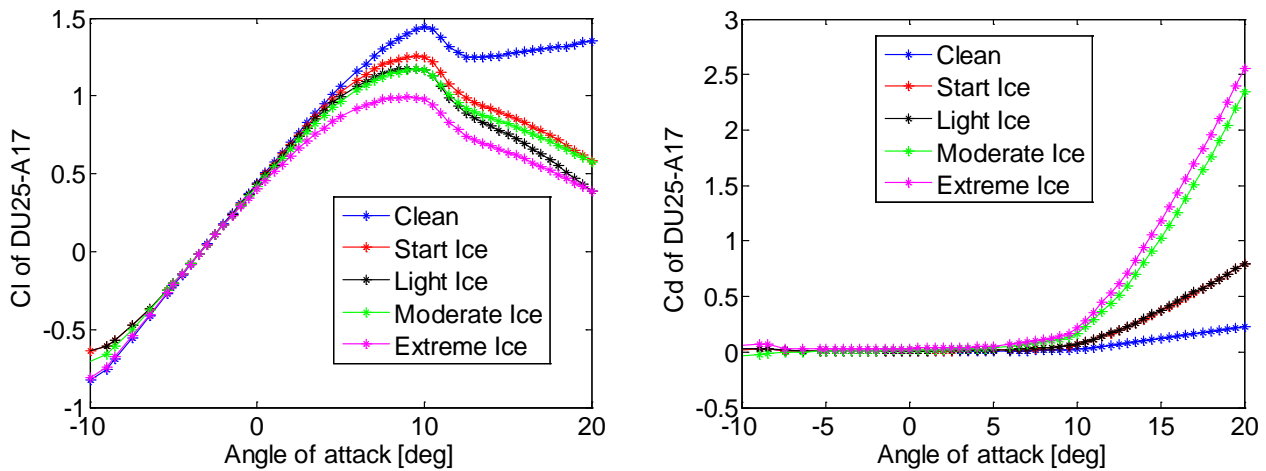

Figure 12 Lift (left) and drag (right) coefficient of NREL 5 MW blade section DU25-A17 at different angle of attack
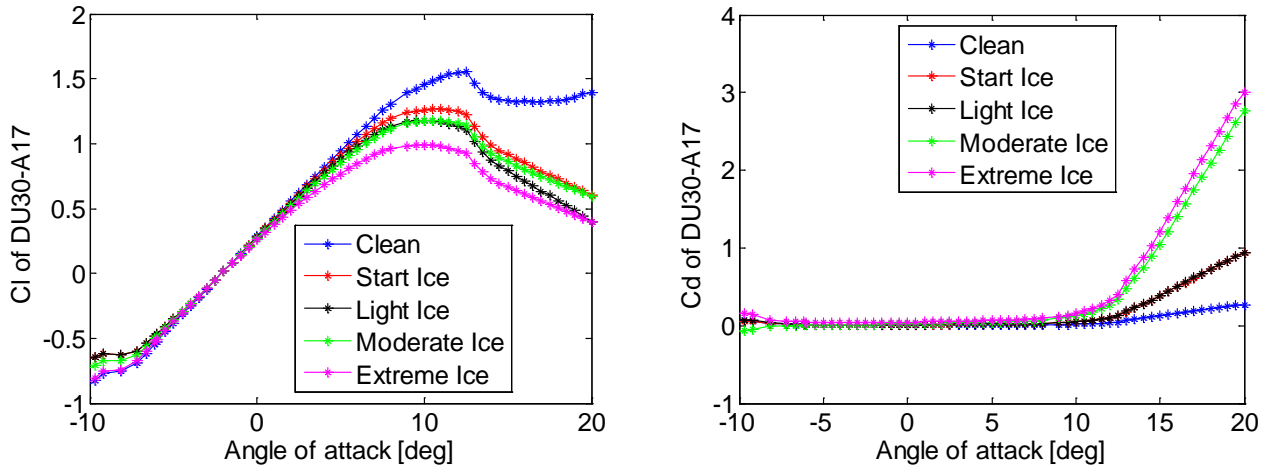
Figure 13 Lift (left) and drag (right) coefficient of NREL 5 MW blade section DU30-A17 at different angle of attack
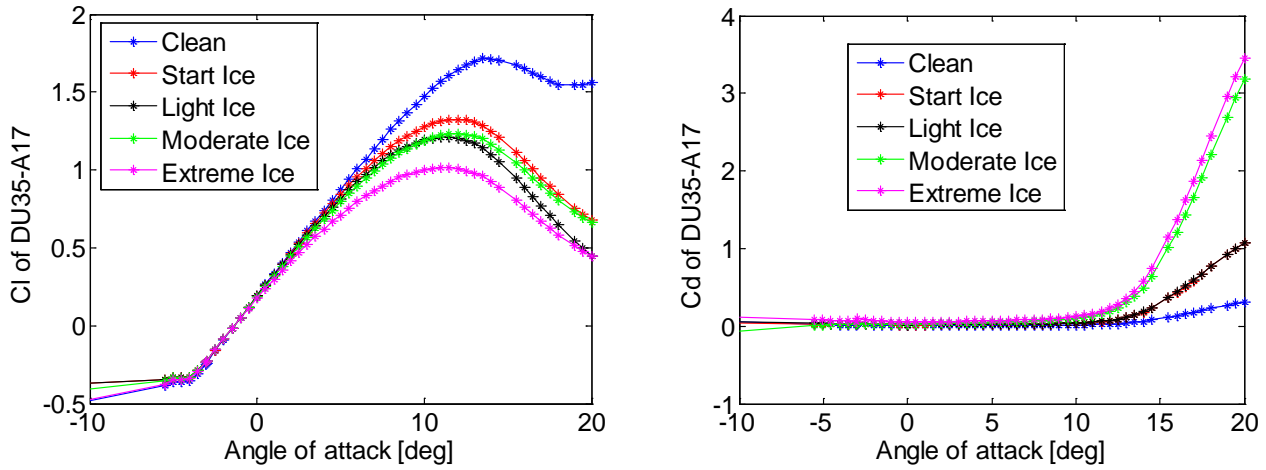

Figure 14 Lift (left) and drag (right) coefficient of NREL 5 MW blade section DU35-A17 at different angle of attack
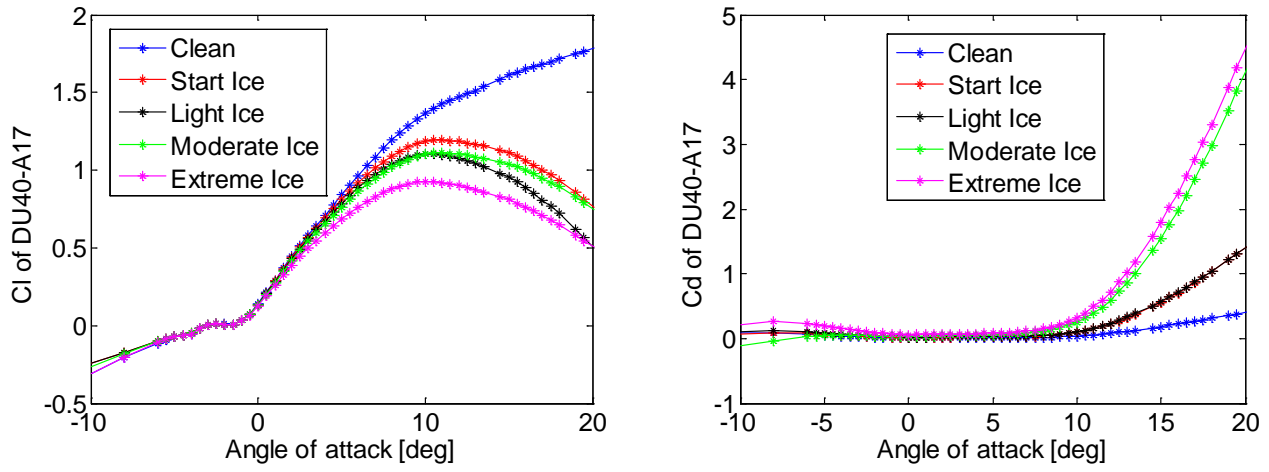
Figure 15 Lift (left) and drag (right) coefficient of NREL 5 MW blade section DU40-A17 at different angle of attack